MECHANISTIC STUDIES OF THE ANTIANGIOGENIC ACTIVITY OF ITRACONAZOLE

By
Sarah Alexandra Head

A dissertation submitted to Johns Hopkins University in conformity with the requirements for the degree of Doctor of Philosophy

Baltimore, Maryland

June 2016

Abstract

Angiogenesis, or the formation of new blood vessels, is an essential process in normal development as well as the pathological development of several diseases, including cancer. In an effort to identify novel angiogenesis inhibitors from existing drugs, the antifungal drug itraconazole was found to possess potent antiangiogenic activity that was unique among members of the azole antifungal class. However, despite promising early results in several phase 2 clinical trials for various types of cancer, its antiangiogenic mechanism of action remained unknown. We therefore sought to identify novel targets of itraconazole using a live cell photoaffinity labeling approach. Using a probe that retained the full cellular activity of itraconazole in endothelial cells, we identified two previously unknown binding partners of the drug: the mitochondrial Voltage-Dependent Anion Channel 1 (VDAC1) and the lysosomal protein Niemann-Pick type C 1 (NPC1). Inhibition of both targets leads to the inhibition of mTOR signaling through distinct pathways: VDAC1 is required for itraconazole-induced activation of the AMPK signaling pathway, an upstream effector of mTOR; and NPC1 inhibition causes a defect in cholesterol trafficking that also leads to mTOR inhibition. The simultaneous inhibition of these two pathways has a synergistic effect on mTOR inhibition, suggesting that the unique dual-targeted mechanism of itraconazole may give it an advantage over other anti-mTOR and antiangiogenic drugs.

Thesis advisor: Dr. Jun O. Liu

Thesis committee: Dr. Michael Wolfgang (reader), Dr. Philip Cole, Dr. Peter Espenshade, Dr. Steven Claypool.

Acknowledgements

I would first like to thank my thesis advisor, Dr. Jun Liu, for making this work possible. For me, Dr. Liu's mentoring style has been an ideal mixture of freedom and support, allowing me the space to pursue my ideas and make my own mistakes while also providing a constant driving force of optimism and excitement about science. I am very grateful for the training I have had in Dr. Liu's lab, as this line of research has touched on a huge breadth of different areas throughout the years, pushing me to constantly be learning a new technique or subject matter and really preparing me to become an independent scientist.

I also want to thank all of the members of the Liu lab, who have been my second family for the past 6 years. We've had a lot of fun together, and I'm so grateful to work with a group of people who I really like, respect, and can always rely on. From the time of my rotation in the Liu lab, it immediately struck me that anybody would drop what they were doing to help you with something. I especially want to thank Drs. Ben Nacev, Feiran Zhang, Yongjun Dang, and Joong Sup Shim, who taught me everything when I first joined the lab, and Wei Shi, Kalyan Kumar, and Ruojing Li who have worked together with me on the itraconazole project.

Thank you to my committee members, Drs. Peter Espenshade, Philip Cole, Michael Wolfgang, and Steven Claypool, for the advice and stimulating discussions. Also, my other rotation mentors –Drs. Jin Zhang and Dr. Heng Zhu – for continuing to be present and interested in my work throughout my Ph.D. Thanks to the Pharmacology staff for their work behind-the-scenes that makes it all possible. I have also had an

enormous amount of help from several collaborators at Hopkins and elsewhere: Thank you to Dr. Marco Colombini, Dr. Tatiana Rostovtseva, Dr. Yingming Zhao, Dr. Liang Zhao, Dr. Bob Cole and the JHMI MS facility, and Dr. William Craigen. I am also grateful to the PhRMA foundation for awarding me a predoctoral fellowship that helped fund this work.

Thanks to the Pharmacology class of 2010 for being so supportive and making the early years of our PhDs a lot of fun. Finally, I want to thank my family, especially my parents for their unconditional love and support, and my husband Joe for always believing in me.

Table of Contents

List of tables

List of Figures

Chapter 1: Introduction

1.1: Approaches to Drug Discovery

The discovery and development of new therapeutics to treat human diseases is arguably one of the most critical endeavors of modern society. It is also one of the most demanding of our society's financial and human resources. From start to finish, the process of bringing one new drug to market now takes on the order of 10-15 years and upwards of $2.5 billion[1], and is a major contributor to the unsustainable cost of healthcare in the United States and around the world. Thus, it is imperative that every measure be taken to make the entire process of drug development, from early preclinical research to approval, as efficient and effective as possible.

Phenotypic vs. Target-based Drug Discovery

In the earliest recorded days of human medicine, illnesses were largely treated using plants and other substances found in nature that were observed to have an effect on the illness. The use of empirical observation to determine whether a given treatment has an effect on the phenotype, or observable traits, of a disease has given rise to thousands of medicines, many of which are still in use today. This so-called "phenotypic" approach to drug discovery is an unbiased, brute force method, but has the advantage that effective treatments can be identified and used without any prior knowledge about how the treatment actually works.

As medical science has progressed through the ages and our understanding of the basic biology underlying human diseases has reached the molecular level, the logic

behind drug discovery has largely shifted. We now understand that drugs fundamentally work by binding to, and altering the function of, one or more "target" molecules in the body, typically proteins. Thus, it was logical to infer that if we could use our understanding of disease pathology to identify a target protein that plays a key role in the disease pathology, we could design drugs with specific activity against that protein. This target-based approach to drug discovery has given rise to the modern era of precision medicine, and over the past 25 or so years the vast majority of drug discovery efforts in the pharmaceutical industry have been focused on targets. The advantage of this approach is that it is hypothesis-driven rather than observational, providing a rational, defined starting point for drug development studies. In addition, simplified systems such as purified proteins can be used to screen very large numbers of compounds for activity; alternatively, if the structure of the target is known, new inhibitors can be rationally designed to bind within a certain binding pocket that may disrupt the protein's function. However, a major drawback to this approach is that there is no guarantee the drug candidate with the best activity against the chosen target will also have the most favorable activity in the context of the human body.

Despite enormous advances in our understanding of and approach to drug development, the rate of new drug approval has stagnated in recent years, while research and development costs have skyrocketed. In trying to elucidate the reasons for this lack of productivity, recent retrospective studies have looked at the successes and failures of drug candidates and assessed which properties were associated with the drugs that were finally approved. Interestingly, it was shown that between 1999-2008, while most R&D efforts were focused on targeted therapeutics, a majority of the approved first-in-class

drugs were actually identified by phenotypic assays[2]. The authors of the study speculate that high attrition rates in clinical trials were often due to incorrect assumptions that activity against a chosen target would translate into efficacy against the disease with an acceptably large therapeutic window. As a result of this and other studies, there has been a resurgence of interest in phenotypic screening in recent years as a potentially more effective and unbiased approach to drug discovery[3]. In addition, the development of more sophisticated technologies for phenotypic screening has allowed for more relevant disease models, including cell and even some animal models, to be miniaturized to the point where compounds can be tested in much higher throughput.

Drug Repurposing

Another important consideration in any drug discovery program is the selection of compounds from which to search for leads. Usually a large collection, or library, of chemical compounds is gathered and prepared in a format that can be used directly in the high-throughput assay of choice. Ideally, these compounds should have a wide range of different scaffolds, functional groups, and other physical properties to increase the likelihood of finding one with activity. The concentration of the chemicals is selected somewhat arbitrarily, at a relatively high level to ensure that compounds with moderate activity will show an effect, but not so high that too many hits are generated to follow up on. A balance must also be found in the number of compounds screened, as higher numbers are more likely to generate hits, but also use up larger amounts of resources and can potentially introduce greater experimental variability.

The makeup of the chemical library used in a particular high-throughput screen should be chosen based on the desired goal of the project. In pharmaceutical industry, where the goal is usually to identify a novel structure with a good likelihood of having favorable pharmacokinetic properties, and where resources are not a large concern, it is common for libraries upwards of 1,000,000 compounds of widely varying properties to be screened. Another popular approach is to screen smaller libraries of chemical fragments, very small compounds of less than 500 daltons, from which moderately active pieces can later be patched together in different combinations to form an optimized ligand. In contrast to these approaches common in industry, more resource-limited programs such as academic labs or other non-profits do not typically handle such large numbers of compounds or chemical reactions. However, because the end goal of programs outside of industry is usually not to produce a commercializable product, but to find the most effective drug from the smallest number of compounds possible, there are different strategies that can be used very successfully in academia.

One powerful strategy to find effective drugs is to search the chemical space of drugs that are already known to be effective. This is the idea behind drug repurposing, or finding new uses for existing drugs. Because drugs that are already approved for clinical use are known to be effective against some condition and have tolerable safety and toxicity profiles, the likelihood of finding an active compound with good drug-like properties improves exponentially. If validated against a disease model in preclinical studies, repurposed drugs can potentially enter later stage clinical trials directly without the need for initial safety and toxicity studies, saving significant time and resources. In addition, once the patent on an approved drug has expired, generic forms of the drug can

be made available to patients very inexpensively, potentially reaching underprivileged populations for whom expensive new drugs are not always readily available.

In summary, of the many different approaches to drug discovery being used today, a strategy that combines high-throughput phenotypic screening and drug repurposing is arguably the most likely to yield effective new treatments that can be most rapidly translated to clinical use while also minimizing the resources required for their discovery. In the remainder of this chapter, I will describe the use of such a strategy to identify a clinically used antifungal drug, itraconazole, which was found through phenotypic screening to have antiangiogenic activity and has been repurposed as an anticancer drug.

1.2: Angiogenesis and Cancer

The term angiogenesis refers to the creation of new blood vessels from preexisting vasculature. This process is important during normal growth and development, but also in the pathology of several diseases, including cancer, macular degeneration, rheumatoid arthritis, pulmonary hypertension, and others[4]. In the case of malignant tumors, the rapidly proliferating, genetically altered cancer cells require a progressively increasing supply of nutrients to continue their uncontrolled growth. Tumors often promote the in-growth of new blood vessels for this purpose, by secreting proangiogenic growth factors including vascular endothelial growth factor (VEGF), basic fibroblast growth factor (bFGF), and others[5]. For this reason, Dr. Judah Folkman postulated in the 1970's that by inhibiting the growth of new blood vessels into the tumor, it might be possible to prevent the tumor from growing beyond a certain size,

rendering it effectively "dormant" and harmless to the host[6]. In addition, because the endothelial cells that line the blood vessels are genetically stable and do not proliferate as rapidly as cancer cells, targeting endothelial cells might lead to a decreased incidence of drug resistance[7].

Since this theory originated, a significant amount of effort has been dedicated to understanding, and designing inhibitors of, angiogenesis. Several clinical drugs have resulted from these studies, which have shown efficacy against various types of cancer alone or in combination with chemotherapy[8]. Based on the work of researchers such as Folkman and others on the molecular mechanisms underlying angiogenesis, the majority of currently used antiangiogenic drugs were developed using a targeted approach to inhibit the VEGF signaling axis. Monoclonal antibodies against VEGF (e.g. Bevacizumab) and its receptor VEGFR (e.g. Ramucirumab) are being used or tested in a variety of different types of cancers, including colorectal, lung, and gastric cancers[9,10]. Another anti-VEGF strategy is the use of soluble "decoy" receptors (e.g. Aflibercept), which bind VEGF in the circulation and prevent it from reaching the VEGFR[11]. Small molecule tyrosine kinase inhibitors (e.g. sorafenib, sunitinib, regorafenib), which inhibit the kinase activity of VEGFR, PDGFR, FGFR, and other proangiogenic receptors, are also being used to treat cancer.

Although these treatments have proven efficacious in certain cancers, they are also generally prone to acquired resistance or insensitivity. As with most other targeted cancer therapies, genetically unstable cancer cells are often able to find ways to overcome the treatment, by developing mutations in the target proteins themselves that prevent the drugs from binding, and/or reducing their dependence on the target through some other

compensatory mechanism. For example, in the case of anti-VEGF therapies, other growth factors such as FGF, PDGF, etc. can stimulate angiogenesis and therefore, once VEGF becomes ineffective, the tumor cells can upregulate production of another factor[12]. These transformations often mean that such therapeutics are only able to provide transient benefits to the patient and do not necessarily translate to increases in overall survival.

In light of these challenges, it is likely that monotargeted therapies will not be the best solution for angiogenesis inhibition going forward, and the use of mechanistically distinct drugs, either sequentially or in combination, will be necessary for sustained responses in these patients. In addition, relying only on our existing knowledge of the mechanisms underlying angiogenesis to design new inhibitors is problematic, as it limits the number of potential targets to a tiny fraction of all druggable space. Logically, it is highly likely that of the 20,000+ genes in the human genome, several regulators of angiogenesis have not yet been identified that could potentially be effective drug targets. Unbiased, phenotypic drug screening is therefore more likely to yield mechanistically distinct drugs that can expand the portfolio of antiangiogenic treatments.

1.3: Repurposing Itraconazole as an Antiangiogenic/Anticancer Drug

With the goal of identifying novel angiogenesis inhibitors from the existing drug space, a library of clinically used, mostly FDA-approved drugs was assembled and screened for inhibitors of primary Human Umbilical Vein Endothelial Cell (HUVEC) proliferation as a proxy for angiogenesis[13]. A promising hit to emerge from this screen was the antifungal drug itraconazole, with an IC_{50} of 150-200 nM for inhibition of HUVEC proliferation. Because the plasma concentration of itraconazole during a

standard course of treatment can reach as high as 3.2 μM, these concentrations are likely to be attainable during normal dosing regimens. The proliferation inhibition was shown to be selective for endothelial cells (both HUVEC and Bovine Aortic Endothelial Cells, BAEC) over other cell types, including Human Foreskin Fibroblasts (HFF), HeLa, and Jurkat T cells, suggesting a specific antiangiogenic effect[13]. Itraconazole's activity was further validated in an *in vivo* matrigel angiogenesis assay, where a growth factor-secreting gel is implanted into mice and the number of blood vessels that grow into the gel is quantified. In addition, itraconazole was shown to inhibit the growth of prostate and lung cancer xenografts in mice, demonstrating its anticancer potential[13,14].

Shortly after the discovery and validation of itraconazole's antiangiogenic activity, another screen of the same clinical drug library identified itraconazole as a novel inhibitor of the Hedgehog signaling pathway[15]. The Hedgehog pathway is most well studied in the context of organismal development, but has also been implicated in adult human diseases including several types of cancer. Hyperactivation of the pathway is observed in a large majority of basal cell carcinomas (BCC) and at least a third of medulloblastoma cases[16]. Thus, there has been considerable interest in the development of Hedgehog pathway inhibitors.

The Hedgehog signaling pathway is initiated by binding of the Hedgehog ligand to its receptor, Patched. Through mechanisms that are not completely understood, Patched then releases its inhibitory hold on Smoothened, allowing Smoothened to translocate to the primary cilium and triggering a cascade of events leading to activation of the Gli transcription factor that controls Hedgehog target gene expression. Using the Gli-responsive luciferase reporter cell line Shh-Light 2, itraconazole was shown to inhibit

pathway activation with an IC_{50} of ~800 nM. This inhibition was shown to occur at the level of Smoothened, preventing its translocation to the primary cilium[15]. Itraconazole also inhibited Gli1 expression in mice, as well as growth of medulloblastoma xenografts and endogenous basal cell carcinomas, demonstrating antihedgehog and anticancer activity *in vivo*.

Clinical Studies of Itraconazole in Cancer

Itraconazole has been in clinical use for decades, and its pharmacokinetic properties and safety and toxicity profiles are thoroughly documented. Because of this, it has been able to move rapidly into clinical trials as an investigational anticancer drug. Several trials have been initiated in different types of cancer, including prostate, breast, lung, and basal cell carcinomas (**Table 1.1**). The results of three of these trials have been published to date. A phase 2 trial in castration-resistant metastatic prostate cancer (CRPC) where patients were given either 200 or 600 mg/day itraconazole demonstrated a median progression-free survival (PFS) of 35.9 weeks in the high-dose arm, which is considered comparable to other investigational treatments in this population, whereas the low-dose arm (200 mg/day) had a median PFS of 11.9 weeks[17]. Additionally, Hedgehog signaling, as measured by Gli1 expression in skin punch biopsies, and circulating tumor cell counts were also suppressed in a majority of the patients in the study. A phase 2 trial in non-small cell lung cancer (NSCLC) in which patients were given pemetrexed with or without itraconazole (200 mg/day) demonstrated an increase in 3-month PFS (67% vs. 27%), median PFS (5.5 months vs. 2.8 months) and median overall survival (32 months vs. 8 months) in the itraconazole arm[18]. A phase 2 trial in basal cell carcinoma (BCC)

showed a decrease in tumor cell proliferation (45%), Hedgehog signaling (65%) and tumor area (24%) after itraconazole treatment[19]. In addition, prior to these three trials specifically assessing itraconazole's anticancer activity, another study had investigated itraconazole as an antifungal prophylactic in patients with neutropenic leukemia receiving daunorubicin and found that the disease-free survival rate of acute lymphoblastic leukemia (ALL) was higher in the itraconazole-treated arm, which was attributed to reversal of multidrug resistance[20]. Several case reports have also been published showing apparent effects of itraconazole treatment in prostate cancer, pancreatic cancer, cutaneous T-cell lymphoma, and infantile hemangiomas[21–24].

Title	Condition	Sponsor/Collaborators
Phase Ib/II Study Evaluating Orteronel (Without Prednisone) Combined With Itraconazole In Men With Castration-Resistant Prostate Cancer (CRPC)	Prostate Cancer	Emmanuel Antonarakis, MD|Millennium Pharmaceuticals, Inc.|Johns Hopkins University
A Phase II Study of Itraconazole in Biochemical Relapse	Prostate Cancer	University of California, San Francisco
Study of Itraconazole in Castrate-resistant Prostate Cancer (CRPC) Post-chemotherapy	Prostate Cancer	Stanford University
A Two-dose Level Clinical Trial of Itraconazole in Patients With Metastatic Prostate Cancer Who Have Had Disease Progression While on Hormonal Therapy	Prostate Cancer	Johns Hopkins University|Memorial Sloan Kettering Cancer Center
Neoadjuvant Itraconazole in Non-small Cell Lung Cancer	Non-small Cell Lung Cancer	University of Texas Southwestern Medical Center|United States Department of Defense
A Randomized Phase II Study of SUBATM-itraconazole in Patients With Untreated Squamous NSCLC.	Non-small Cell Lung Cancer	Sidney Kimmel Comprehensive Cancer Center
A Randomized Phase II Study of Itraconazole and Pemetrexed in Patients With Previously Treated Non-Squamous Non-Small Cell Lung Cancer	Non Small Cell Lung Cancer	Sidney Kimmel Comprehensive Cancer Center
A Pilot Trial of Itraconazole Pharmacokinetics in Patients With Metastatic Breast Cancer	Breast Cancer	Indiana University
Open-label Trial of SUBA™ -Itraconazole (SUBA-Cap) in Subjects With Basal Cell Carcinoma Nevus Syndrome (BCCNS)	Basal Cell Carcinoma in Basal Cell Nevus Syndrome	HedgePath Pharmaceuticals, Inc.
Topical Itraconazole in the Treatment of Basal Cell Carcinoma	Basal Cell Carcinoma	Johns Hopkins University
Pilot Biomarker Trial to Evaluate the Efficacy of Itraconazole in Patients w/ Basal Cell Carcinomas	Basal Cell Carcinoma	Stanford University

Table 1.1: Ongoing and recently completed clinical trials investigating itraconazole as an anticancer agent in the US
(information compiled from http://www.clinicaltrials.gov)

Because itraconazole has been in clinical use for many years, retrospective studies have also been performed to evaluate the outcomes of patients with various cancers who were treated with itraconazole. These studies have shown a potential benefit of itraconazole treatment in ovarian clear cell carcinoma[25], refractory ovarian cancer[26], recurrent triple-negative breast cancer[27], metastatic pancreatic cancer[28], and metastatic biliary tract cancer[29], providing a rationale for further studies with itraconazole in these cancer types. However, it is worth noting that in all of the above clinical studies, there can be no conclusive determination that the observed effects of itraconazole are due to angiogenesis inhibition, Hedgehog inhibition, MDR reversal, or some other undescribed activity.

Although itraconazole is well tolerated and side effects are generally mild, it has been shown to cause hepatotoxicity in a small subset of patients due to its interaction with CYP450 enzymes. Participants in the above phase 2 trials had their liver function monitored throughout the course of their treatment and no liver toxicities were reported, although the duration of these trials was relatively short. Depending on the prognosis of the patient, the low risk of liver toxicity may be outweighed by the potential benefit if life expectancy is short otherwise. The commercial formulation of itraconazole contains a mixture of the 4 cis-stereoisomers in a 1:1:1:1 ratio, and a recent study found that the antiangiogenic activity of these 4 stereoisomers did not track with their hepatotoxicity, suggesting the two effects can be separated[30]. Stereochemistry at the 2 and 4 positions had a greater influence on antiangiogenic activity while the 2' position affected hepatotoxicity (**Figure 1.1**). One stereoisomer designated IT-C (2S,4R,2'S) had both

better antiangiogenic potency and less hepatotoxicity than the commercial mixture, suggesting it may be a better anticancer drug candidate for further clinical studies.

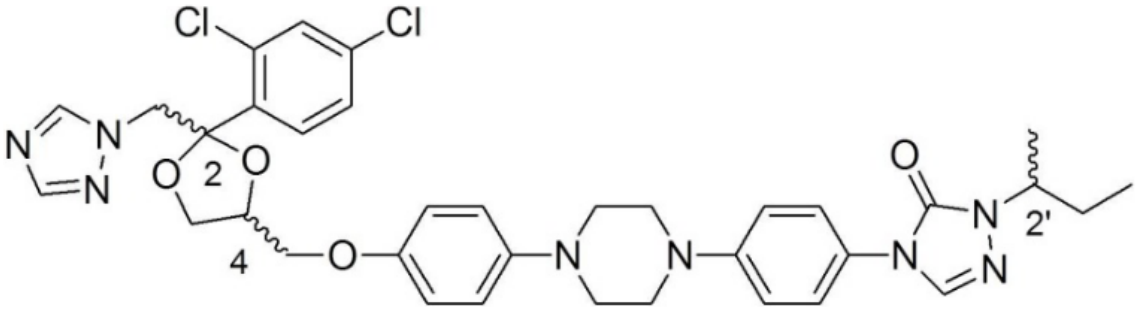

Figure 1.1: Itraconazole structure and stereocenters[30]. Itraconazole has three stereocenters, designated 2, 4, and 2', giving rise to 8 possible stereoisomers. The commercial itraconazole formulation is a mixture of equal amounts of the 4 cis-stereoisomers, where the triazole and ethoxyphenyl-containing substituents are on the same side of the dioxolane ring (i.e. 2S4R or 2R4S).

Mechanistic Studies

Like other azole antifungal drugs, itraconazole exerts its activity through binding to the fungal P450 enzyme lanosterol 14-α-demethylase (14DM; CYP51). This enzyme catalyzes the first step in the conversion of lanosterol to ergosterol, an important structural sterol required for maintenance of membrane integrity in fungal cells. The azole drugs bind in the active site of the enzyme and one of the basic azole nitrogen atoms (N3 for imidazole drugs and N4 for triazoles) coordinates the iron of the heme group, leading to reversible enzyme inhibition[31]. 14DM is also expressed in mammalian cells, where it is analogously involved in the cholesterol biosynthetic pathway; however, it has been shown that the azole drugs, including itraconazole, have a significantly lower affinity for the human enzyme than the fungal enzyme[32,33].

Although itraconazole's antifungal mechanism of action is well established, several pieces of evidence suggested that the antiangiogenic activity is likely not mediated by 14DM inhibition. First, other azole antifungals that have been shown to have greater potency against human 14DM have significantly lower potency for HUVEC inhibition[13]. Second, a similar lack of correlation was observed when all eight individual stereoisomers of itraconazole were synthesized and tested in HUVEC and yeast, strongly suggesting the two activities are likely to be mediated by different targets[34]. Finally, an analog of itraconazole that lacks the triazole ring was synthesized and shown to retain significant antiproliferative activity in HUVEC (**Figure 1.2**)[35]. These results suggest that there may be one or more other molecular targets of itraconazole that contribute to its antiangiogenic activity.

A

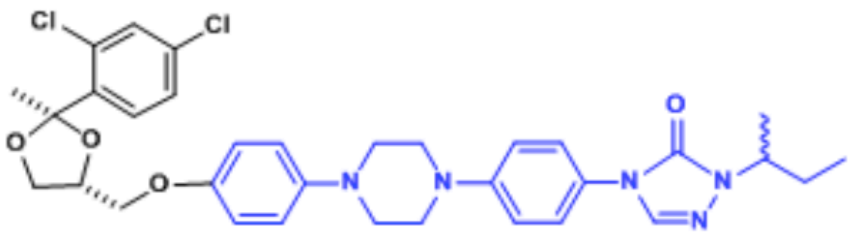

B

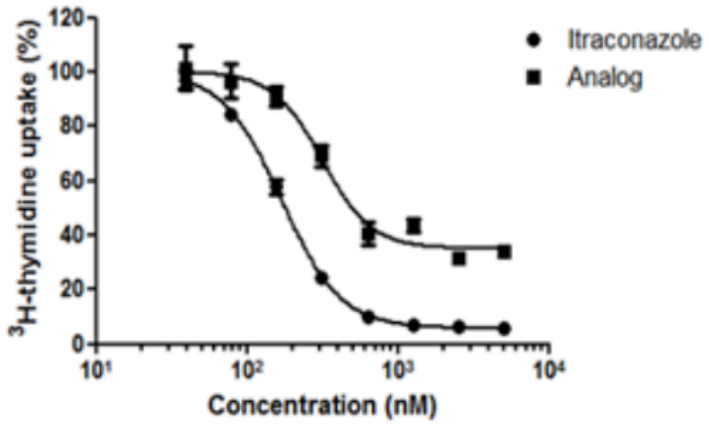

Figure 1.2: Structure and activity of triazole-deleted itraconazole. (A) Structure of triazole-deleted itraconazole (TD-itra) and (B) its antiproliferative activity in HUVEC, as measured by thymidine incorporation.

In attempting to elucidate the mechanism of action of itraconazole, several key phenotypes were observed that possibly contribute to its activity in endothelial cells. Itraconazole was shown to induce cell cycle arrest in the G1 phase, which was associated with decreased expression of the cell cycle regulatory proteins Cyclin A, Cyclin E and p21, and increased expression of p27[36]. Similar effects had been previously reported for the natural product rapamycin, which inhibits the mechanistic target of rapamycin (mTOR) signaling pathway and also has antiangiogenic activity[37,38]. Similarly, itraconazole was shown to inhibit mTOR signaling in HUVEC, as measured by phosphorylation of the mTOR kinase substrates ribosomal protein s6 kinase (S6K) and eukaryotic translation initiation factor 4E binding protein 1 (4EBP1). Because the IC_{50} for mTOR inhibition in HUVEC was the same as for proliferation inhibition (between 100-300 nM after 24 hours treatment), it was thought that the antiangiogenic activity of itraconazole was likely mediated by this mTOR inhibitory activity.

It was also shown that itraconazole induced accumulation of cholesterol into perinuclear vesicles that colocalized with the late endosomal-lysosomal resident protein LAMP1, preventing its trafficking to the plasma membrane and other organelle membranes[36]. This cholesterol trafficking defect is characteristic of cells from patients with Niemann-Pick type C (NPC) disease, where a deficiency in one of two lysosomal proteins, NPC1 and NPC2, prevents cholesterol from being properly transported out of the lysosome to the rest of the cell (referred to as NPC phenotype). It was shown that adding exogenous cholesterol delivered in complex with the carrier molecule β-cyclodextrin to itraconazole-treated cells partially reversed both the proliferation inhibition and mTOR inhibition. In addition, shRNA knockdown of NPC1 or NPC2 led

to inhibition of mTOR signaling in HUVEC, and other small molecules known to induce NPC phenotype (U18666a and imipramine) had a similar effect, suggesting a connection between cholesterol trafficking and mTOR signaling in endothelial cells.

Another interesting effect of itraconazole in HUVEC was discovered while monitoring levels of VEGFR2 protein, an important mediator of VEGF-induced angiogenesis. It was found that treatment with itraconazole caused a change in the electrophoretic mobility of the protein, leading to a downward shift on SDS-PAGE. This gel shift was eventually attributed to hypoglycosylation of the receptor[39]. Proper glycosylation of VEGFR2 is required for the correct localization of the receptor at the cell surface and thus its availability for binding and activation by its ligand; accordingly, inhibition of glycosylation leads to intracellular accumulation and failure to stimulate the proangiogenic signaling pathway. This effect was specific to itraconazole over other azole antifungals tested, suggesting that it was not due to inhibition of 14DM, and it was also not a consequence of mTOR inhibition or cholesterol trafficking as other mTOR/cholesterol trafficking inhibitors failed to induce the same defect in VEGFR2 glycosylation. Likewise, other glycosylation inhibitors failed to inhibit mTOR or cholesterol trafficking, suggesting that the two phenotypes were likely parallel consequences of itraconazole treatment. Similar to the mTOR/NPC phenotype, however, the glycosylation defect was also partially reversed by adding cholesterol/cyclodextrin complex to itraconazole-treated cells. In addition to VEGFR2, effects of itraconazole on the glycosylation of VEGFR1, EGFR, Fcγ and CD14 receptors have been reported, suggesting a global defect in N-linked glycosylation[39–41].

In order to determine whether the effects of itraconazole observed in endothelial cells were related to the Hedgehog inhibition, a structure-activity relationship (SAR) study was performed using a number of itraconazole analogs with modifications to the isobutyl side-chain[42]. Analogs were assayed for HUVEC proliferation and VEGFR2 glycosylation, as well as proliferation and Gli1 transcription in a medulloblastoma culture. Overall, a lack of correlation between antiproliferative potency in the two cultures was observed, and the apparent structural determinants for VEGFR2 glycosylation inhibition (≥4 carbon side-chain length with branching at the α or β carbon) differed from those for Gli1 transcription inhibition (≥3 carbon length, no branching at β carbon or polar modifications), suggesting that the antiangiogenic and anti-hedgehog effects of itraconazole are likely mediated by different targets. In light of these results, I have focused on itraconazole's antiangiogenic effects in this thesis work, although it is worth noting that both aspects of itraconazole's mechanism may play a role in its anticancer activity.

1.4: Target Identification

Although a significant amount of work has been performed in trying to understand itraconazole's molecular mechanism of action (MMOA), the direct target(s) mediating its antiangiogenic activity had not been found. Target identification is an important step not just in understanding how a particular drug works at a molecular level, but also illuminating the underlying biological processes governing a disease and potentially identifying improved treatment strategies.

Approaches to identifying the targets of small molecules can be broadly grouped into two categories: top-down, where the cellular phenotype of the drug is used to narrow

down its potential targets based on their known functions, or bottom-up, where the target is identified directly by chemical or genetic means (**Figure 1.3**)[43]. The studies described above, where the effects of itraconazole were observed in cells, fall into the category of a top-down approach. These studies provided clues to the cellular changes that might underlie the ultimate phenotype of angiogenesis inhibition, which helps narrow down the list of potential targets to proteins involved in those cellular processes affected by the drug (e.g. cholesterol trafficking, mTOR signaling, glycosylation, etc.). However, a major disadvantage of the top-down approach is that it relies on what is already known about these processes, and does not account for the possibility that the real target is a protein whose function has not been characterized or has not been previously described to be involved in a given process.

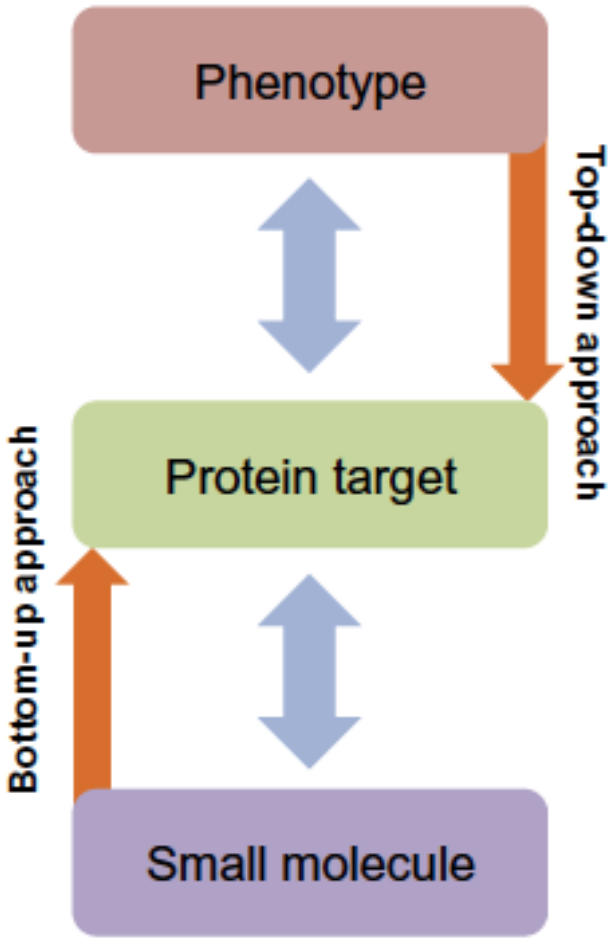

Figure 1.3: Two approaches to target identification. The top-down approach begins with observation of a phenotype and narrows down the possible targets based on their known functions. The bottom-up approach starts with direct identification of the target protein and then up to connect that target with the observed phenotype. Figure from Titov and Liu, 2012[43].

The bottom-up approach circumvents this problem by identifying the target directly in an unbiased manner. This can be accomplished by genetic means; for example, by screening an shRNA library for knockdown cell lines that confer resistance or hypersensitivity to the drug, or by isolating drug-resistant cell lines and using deep sequencing to determine which genes contain mutations that confer resistance. These types of experiments can identify key proteins or pathways related to the activity of the drug, but do not necessarily prove direct binding to the identified protein. Chemical approaches, on the other hand, typically involve the use of a chemical probe to bind to the target protein directly and allow its isolation and identification. Designing a probe that retains its ability to bind to the target protein requires the use of structure-activity relationship (SAR) studies to identify a position on the molecule that can be modified without significant loss of activity. It also requires that the probe be able to bind its target with high enough affinity that it can be isolated from other cellular proteins (i.e. affinity purified), and that these proteins retain their ability to bind the small molecule outside of their native cellular environment. This requirement can be problematic for certain targets; for example, integral membrane proteins often require a specific lipid environment to maintain their active conformation, and may become aggregated or improperly oriented for ligand binding once cells are lysed. One way to circumvent this issue is to design a chemical probe containing a crosslinking moiety that can covalently attach to the target protein and thus allow it to be isolated without regard to affinity. A common crosslinking strategy for such probes is to use a photolabile group, such as a diazirine or benzophenone, which becomes activated upon irradiation with UV light and covalently inserts into whatever protein is nearest.

The goal of this thesis work has been to identify the direct target(s) of itraconazole that mediate its antiangiogenic activity, with the aim of understanding its MMOA as well as uncovering new potential targets for the future development of mechanistically distinct antiangiogenic drugs. To accomplish this, I used a cell-active photoaffinity probe of itraconazole to identify its binding proteins in live cells, and performed target validation studies to identify these proteins' connection to known phenotypes of itraconazole in endothelial cells. In the course of this work, I identified a previously unknown connection between the outer mitochondrial membrane channel VDAC1 and the mTOR signaling pathway in endothelial cells (Chapter 2), and uncovered a novel dual-targeted mechanism of small-molecule-induced mTOR inhibition (Chapter 3). The relevance of these studies and future directions will be discussed in Chapter 4.

1.5: References

1. DiMasi, J. A., Grabowski, H. G. & Hansen, R. W. The cost of drug development. *N. Engl. J. Med.* **372,** 1972 (2015).
2. Swinney, D. C. & Anthony, J. How were new medicines discovered? *Nat. Rev. Drug Discov.* **10,** 507–519 (2011).
3. Wagner, B. K. The resurgence of phenotypic screening in drug discovery and development. *Expert Opin. Drug Discov.* 1–5 (2015). doi:10.1517/17460441.2016.1122589
4. Carmeliet, P. Angiogenesis in health and disease. *Nat. Med.* **9,** 653–660 (2003).
5. Distler, J. H. W. *et al.* Angiogenic and angiostatic factors in the molecular control of angiogenesis. *Q. J. Nucl. Med. Off. Publ. Ital. Assoc. Nucl. Med. AIMN Int. Assoc. Radiopharmacol. IAR* **47,** 149–161 (2003).
6. Folkman, J. Tumor angiogenesis: therapeutic implications. *N. Engl. J. Med.* **285,** 1182–1186 (1971).
7. Boehm, T., Folkman, J., Browder, T. & O'Reilly, M. S. Antiangiogenic therapy of experimental cancer does not induce acquired drug resistance. *Nature* **390,** 404–407 (1997).
8. Abdollahi, A. & Folkman, J. Evading tumor evasion: current concepts and perspectives of anti-angiogenic cancer therapy. *Drug Resist. Updat. Rev. Comment. Antimicrob. Anticancer Chemother.* **13,** 16–28 (2010).
9. Grothey, A. & Galanis, E. Targeting angiogenesis: progress with anti-VEGF treatment with large molecules. *Nat. Rev. Clin. Oncol.* **6,** 507–518 (2009).
10. Fala, L. Cyramza (Ramucirumab) Approved for the Treatment of Advanced Gastric Cancer and Metastatic Non-Small-Cell Lung Cancer. *Am. Health Drug Benefits* **8,** 49–53 (2015).
11. Holash, J. *et al.* VEGF-Trap: a VEGF blocker with potent antitumor effects. *Proc. Natl. Acad. Sci. U. S. A.* **99,** 11393–11398 (2002).

12. Bergers, G. & Hanahan, D. Modes of resistance to anti-angiogenic therapy. *Nat. Rev. Cancer* **8,** 592–603 (2008).

13. Chong, C. R. *et al*. Inhibition of angiogenesis by the antifungal drug itraconazole. *ACS Chem. Biol*. **2,** 263–270 (2007).

14. Aftab, B. T., Dobromilskaya, I., Liu, J. O. & Rudin, C. M. Itraconazole inhibits angiogenesis and tumor growth in non-small cell lung cancer. *Cancer Res*. **71,** 6764–6772 (2011).

15. Kim, J. *et al*. Itraconazole, a commonly used antifungal that inhibits Hedgehog pathway activity and cancer growth. *Cancer Cell* **17,** 388–399 (2010).

16. Rubin, L. L. & de Sauvage, F. J. Targeting the Hedgehog pathway in cancer. *Nat. Rev. Drug Discov*. **5,** 1026–1033 (2006).

17. Antonarakis, E. S. *et al*. Repurposing itraconazole as a treatment for advanced prostate cancer: a noncomparative randomized phase II trial in men with metastatic castration-resistant prostate cancer. *The Oncologist* **18,** 163–173 (2013).

18. Rudin, C. M. *et al*. Phase 2 Study of Pemetrexed and Itraconazole as Second-Line Therapy for Metastatic Non-Squamous Non-Small Cell Lung Cancer. *J. Thorac. Oncol. Off. Publ. Int. Assoc. Study Lung Cancer* **8,** 619–623 (2013).

19. Kim, D. J. *et al*. Open-Label, Exploratory Phase II Trial of Oral Itraconazole for the Treatment of Basal Cell Carcinoma. *J. Clin. Oncol*. **32,** 745–751 (2014).

20. Vreugdenhil, G., Raemaekers, J. M., van Dijke, B. J. & de Pauw, B. E. Itraconazole and multidrug resistance: possible effects on remission rate and disease-free survival in acute leukemia. *Ann. Hematol*. **67,** 107–109 (1993).

21. Suzman, D. L. & Antonarakis, E. S. High-Dose Itraconazole As a Noncastrating Therapy for a Patient With Biochemically Recurrent Prostate Cancer. *Clin. Genitourin. Cancer* **12,** e51–e53 (2014).

22. Lockhart, N. R., Waddell, J. A. & Schrock, N. E. Itraconazole therapy in a pancreatic adenocarcinoma patient: A case report. *J. Oncol. Pharm. Pract. Off. Publ. Int. Soc. Oncol. Pharm. Pract.* (2015). doi:10.1177/1078155215572931

23. Cooper, S. M., Sheridan, A. & Burge, S. Mycosis fungoides responding to systemic itraconazole. *J. Eur. Acad. Dermatol. Venereol. JEADV* **17,** 588–590 (2003).

24. Ran, Y. *et al*. Successful treatment of oral itraconazole for infantile hemangiomas: A case series. *J. Dermatol.* **42,** 202–206 (2015).

25. Tsubamoto, H., Sonoda, T., Yamasaki, M. & Inoue, K. Impact of combination chemotherapy with itraconazole on survival for patients with recurrent or persistent ovarian clear cell carcinoma. *Anticancer Res.* **34,** 2007–2014 (2014).

26. Tsubamoto, H., Sonoda, T., Yamasaki, M. & Inoue, K. Impact of combination chemotherapy with itraconazole on survival of patients with refractory ovarian cancer. *Anticancer Res.* **34,** 2481–2487 (2014).

27. Tsubamoto, H., Sonoda, T. & Inoue, K. Impact of itraconazole on the survival of heavily pre-treated patients with triple-negative breast cancer. *Anticancer Res.* **34,** 3839–3844 (2014).

28. Tsubamoto, H. *et al*. Combination Chemotherapy with Itraconazole for Treating Metastatic Pancreatic Cancer in the Second-line or Additional Setting. *Anticancer Res.* **35,** 4191–4196 (2015).

29. Tsubamoto, H. *et al*. Impact of Itraconazole After First-line Chemotherapy on Survival of Patients with Metastatic Biliary Tract Cancer. *Anticancer Res.* **35,** 4923–4927 (2015).

30. Shim, J. S. *et al*. Divergence of Anti-angiogenic Activity and Hepatotoxicity of Different Stereoisomers of Itraconazole. *Clin. Cancer Res. Off. J. Am. Assoc. Cancer Res.* (2016). doi:10.1158/1078-0432.CCR-15-1888

31. Hitchcock, C. A. Cytochrome P-450-dependent 14 alpha-sterol demethylase of Candida albicans and its interaction with azole antifungals. *Biochem. Soc. Trans.* **19,** 782–787 (1991).

32. Lamb, D. C. *et al*. Purification, Reconstitution, and Inhibition of Cytochrome P-450 Sterol Δ22-Desaturase from the Pathogenic Fungus Candida glabrata. *Antimicrob. Agents Chemother*. **43,** 1725–1728 (1999).

33. Trösken, E. R. *et al*. Comparison of lanosterol-14α-demethylase (CYP51) of human and Candida albicans for inhibition by different antifungal azoles. *Toxicology* **228,** 24–32 (2006).

34. Shi, W., Nacev, B. A., Bhat, S. & Liu, J. O. Impact of Absolute Stereochemistry on the Antiangiogenic and Antifungal Activities of Itraconazole. *ACS Med. Chem. Lett*. **1,** 155–159 (2010).

35. Head, S. A. *et al*. Antifungal drug itraconazole targets VDAC1 to modulate the AMPK/mTOR signaling axis in endothelial cells. *Proc. Natl. Acad. Sci. U. S. A*. **112,** E7276–7285 (2015).

36. Xu, J., Dang, Y., Ren, Y. R. & Liu, J. O. Cholesterol trafficking is required for mTOR activation in endothelial cells. *Proc. Natl. Acad. Sci. U. S. A*. **107,** 4764–4769 (2010).

37. Nourse, J. *et al*. Interleukin-2-mediated elimination of the p27Kip1 cyclin-dependent kinase inhibitor prevented by rapamycin. *Nature* **372,** 570–573 (1994).

38. Guba, M. *et al*. Rapamycin inhibits primary and metastatic tumor growth by antiangiogenesis: involvement of vascular endothelial growth factor. *Nat. Med*. **8,** 128–135 (2002).

39. Nacev, B. A., Grassi, P., Dell, A., Haslam, S. M. & Liu, J. O. The antifungal drug itraconazole inhibits vascular endothelial growth factor receptor 2 (VEGFR2) glycosylation, trafficking, and signaling in endothelial cells. *J. Biol. Chem*. **286,** 44045–44056 (2011).

40. Niño, D. F., Cauvi, D. M. & De Maio, A. Itraconazole, a commonly used antifungal, inhibits Fcγ receptor-mediated phagocytosis: alteration of Fcγ receptor glycosylation and gene expression. *Shock Augusta Ga* **42,** 52–59 (2014).

41. Frey, T. & De Maio, A. The antifungal agent itraconazole induces the accumulation of high mannose glycoproteins in macrophages. *J. Biol. Chem*. **284,** 16882–16890 (2009).

42. Shi, W. *et al*. Itraconazole Side Chain Analogues: Structure–Activity Relationship Studies for Inhibition of Endothelial Cell Proliferation, Vascular Endothelial Growth Factor Receptor 2 (VEGFR2) Glycosylation, and Hedgehog Signaling. *J. Med. Chem*. **54,** 7363–7374 (2011).

43. Titov, D. V. & Liu, J. O. Identification and validation of protein targets of bioactive small molecules. *Bioorg. Med. Chem*. **20,** 1902–1909 (2012).

Chapter 2: VDAC1 as a Direct Target of Itraconazole and Mediator of AMPK Activation in Endothelial Cells[1]

2.1: Abstract

Itraconazole, a clinically used antifungal drug, was found to possess potent antiangiogenic and anticancer activity that is unique among the azole antifungals. Previous mechanistic studies have shown that itraconazole inhibits the mechanistic target of rapamycin (mTOR) signaling pathway, which is known to be a critical regulator of endothelial cell function and angiogenesis. However, the molecular target of itraconazole that mediates this activity has remained unknown. In this chapter, I describe the identification of the major binding protein of itraconazole in endothelial cells as the mitochondrial protein voltage-dependent anion channel 1 (VDAC1), which regulates mitochondrial metabolism by controlling the passage of ions and small metabolites through the outer mitochondrial membrane. VDAC1 knockdown profoundly inhibits mTOR activity and cell proliferation in primary human umbilical vein endothelial cells (HUVEC), uncovering a previously unknown connection between VDAC1 and mTOR. Inhibition of VDAC1 by itraconazole disrupts mitochondrial metabolism, leading to an increase in the cellular AMP:ATP ratio and activation of the AMP-activated protein kinase (AMPK), an upstream regulator of mTOR. VDAC1-knockout cells are resistant to

[1] The following chapter is adapted from Head, S. A. *et al.* Antifungal drug itraconazole targets VDAC1 to modulate the AMPK/mTOR signaling axis in endothelial cells. *Proc. Natl. Acad. Sci. U.S.A.* **112,** E7276–7285 (2015).

AMPK activation and mTOR inhibition by itraconazole, demonstrating that VDAC1 is the mediator of this activity. In addition, another known VDAC-targeting compound, erastin, also activates AMPK and inhibits mTOR and proliferation in HUVEC. VDAC1 thus represents a novel upstream regulator of mTOR signaling in endothelial cells and a promising target for the development of angiogenesis inhibitors.

ABBREVIATIONS

14DM, lanosterol 14-α-demethylase; 2DG, 2-deoxyglucose; ABKAR, AMPK and BRSK kinase activity reporter; ACC, acetyl coA carboxylase; AMPK, AMP-activated protein kinase; AXP, adenine nucleotides (AMP/ADP/ATP); CPT2, carnitine palmitoyltransferase 2; DMSO, dimethyl sulfoxide; FRET, fluorescence resonance energy transfer; GAPDH, glyceraldehyde 3-phosphate dehydrogenase; HUVEC, human umbilical vein endothelial cells; IC50, 50% inhibitory concentration; Itra, itraconazole; JHDL, Johns Hopkins Drug Library; MEF, mouse embryonic fibroblast; mEH, microsomal epoxide hydrolase; MS, mass spectroscopy; mTOR, mechanistic target of rapamycin; NPC, Niemann-Pick type C; Raptor, regulatory associated protein of TOR; S6K, ribosomal protein S6 kinase; TD-itra, triazole deleted itraconazole; TSC2, tuberous sclerosis complex 2; VDAC, voltage-dependent anion channel; VEGF, vascular endothelial growth factor; VEGFR2, vascular endothelial growth factor receptor 2.

2.2: Introduction

Angiogenesis, or the formation of new blood vessels from preexisting vasculature, is a critical process both in normal development and in the pathogenesis of a myriad of diseases. In particular, it has long been recognized that angiogenesis is required for tumor growth and metastasis, and growing tumors can promote angiogenesis by secreting pro-angiogenic factors, such as VEGF, bFGF, EGF, and others[1,2]. These pro-angiogenic factors stimulate the proliferation, migration, and differentiation of the endothelial cells that make up the inner layer of all blood vessels, causing them to form new vessels that grow toward the source of these factors. This process, termed tumor angiogenesis, allows the tumor to keep up with an increasing demand for oxygen and nutrients as it grows, eliminate accumulating waste products, and shed cancerous cells into circulation leading to metastasis. Without angiogenesis, a tumor cannot grow larger than about 1-2 mm in diameter, the largest size at which nutrients can permeate by diffusion alone, and is thus rendered essentially harmless to the host[3]. Inhibition of angiogenesis is emerging as a useful strategy for treating cancer. The discovery and development of angiogenesis inhibitors as novel therapeutics for cancer has culminated in the FDA approval of a few antiangiogenic drugs. Bevacizumab (Avastin), a monoclonal antibody targeting VEGF, gained FDA approval for the treatment of metastatic colorectal cancer[4,5]. Pegaptanib (Macugen), a polynucleotide-based aptamer targeting VEGF[6], has also been approved by the FDA for the treatment of age-dependent macular degeneration. More recently, several kinase inhibitors, including sorafenib, sunitinib, pazopanib and everolimus, that have a major, albeit non-specific, effect on angiogenesis have also entered the clinic[7].

Drug discovery and development is a time-consuming and costly process. The

discovery and development of anti-angiogenic drugs is no exception. To accelerate the process, our lab began a new initiative to collect known drugs and assemble them into what is now known as the Johns Hopkins Drug Library (JHDL). Screening of JHDL using an endothelial cell proliferation assay led to the discovery of a number of hits. Among the novel and most interesting hits is the antifungal drug itraconazole[8]. Itraconazole potently inhibits endothelial cell proliferation with an IC_{50} value (ca. 200 nM) that is significantly below its peak plasma levels (> 2 μM)[9], suggesting that it is likely to have antiangiogenic activity under existing drug administration regimens. It also displays high cell type selectivity, being most potent against primary human endothelial cells in comparison to human foreskin fibroblasts and most human cancer cell lines. Moreover, it is over 30-fold more potent than other members of the azole family of antifungal drugs, including ketoconazole and terconazole[8].

Itraconazole was originally developed as an antifungal drug, and has been used clinically for over 30 years with a well-established safety record. Upon validation of its antiangiogenic and antitumor activity in a number of models both *in vitro* and *in vivo*[8,10,11], it entered multiple phase 2 clinical trials for treating cancer. To date, the pilot trials in non-small cell lung cancer, prostate cancer, and basal cell carcinoma have been completed; itraconazole has been shown to increase the progression-free and overall survivals of patients taking the drug[12–14]. Thus, itraconazole has great potential in becoming a new drug to treat cancer and other angiogenesis-dependent diseases such as macular degeneration and diabetic retinopathy.

Despite these promising clinical results, the mechanism of angiogenesis inhibition by itraconazole has remained largely unknown. Like other azole-containing antifungal

drugs, itraconazole exerts its antifungal activity by inhibiting the CYP450 enzyme lanosterol 14-α demethylase (14DM), which is required for synthesis of the lipid ergosterol that maintains cell wall integrity in these organisms. However, the potency of itraconazole against human 14DM has been shown to be greatly reduced as compared to the fungal enzyme[15,16]. Moreover, itraconazole is unique among this class of antifungal drugs in its antiangiogenic activity, including those which are more potent inhibitors of human 14DM[8]. Taken together, these lines of evidence strongly suggest that 14DM inhibition cannot explain the antiangiogenic activity of itraconazole.

In an attempt to identify cellular pathways affected by itraconazole, we found that the mechanistic target of rapamycin (mTOR) signaling pathway, which regulates cell proliferation and is known to be required for angiogenesis, is potently inhibited by itraconazole at concentrations similar to those required for proliferation inhibition[17]. This mTOR inhibitory activity is also more potent in endothelial cells, both primary and immortalized, as compared with other common cell lines such as HEK-293T and HeLa. We found that inhibition of mTOR was mediated, only in part, by inhibition of cholesterol trafficking through the endolysosome, leaving unanswered the question of what is the direct molecular target of itraconazole.

In this chapter, I describe the use of a photoaffinity probe of itraconazole to isolate and identify its binding proteins from live endothelial cells. Importantly, the probe retained full activity in endothelial cells, indicating that it binds to the same target proteins as itraconazole itself. Using a combination of affinity pull-down and mass spectrometry, VDAC1 was identified as a primary binding protein of itraconazole. I demonstrate that itraconazole not only directly binds to VDAC1, but also interferes with

its primary cellular function of regulating mitochondrial metabolism, causing a drop in cellular energy levels that triggers the energy-sensing protein AMP-activated protein kinase (AMPK). Subsequently, AMPK downregulates mTOR activity through direct phosphorylation of the regulatory-associated protein of mTOR (raptor), ultimately leading to inhibition of endothelial cell proliferation.

2.3: Materials and Methods

Reagents and antibodies

Itraconazole was purchased from TCI Chemicals (I0732; Philadelphia, PA). Erastin (E7781) and Ionomycin (I9657) were from Sigma-Aldrich (St Louis, MO). 2DG was from LKT laboratories (D1859; St. Paul, MN). STO-609 was from Enzo Life Sciences (BML-EI389; Farmingdale, NY). Alexa Fluor 647-azide (A10277), TCEP (20490) and High Capacity Streptavidin Agarose beads (20359) were from Life Technologies (Grand Island, NY). Biotin-azide was from Click Chemistry Tools (AZ104-100; Scottsdale, AZ). TBTA was from Anaspec (63360-50; Fremont, CA). Copper Sulfate was from LabChem Inc (LC13440-1; Pittsburgh, PA). A769662 was from Abcam (ab120335; Cambridge, MA). Compound C was from Calbiochem (171261; San Diego, California). Antibodies against AMPKα (2532), phospho-AMPKα Thr172 (2535), ACC (3676), phospho-ACC Ser79 (3661), phospho-p70 S6K Thr389 (9205), raptor (2280), phospho-raptor Ser792 (2083), TSC2 (3990), phospho-TSC2 Ser1387 (5584) and AMPKγ2 (2536) were from Cell Signaling Technologies (Danvers, MA). Antibodies against p70 S6K (sc-8418), GAPDH (sc-20357), Tubulin (sc-5286), VDAC1 (sc-58649), and Tom 40 (sc-11414) were from Santa Cruz Biotechnologies (Santa Cruz, CA). The antibody against 14DM was from Proteintech (13431-1-AP; Chicago, IL). The antibody against AMPKγ1 was from Abcam (ab32382; Cambridge, MA). DOPC and DOPE were from Avanti Polar Lipids, Inc. (Alabaster, AL).

Synthesis of itraconazole probe and triazole-deleted itraconazole

The itraconazole photoaffinity probe was synthesized by Dr. Wei Shi, and the triazole-deleted itraconazole was synthesized by Dr. Kalyan Kumar, both former Liu lab

members. The details of these syntheses have been published[18].

Cell culture

Primary HUVEC pooled from 4 donors (Lonza) were cultured in complete EGM-2 (Lonza) and subcultured every 2 days at a density of 1:4, or 3 days at 1:8, and discarded after passage 8. HEK 293T, HeLa, and A549 were cultured in low glucose DMEM (Gibco; Gaithersburg, MD) supplemented with 10% filtered FBS (Gibco) and 1% penicillin/streptomycin (Gibco). VDAC1 wild-type and knockout MEFs were generated as previously reported[19] and cultured in high glucose DMEM supplemented with 10% filtered FBS and 1% penicillin/streptomycin. All cells were cultured at 37°C with 5% CO_2.

Photoaffinity labeling

Photoaffinity labeling was performed according to the protocol of MacKinnon and Taunton, with modifications[20]. Cells were seeded into 6-cm dishes in 4 mL of culture media to achieve near complete confluence after settling overnight. Cells were pre-treated with competitor (as noted in text) or an equal volume of DMSO vehicle for 30 min, before addition of 200 nM probe or DMSO, with a final DMSO concentration in all samples of 0.5%. After a 1-h incubation with the probe, the dishes were placed on ice. Cells were washed 1x with 5 mL ice-cold PBS (pH 7.4) to remove excess probe, and re-covered with 4 mL ice-cold PBS before being placed 3 cm under a Spectroline FC100 365 nm UV lamp (Westbury, NY) for 3 min on top of an ice pack to minimize heating from the lamp. After irradiation, the PBS was aspirated completely and 200 μL of ice-cold PBS (pH 8.5) containing protease inhibitor cocktail (Roche Life Science, Indianapolis, IN) was added to the dish. Cells were removed from the dish by scraping

and transferred to an Eppendorf tube kept on ice, and SDS was added to a final concentration of 0.4%. The cell suspension was then sonicated for 10 pulses using a Branson Sonifier 250 (Danbury, CT) set to output 1, duty cycle 30%, and incubated on ice for 1 min before a second round of 10 pulses. After sonication, samples were incubated at 95°C for 5 min to complete cell lysis and denature all of the proteins. The concentration of total proteins in the lysate was then measured by the detergent compatible (Dc) protein assay kit (BioRad, Hercules, CA), and normalized to 2.5 mg/mL (or in the case of HUVEC, the highest concentration possible). For the click reaction with fluor-azide, 40 µL of lysate was removed and transferred to a new tube, and 0.2 µL Alexa Fluor 647 azide (1 mM stock solution in DMSO), 0.58 µL TCEP (100 mM stock with 4 equivalents NaOH added), 3.38 µL TBTA (1.7 mM stock in 4:1 t-butanol:DMSO) were added sequentially and vortexed to mix. $CuSO_4$-$5H_2O$ (1.14 µL, 50 mM stock in water) was then added to start the reaction. The samples were briefly vortexed again and incubated at room temperature for 30 min in the dark. Aliquots of 50 µL 2X SDS sample buffer were then added and samples subjected to SDS-PAGE before being scanned on a Typhoon FLA 9500 gel scanner (GE Healthcare Life Sciences; Piscataway Township, NJ) using a red excitation laser. For the click reaction with biotin-azide, the maximum amount of lysate obtained after protein normalization was used, and 1.38 µL biotin-azide (10 mM stock in DMSO), 5.5 µL TCEP, 32.5 µL TBTA, and 11 µL $CuSO_4$-$5H_2O$ were added per 500 µL of lysate. The samples were vortexed and incubated at room temperature for 30 min, after which time 4 volumes of cooled acetone (-20 °C) were added to the lysate to precipitate the proteins, and samples were incubated overnight at -80 °C. The precipitated proteins were pelleted by centrifugation at 17,000 x g for 15 min

at 4 °C. The supernatant was aspirated completely. The pellet was then completely resuspended by sonication in 150 μL PBS containing 1% SDS, after which 600 μL of PBS was added to dilute the SDS to 0.2%. The lysates were then added to 30-40 μL high capacity streptavidin agarose beads pre-washed 2x in PBS, and incubated with rotation at 4 °C for 1 h. The beads were collected by centrifugation at 800 x g at room temperature for 3 min, and washed 3x with wash buffer (400 mM NaCl, 50 mM Tris, 0.2% SDS, pH 7.4) for 5 min each with rotation at room temperature. After the final wash, beads were boiled in 40 μL 2X SDS sample buffer, and subjected to SDS-PAGE before silver staining or transfer to nitrocellulose membranes for Western blot.

Target identification by MS

Silver stained SDS-PAGE bands were cut out and destained with the SilverQuest kit following the manufacture's protocol (Thermofisher Inc., Waltham, MA). Each gel band was then cut into small pieces and placed in a 1.5 ml Eppendorf tube. The gel pieces were washed with water for 1 hour and then with 25 mM ammonium bicarbonate solution in 50% acetonitrile for 10 min. The sample was dehydrated by 100% acetonitrile and dried in a SpeedVac (Thermofisher Inc.). Sequencing-grade trypsin (Promega, Madison, WI) was reconstituted in 50 mM ammonium bicarbonate solution and added to the sample for overnight digestion at 37 °C. The tryptic peptides were extracted from the gel pieces with sequential wash in 50% acetonitrile and 100% acetonitrile, respectively. The solution from both extractions were pooled and dried by SpeedVac. The sample was then desalted with a C18 Ziptip following the manufacturer's protocol (Millipore Inc., Billerica, MA). The tryptic peptides were dissolved in HPLC buffer A (0.1% formic acid in water) and then manually injected into the LCMS system with Eksigent 1D plus nano

HPLC (AB Sciex Inc., Framingham, MA) and LTQ Orbitrap Velos mass spectrometer (Thermofisher Inc.). The peptides were analyzed on an in-house packed capillary C18 column (75 μm ID and 10 cm in length, 3 μm C18 beads (Dr. Maisch Inc., Ammerbuch, Germany)) using a linear gradient of 5-30% HPLC buffer B (0.1% formic acid in acetonitrile) for 60 minutes at 200 nL/min. The data were analyzed by Mascot v2.1 (Matrix Science, London, UK) for protein identification with a default p-value cutoff of 0.05. Identified peptides were manually evaluated to remove false positive identifications.

Western blot

Cells (100,000/well in 2 mL media) were seeded in 6-well plates 24 h before drug treatment. Drugs were then added to each well from 200x DMSO stock solutions (final DMSO concentration of 0.5%), and incubated for the indicated times. Plates were then placed on ice and washed once with ice-cold PBS before addition of 2X Laemmli sample buffer directly to the cells. Lysates were collected after 10 min and incubated for 5 min at 95°C before being subjected to SDS-PAGE. Proteins were then transferred to nitrocellulose membranes (Bio-Rad) and stained with ponceau to confirm the quality of protein transfer and equal loading of samples. Membranes were then incubated in 5% w/v blotto (Santa Cruz Biotechnologies) dissolved in TBS containing 0.05% Tween-20 (TBST) for 1 h at room temperature before overnight incubation with primary antibodies at 4 °C. Membranes were washed 3 times for 5 min each with TBST, and then incubated with HRP-conjugated secondary antibodies (GE healthcare) diluted in 5% blotto/TBST for 1 h at room temperature. Membranes were then washed another 3 times for 5 min with TBST before the immune complexes were detected with Chemiluminescent ECL

substrate (Millipore) on a Kodak Image Station (440CF). Band intensity was quantified using ImageJ.

VDAC1/2/3-V5 expression plasmids

VDAC1 and VDAC2 expression plasmids in pLX304 backbone and VDAC3 entry clone in pENTR223 backbone were provided by The ORFeome Collaboration[21], (PlasmID clone IDs HsCD00420021, HsCD00421586, and HsCD00370222; PMIDs 21706014 and 154893350). Storage and distribution provided by the PlasmID Repository at Harvard Medical School and funded in part by NCI Cancer Center Support Grant #NIH 5 P30 CA06516. The VDAC3 expression plasmid was obtained by Gateway recombination of the entry clone into the pEF-DEST51 destination vector (Invitrogen, Carlsbad, CA).

Thymidine incorporation assay

HUVEC or MEFs were seeded in 96-well plates (Costar, Corning, NY) at a density of 2000/well and allowed to attach overnight. Drugs were serially diluted in DMSO at 200x final concentrations (0.5% DMSO), then diluted in media before addition to the cells. Cells were incubated with drugs for 24 hours before addition of 1μCi per well of [^{3}H]-labeled thymidine (American Radiolabeled Chemicals, St. Louis, MO) for a further 6 hours. Cells were then harvested onto glass fiber filters (PerkinElmer, Norwalk, CT) using a Mach III M Harvester 96 (Tomtec Inc., Hamden, CT). Filters were dried overnight before being sealed in sample bags with 4 mL of Betaplate Scint scintillation fluid (PerkinElmer), and then scintillation was counted using a 1450 Microbeta apparatus (PerkinElmer). The counts-per-minute (CPM) of drug-treated cells were normalized to control cells treated with DMSO alone. Drug dose-response curves and IC_{50} values were

generated using GraphPad Prism 5 software.

shRNA plasmids

Short hairpins were designed targeting two non-overlapping sequences within the coding region of human VDAC1, mEH, and CPT2. Complimentary sets of page-purified oligonucleotides were ordered from IDT technologies, and the sequences are shown in **Table 2.1**. Forward and reverse primers were annealed and ligated into the lentiviral vector pSicoR digested with HpaI/XhoI, before being confirmed by sequencing.

Table 2.1: shRNA primers

Primer	**Sequence (5'→3')**
CPT2sh1+	TTGGGACTAGATCACAACTGAATTCAAGAGATTCAGTTGTGATCTAGTCCCATTTTTTC
CPT2sh1-	TCGAGAAAAAATGGGACTAGATCACAACTGAATCTCTTGAATTCAGTTGTGATCTAGTCCCAA
CPT2sh2+	TCAGCTACAGGCTTGAGCTTTATTCAAGAGATAAAGCTCAAGCCTGTAGCTGTTTTTTC
CPT2sh2-	TCGAGAAAAAACAGCTACAGGCTTGAGCTTTATCTCTTGAATAAAGCTCAAGCCTGTAGCTGA
VDAC1sh1+	TCACTAGGCACCGAGATTATTTCAAGAGAATAATCTCGGTGCCTAGTGTTTTTTC
VDAC1sh1-	TCGAGAAAAAACACTAGGCACCGAGATTATTCTCTTGAAATAATCTCGGTGCCTAGTGA
VDAC1sh2+	TGTGACGGGCAGTCTGGAATTTCAAGAGAATTCCAGACTGCCCGTCACTTTTTTC
VDAC1sh2-	TCGAGAAAAAAGTGACGGGCAGTCTGGAATTCTCTTGAAATTCCAGACTGCCCGTCACA
EPHX1sh5+	TCAACATGGCTTTGATGATAAATTCAAGAGATTTATCATCAAAGCCATGTTGTTTTTTC
EPHX1sh5-	TCGAGAAAAAACAACATGGCTTTGATGATAAATCTCTTGAATTTATCATCAAAGCCATGTTGA
EPHX1sh8+	TATGTGGCTAGAAATCCTCTTCAAGAGAGAGGATTTCTAGCCACATTTTTTTC
EPHX1sh8-	TCGAGAAAAAAATGTGGCTAGAAATCCTCTCTCTTGAAGAGGATTTCTAGCCACATA

Adenine nucleotide extraction

AXP were extracted by the hot methanol method described by Shryock et. al[24]. HUVEC were plated in 10-cm dishes at a density of 700k/dish and allowed to settle

overnight. Cells were treated with DMSO or drugs as indicated, with a final DMSO concentration of 0.5%. After drug treatment, the cells were washed twice with 10 mL of PBS, before the addition of 1 mL of extractant (80% methanol with 0.5 mM EGTA) preheated to 70°C. Cells were scraped immediately from the plate, transferred to an ice-cold microcentrifuge tube, and centrifuged for 5 min at 1000 x g at 4°C to pellet precipitated matter. The supernatants were then transferred to a new ice-cold tube, dried by Speedvac, and stored at -20°C until immediately before analysis. The extracts were then reconstituted in 100 µL 50% acetonitrile, and centrifuged at 14,000 x g for 5 min at 4°C before supernatants were taken for analysis.

AMP/ATP analysis by LC-MS/MS

AMP and ATP analysis were performed on an Agilent 6490 triple quadrupole LC-MS/MS system with iFunnel and Jet-Stream® technology (AgilentTechnologies, Santa Clara, CA) equipped with an Agilent 1260 infinity pump and autosampler. Chromatographic separation was performed on a Diamond Hydride column (150mm x 2.1 mm i.d., 4µm particle size, Microsolv, Eatontown, NJ). The LC parameters were as follows: autosampler temperature, 4°C; injection volume, 4 µl; column temperature, 35°C; and flow rate, 0.4 ml/min. The solvents and optimized gradient conditions for LC were: Solvent A, water with 5mM ammonium acetate, pH=7.2; Solvent B, 90% acetonitrile with 10mM ammonium acetate, pH=6.5; elution gradient: 0 min 95% B; 15–20 min 25% B; post-run time for equilibration, 5 min in 95% B. MS was operated in positive-ion electrospray mode (unit resolution) with all analytes monitored by SRM. AMP was monitored by the transition of 348→136 (collision energy: 23ev). ADP was monitored by the transition of 428→136 (collision energy: 30ev). ATP was monitored by

the transition of 508→136 (collision energy: 35ev). Compound identity was confirmed by comparison to the retention times of pure standards. The optimized operating ESI conditions were: gas temperature 230°C (nitrogen); gas flow 15 L/min; nebulizer pressure 40 psi; sheath gas temperature 350°C and sheath gas flow 12 L/min. Capillary voltages were optimized to 4000V in positive mode with nozzle voltages of 2000 V. The iFunnel parameters were: 130V for high pressure RF and 80V for low pressure RF. All data processing was performed with Mass Hunter Quantitative Analysis software package.

Lentivirus production

Lentivirus was produced using the second generation system developed by the laboratory of Didier Trono[25]. HEK293T cells were plated 2.0 x 10^7 in a 15-cm dish and allowed to settle overnight. Each dish was co-transfected with 9 μg lentiviral expression vector, 6 μg of the packaging vector psPAX2, and 3 μg of the envelope vector pMD2.G, using 45 μL of Lipofectamine 2000 (Life Technologies). The culture media was harvested 48 hours later and virus particles were concentrated by ultracentrifugation at 25,000 rpm (~100,000 x g) for 2.5 hours using a Beckman Optima LE-80k ultracentrifuge (Beckman Coulter, Fullerton, CA) and a Beckman SW-28 rotor, before being resuspended in EGM-2 media and aliquoted into 4 cryotubes stored at -80°C. One tube of virus was used to transduce 100,000 HUVEC, and experiments were performed 2-5 days later.

FRET imaging

The generation of ABKAR was previously described[26,27] and the construct was verified by sequencing. HUVEC were nucleofected with ABKAR using a nucleofection

kit from Lonza (VAPB-1002; Walkersville, MD) according to the manufacturer's protocol, and plated into 35-mm glass bottom dishes to 50-70% confluence. Cells were imaged 24 h after nucleofection. Itraconazole and 2-deoxyglucose were added directly to the culture media as indicated. Images were acquired using a Zeiss Axiovert 200M inverted fluorescence microscope (Carl Zeiss, Thornwood, NY) with a 40x/1.3 NA oil-immersion objective lens and a cooled charge-coupled device camera (Roper Scientific, Trenton, NJ) controlled by Metafluor 7.7 software (Molecular Devices, Sunnyvale, CA). Dual cyan/yellow emission ratio imaging was performed using a 420DF20 excitation filter, a 450DRLP dichroic mirror, and two emission filters (475DF40 for CFP and 535DF25 for YFP). Filter sets were alternated using a Lambda 10–2 filter changer (Sutter Instruments, Novato, CA). Exposure time was set to 500 ms, and images were taken every 30-180 s. Raw fluorescence images were corrected by subtracting the background fluorescence intensity of a cell-free region from the emission intensities of biosensor expressing cells. Emission ratios (yellow/cyan or cyan/yellow) were then calculated at each time point. All time-courses were normalized by dividing the emission ratio at each time point by the basal value immediately preceding drug addition.

Fatty acid oxidation assay

300,000 HUVEC were seed in T25 flasks (~80% confluent) in 5 mL fresh EGM-2, along with 2 control flasks containing media only. ^{14}C oleic acid (1 μL/sample) was added to pre-warmed media (0.5 mL/sample) containing 1% BSA + 100 μM carnitine and incubated in a 37°C water bath for 1 h. During this hour, cells were pretreated with drug or DMSO. The oleic acid mixture was then added to each flask (0.5 mL/sample), the flasks were sealed with a rubber stopper containing a piece of folded filter paper to catch

the $^{14}CO_2$ produced, and returned to the culture incubator for 6 h. The reaction was quenched by injection of 200 µL 1M perchloric acid through the stopper into the media, and 200 µL 1M NaOH was injected onto the filter paper. The flasks were then incubated at 60°C for 1 h, after which time the stoppers were removed from the flasks in a fume hood and the filter paper was moved to a vial for scintillation counting.

Mitochondrial swelling assay

Mitochondria were isolated from livers of male Sprauge-Dawley rats according to a previously published protocol[28]. Mitochondria were diluted to a final protein concentration of 250 µg/mL into H-buffer (70 mM sucrose, 210 mM mannitol, 0.1 mM EGTA, 5.0 mM HEPES, pH 7.5) plus 5 mM phosphate buffer, pH 7.4, in a 3 mL volume in a glass test tube pre-washed in H-buffer. Diluted mitochondria were then gently vortexed during the addition of 3 µL DMSO or 1000x drug stock (0.1% DMSO final concentration) to ensure adequate mixing of the drug and mitochondria. The samples were transferred to a quartz cuvette containing a mini stir bar and placed into a CHEMUSB4-UV-VIS spectrophotometer (Ocean Optics, Dunedin, FL) on top of a stir plate, and baseline absorbance at 400 nm was recorded for 5 min before the addition of 400 µL 1 mM $CaCl_2$ diluted in H-buffer. Traces of absorbance vs. time were plotted in Microsoft Excel and the maximum rate of swelling during a 10-second interval shortly after calcium addition was calculated using the linear fitting function.

VDAC purification and planar lipid bilayer electrophysiology

VDAC channels were purified from rat liver mitochondria[29] and channel experiments were conducted as previously described[30]. All experiments were performed in the laboratory of Drs. Sergei Bezrukov and Tatiana Rostovtseva at the National

Institutes of Health using custom equipment. Purified channels were reconstituted in a planar bilayer made up of the lipids DOPC and DOPE in a 1:1 mixture. Membranes were formed across a hole of 2 divisions in diameter in the partition separating cis and trans compartments, and hexadecane was used to coat the hole prior to membrane formation. Multichannel experiments were performed using a triangular wave of voltage between +/- 60 mV and with a frequency of 5 mHz. For single channel recordings, a constant voltage was applied either in 5 sec pulses or continuously until channel closure was achieved. Channel recordings were filtered with 500 Hz Bessel filter. Single channel experiments in the presence of tubulin were performed at voltages between 15-30 mV and pH 7.4, and single channel experiments in the absence of tubulin were performed at 50-60 mV and pH 6. Itraconazole was added to both sides of the membrane from DMSO stock solutions in final concentrations between 500 nM-10 μM as indicated. The final concentration of DMSO was always ≤0.2%.

2.4: Results

Design of a photoaffinity probe of itraconazole that retains full cellular activity

In order to identify molecular target(s) of itraconazole, we turned to a live-cell photoaffinity labeling approach, which allows capture of drug-binding proteins in their native environment and unbiased target identification by mass spectrometry. For this approach to be successful, a probe must be designed that can bind to the same target proteins and induce the same effects as the parent drug with a similar potency. Our previous studies on all eight individual stereoisomers of itraconazole revealed that the stereochemistry in the *sec*-butyl side chain is least important for the growth inhibition of HUVEC[31]. Therefore, we speculated that the alkyl group attached to the triazolone ring might be a suitable position for derivatization to make a chemical probe for target identification. Further elaborated structure–activity relationship (SAR) studies proved this hypothesis[32]. It was found that a relatively large alkyl substituent with sufficient lipophilicity could replace the *sec*-butyl group without a significant loss of activity in HUVEC. Thus, we designed a photoaffinity probe of itraconazole by replacing the isobutyl sidechain with a bifunctional "tail" containing a photosensitive diazirine moiety, which covalently crosslinks the probe to its binding protein(s), and a terminal alkyne for attachment of an affinity tag through click chemistry (**Figure 2.1**). The probe was confirmed to induce all of the same previously reported effects in HUVEC as itraconazole, including mTOR inhibition, NPC phenotype, VEGFR2 hypoglycosylation, and proliferation inhibition, with a similar potency as itraconazole (**Figure 2.2**), giving confidence that the probe is likely acting upon the same molecular target as itraconazole itself.

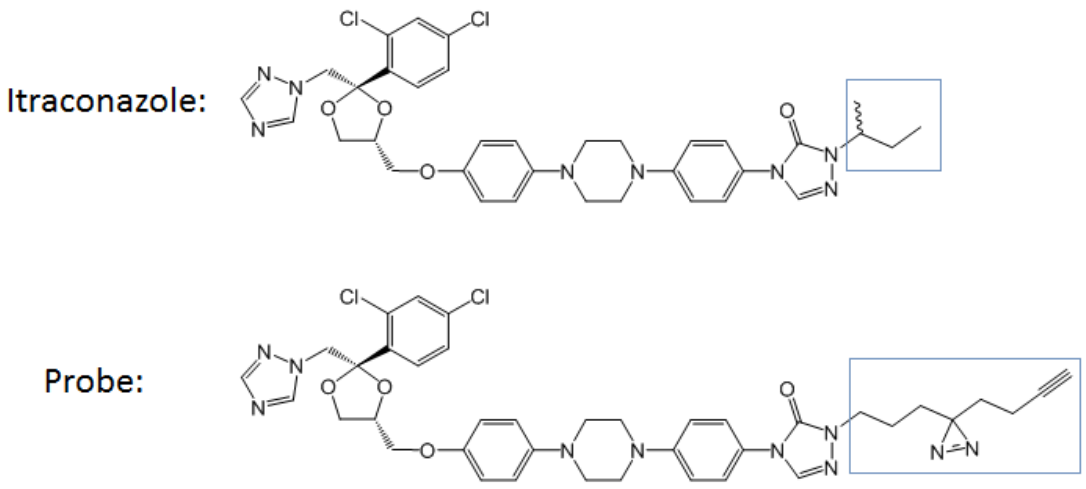

Figure 2.1: Itraconazole and photoaffinity probe structure. The modification to the isobutyl side chain is highlighted in blue.

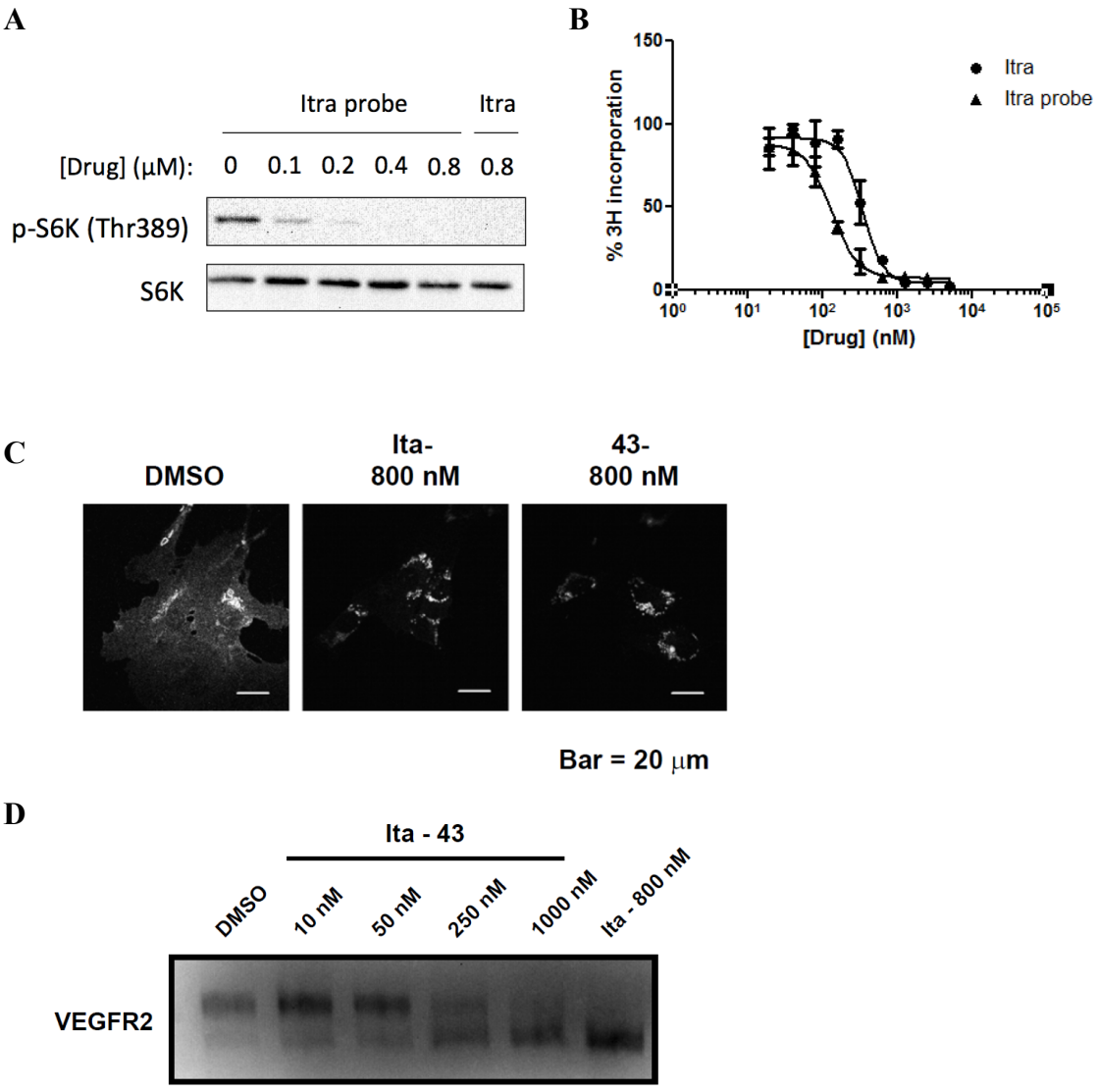

Figure 2.2: The photoaffinity probe is active in HUVEC. The probe induces the same effects in HUVEC as itraconazole, including: A) mTOR inhibition, as measured by phosphorylation of S6K; B) proliferation inhibition, as measured by 3H-thymidine incorporation; C) NPC phenotype, observed by filipin staining; and D) VEGFR2 hypoglycosylation, as measured by mobility shift on SDS-PAGE. The experiments shown in panels C and D were performed by Dr. Benjamin Nacev (Ita-43 = probe).

Identification of three itraconazole-binding proteins by photoaffinity labeling

Initial photoaffinity labeling experiments were performed in 293T cells, due to the difficulty of obtaining large amounts of protein from HUVEC. The workflow of the photoaffinity labeling experiment is depicted in **Figure 2.3**. Live cells in culture were treated with 200 nM probe for 1 hour, with or without pretreatment with 5 μM itraconazole for 30 minutes to compete with the binding of the probe to specific binding proteins. The cells were then placed under a UV lamp for 3 minutes to activate the photolabile diazirine and covalently crosslink the probe to its binding proteins, after which the cells were lysed and proteins denatured. The denatured lysates were then reacted with fluor-azide in the presence of copper, which reacts with the terminal acetylene of the probe to covalently attach the fluorophore via click chemistry. The proteins were then resolved on an SDS-PAGE gel, which was scanned on a fluorescence gel scanner to detect fluorescently labeled proteins.

Probe:

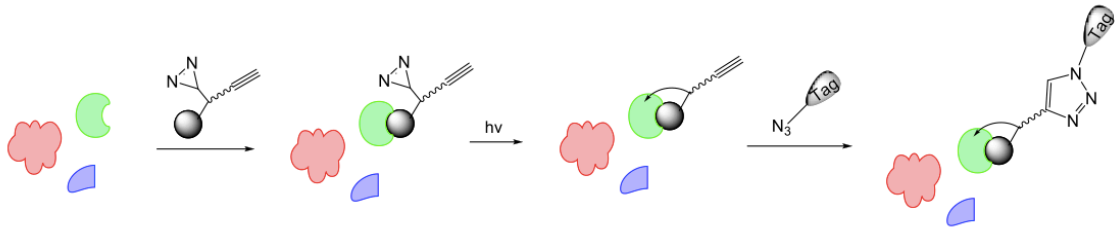

Competition:

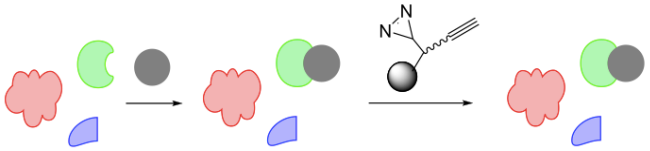

Figure 2.3: Schematic depicting the photoaffinity labeling experiment workflow. Live cells are treated with the probe, which binds to its target protein in the cell. After UV irradiation, the diazirine is crosslinked to the target protein. Click reaction with an azide-linked affinity tag (i.e. biotin or fluorophore) then covalently attaches the tag to the probe for subsequent detection or isolation. In a parallel competition experiment, the cells are pretreated with an excess of unmodified parent compound (grey circle), which binds to the target protein and prevents the binding of the probe. Thus, specific binding proteins will show a decreased signal in the competition sample. Cartoons were created by Dr. Wei Shi.

By comparing the background bands present in the DMSO control sample to the probe-treated sample, we observed that there were 3 proteins clearly photolabeled by the probe, of approximately 35, 50, and 70 kDa (**Figure 2.4**). The labeling of these proteins was also reduced in the competition sample containing excess itraconazole, indicating that these were specific binding proteins of itraconazole. To isolate and identify these itraconazole-binding proteins, the photocrosslinking experiment was repeated using biotin-azide instead of fluor-azide, and the biotinylated proteins were isolated on streptavidin-agarose beads before being resolved by SDS-PAGE. The isolated proteins were then visualized by silver staining, and the silver-stained protein bands were cut out of the gel and subjected to in-gel trypsin digestion and mass-spectrometry analysis. A slice of gel from the same region of the DMSO control lane was analyzed in parallel to subtract any non-specific proteins present in the samples (**Tables 2.2-2.7**). The highest scoring proteins for the 35, 50, and 70 kDa bands present only in the probe sample were Voltage Dependent Anion Channel 1 (VDAC1), microsomal Epoxide Hydrolase (EPHX1, or mEH), and Carnitine Palmitoyl Transferase II (CPT2), respectively.

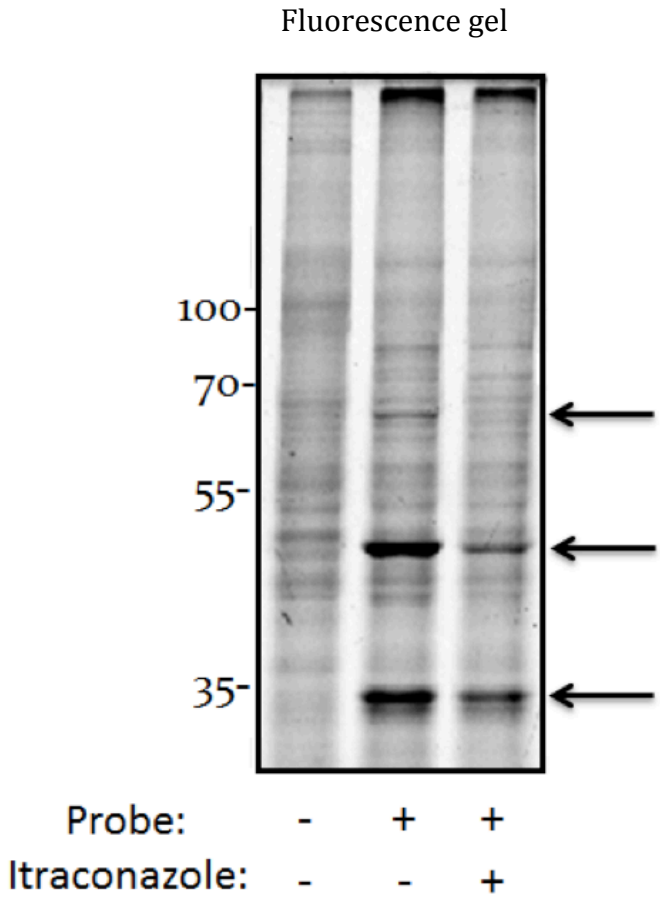

Figure 2.4: Live cell photolabeling experiment in 293T cells. The itraconazole photoaffinity probe labels 3 predominant bands, as detected by fluorescence gel scanning after click reaction with fluor-azide. The intensity of the bands is decreased in the competition sample, demonstrating that they are specific binding proteins of itraconazole.

Table 2.2: MS results from DMSO sample (35 kDa)

rank	prot_acc	prot_desc (Tax_Id=9606 Gene_Symbol)	prot_score	prot_mass
1	IPI00291006	MDH2 Malate dehydrogenase, mitochondrial	752	35481
2	IPI00219217	LDHB L-lactate dehydrogenase B chain	700	36615
3	IPI00022434	ALB Putative uncharacterized protein ALB	227	71658
4	IPI00027462	S100A9 Protein S100-A9	226	13234
5	IPI00013933	DSP Isoform DPI of Desmoplakin	223	331569
6	IPI00027547	DCD Dermcidin	218	11277
7	IPI00398625	HRNR Hornerin	178	282228
8	IPI00008530	RPLP0 60S acidic ribosomal protein P0	167	34252
9	IPI00396378	HNRNPA2B1 Isoform B1 of Heterogeneous nuclear ribonucleoproteins A2/B1	159	37407
10	IPI00789324	JUP cDNA FLJ60424, highly similar to Junction plakoglobin	156	62577
11	IPI00021700	PCNA Proliferating cell nuclear antigen	156	28750
12	IPI00219221	LGALS7;LGALS7B Galectin-7	148	15066
13	IPI00397801	FLG2 Filaggrin-2	148	247928
14	IPI00025753	DSG1 Desmoglein-1	138	113644
15	IPI00217966	LDHA Isoform 1 of L-lactate dehydrogenase A chain	127	36665
16	IPI00007047	S100A8 Protein S100-A8	123	10828
17	IPI00025447	EEF1A1 Elongation factor 1-alpha	122	47839
18	IPI00021439	ACTB Actin, cytoplasmic 1	117	41710
19	IPI00219018	GAPDH Glyceraldehyde-3-phosphate dehydrogenase	86	36030
20	IPI00790298	- 20 kDa protein	86	19534
21	IPI00915869	MDH1 Malate dehydrogenase	80	23024
22	IPI00005969	CAPZA1 F-actin-capping protein subunit alpha-1	78	32902
23	IPI00654755	HBB Hemoglobin subunit beta	76	15988
24	IPI00014587	CLTA Isoform Brain of Clathrin light chain A	76	27060
25	IPI00019038	LYZ Lysozyme C	75	16526
26	IPI00022974	PIP Prolactin-inducible protein	69	16562

27	IPI00032325	CSTA Cystatin-A	67	11000
28	IPI00166729	AZGP1 alpha-2-glycoprotein 1, zinc precursor	65	34237
29	IPI00329332	STX12 Syntaxin-12	63	31622
30	IPI00216099	DSC1 Isoform 1A of Desmocollin-1	60	99924
31	IPI00554711	JUP Junction plakoglobin	57	81693
32	IPI00013885	CASP14 Caspase-14	54	27662
33	IPI00219806	S100A7 Protein S100-A7	51	11464
34	IPI00387020	MYOZ2 Myozenin-2	51	29879
35	IPI00215911	APEX1 DNA-(apurinic or apyrimidinic site) lyase	50	35532
36	IPI00418169	ANXA2 Isoform 2 of Annexin A2	47	40386

Table 2.3: MS results from Probe sample (35 kDa)

rank	prot_acc	prot_desc (Tax_Id=9606 Gene_Symbol)	prot_score	prot_mass
1	IPI00013933	DSP Isoform DPI of Desmoplakin	847	331569
2	***IPI00216308***	***VDAC1 Voltage-dependent anion-selective channel protein 1***	***749***	***30754***
3	IPI00027462	S100A9 Protein S100-A9	673	13234
4	IPI00745872	ALB Isoform 1 of Serum albumin	649	69321
5	IPI00219217	LDHB L-lactate dehydrogenase B chain	560	36615
6	IPI00291006	MDH2 Malate dehydrogenase, mitochondrial	495	35481
7	IPI00789324	JUP cDNA FLJ60424, highly similar to Junction plakoglobin	398	62577
8	IPI00025753	DSG1 Desmoglein-1	341	113644
9	IPI00218918	ANXA1 Annexin A1	300	38690
10	IPI00397801	FLG2 Filaggrin-2	272	247928
11	IPI00398625	HRNR Hornerin	262	282228
12	IPI00554711	JUP Junction plakoglobin	236	81693
13	IPI00021439	ACTB Actin, cytoplasmic 1	222	41710
14	IPI00219806	S100A7 Protein S100-A7	209	11464
15	IPI00011229	CTSD Cathepsin D	192	44524
16	IPI00007047	S100A8 Protein S100-A8	190	10828
17	IPI00019038	LYZ Lysozyme C	189	16526
18	IPI00179330	UBC;RPS27A;UBB ubiquitin and ribosomal protein S27a precursor	169	17953
19	IPI00060800	ZG16B Zymogen granule protein 16 homolog B	169	22725
20	IPI00032325	CSTA Cystatin-A	167	11000
21	IPI00790298	- 20 kDa protein	163	19534
22	IPI00022204	SERPINB3 Isoform 1 of Serpin B3	155	44537
23	IPI00219221	LGALS7;LGALS7B Galectin-7	152	15066
24	IPI00027547	DCD Dermcidin	145	11277
25	IPI00418169	ANXA2 Isoform 2 of Annexin A2	131	40386
26	IPI00300376	TGM3 Protein-glutamine gamma-glutamyltransferase E	128	76584

27	IPI00219018	GAPDH Glyceraldehyde-3-phosphate dehydrogenase	124	36030
28	IPI00216298	TXN Thioredoxin	112	11730
29	IPI00007797	FABP5;FABP5L2;FABP5L7;FABP5L9 Fatty acid-binding protein, epidermal	107	15155
30	IPI00947285	SBSN suprabasin isoform 1 precursor	106	60505
31	IPI00008530	RPLP0 60S acidic ribosomal protein P0	104	34252
32	IPI00216099	DSC1 Isoform 1A of Desmocollin-1	103	99924
33	IPI00154742	IGL@;IGLV1-40;IGLC1;IGLV3-21;IGLC3;LOC100293277;IGLV2-14;LOC100293440;IGLV1	100	24777
34	IPI00021536	CALML5 Calmodulin-like protein 5	97	15883
35	IPI00022974	PIP Prolactin-inducible protein	96	16562
36	IPI00166729	AZGP1 alpha-2-glycoprotein 1, zinc precursor	95	34237
37	IPI00010303	SERPINB4 Serpin B4	93	44825
38	IPI00217966	LDHA Isoform 1 of L-lactate dehydrogenase A chain	91	36665
39	IPI00025447	EEF1A1 Elongation factor 1-alpha	89	47839
40	IPI00396378	HNRNPA2B1 Isoform B1 of Heterogeneous nuclear ribonucleoproteins A2/B1	88	37407
41	IPI00024145	VDAC2 Isoform 2 of Voltage-dependent anion-selective channel protein 2	87	30393
42	IPI00013885	CASP14 Caspase-14	85	27662
43	IPI00013877	HNRNPH3 Isoform 1 of Heterogeneous nuclear ribonucleoprotein H3	82	36903
44	IPI00103242	POF1B Isoform 1 of Protein POF1B	80	68653
45	IPI00015614	PRSS3 Isoform A of Trypsin-3	76	32508
46	IPI00384938	LOC100290320;IGHG1;IGHV4-31;LOC100294459 Putative uncharacterized protein D	73	52819
47	IPI00031564	GGCT Isoform 1 of Gamma-glutamylcyclotransferase	70	20994
48	IPI00910602	NEFH Isoform 1 of Neurofilament heavy polypeptide	67	112411
49	IPI00005969	CAPZA1 F-actin-capping protein subunit alpha-1	63	32902
50	IPI00033583	SERPINB12 Serpin B12	58	46247
51	IPI00019502	MYH9 Isoform 1 of Myosin-9	58	226392
52	IPI00152881	SHROOM3 shroom family member 3 protein	56	216724
53	IPI00003348	GNB2 Guanine nucleotide-binding protein G(I)/G(S)/G(T) subunit beta-2	55	37307
54	IPI00291560	ARG1 Isoform 1 of Arginase-1	52	34713

55	IPI00915869	MDH1	Malate dehydrogenase	32	23024

Table 2.4: MS results from DMSO sample (50 kDa)

rank	prot_acc	prot_desc (Tax_Id=9606 Gene_Symbol)	prot_score	prot_mass
1	IPI00025491	SNORA67;EIF4A1 Eukaryotic initiation factor 4A-I	740	46125
2	IPI00013933	DSP Isoform DPI of Desmoplakin	665	331569
3	IPI00396485	EEF1A1 Elongation factor 1-alpha 1	572	50109
4	IPI00000875	TUT1;EEF1G cDNA FLJ56389, highly similar to Elongation factor 1-gamma	526	56114
5	IPI00025753	DSG1 Desmoglein-1	463	113644
6	IPI00003881	HNRNPF Heterogeneous nuclear ribonucleoprotein F	414	45643
7	IPI00789324	JUP cDNA FLJ60424, highly similar to Junction plakoglobin	344	62577
8	IPI00009328	EIF4A3 Eukaryotic initiation factor 4A-III	328	46841
9	IPI00554711	JUP Junction plakoglobin	297	81693
10	IPI00031461	GDI2 cDNA FLJ60299, highly similar to Rab GDP dissociation inhibitor beta	293	51121
11	IPI00299000	PA2G4 Proliferation-associated protein 2G4	281	43759
12	IPI00021435	PSMC2 26S protease regulatory subunit 7	235	48603
13	IPI00027547	DCD Dermcidin	228	11277
14	IPI00398625	HRNR Hornerin	206	282228
15	IPI00219525	PGD 6-phosphogluconate dehydrogenase, decarboxylating	174	53106
16	IPI00021439	ACTB Actin, cytoplasmic 1	174	41710
17	IPI00219575	BLMH Bleomycin hydrolase	165	52528
18	IPI00009032	SSB Lupus La protein	160	46808
19	IPI00001661	RCC1 regulator of chromosome condensation 1 isoform a	157	48115
20	IPI00013847	UQCRC1 Cytochrome b-c1 complex subunit 1, mitochondrial	150	52612
21	IPI00397801	FLG2 Filaggrin-2	140	247928
22	IPI00015614	PRSS3 Isoform A of Trypsin-3	123	32508
23	IPI00032140	SERPINH1 Serpin H1	120	46411
24	IPI00300376	TGM3 Protein-glutamine gamma-glutamyltransferase E	87	76584
25	IPI00027230	HSP90B1 Endoplasmin	85	92411
26	IPI00012835	CTBP1 C-terminal-binding protein 1	83	47505
27	IPI00013885	CASP14 Caspase-14	83	27662
28	IPI00013068	EIF3E Eukaryotic translation initiation factor 3 subunit E	77	52187

29	IPI00026256	FLG Filaggrin	76	434922
30	IPI00790298	- 20 kDa protein	75	19534
31	IPI00022434	ALB Putative uncharacterized protein ALB	75	71658
32	IPI00071509	PKP1 Isoform 2 of Plakophilin-1	56	82808
33	IPI00103242	POF1B Isoform 1 of Protein POF1B	55	68653
34	IPI00550746	NUDC Nuclear migration protein nudC	50	38219
35	IPI00010154	GDI1 Rab GDP dissociation inhibitor alpha	50	50550
36	IPI00334627	ANXA2P2 Putative annexin A2-like protein	50	38635
37	IPI00387020	MYOZ2 Myozenin-2	50	29879

Table 2.5: MS results from Probe sample (50 kDa)

rank	prot_acc	prot_desc (Tax_Id=9606 Gene_Symbol)	prot_score	prot_mass
1	IPI00013933	DSP Isoform DPI of Desmoplakin	929	331569
2	IPI00025753	DSG1 Desmoglein-1	738	113644
3	***IPI00009896***	***EPHX1 Epoxide hydrolase 1***	***708***	***52915***
4	IPI00000875	TUT1;EEF1G cDNA FLJ56389, highly similar to Elongation factor 1-gamma	579	56114
5	IPI00396485	EEF1A1 Elongation factor 1-alpha 1	447	50109
6	IPI00397801	FLG2 Filaggrin-2	439	247928
7	IPI00789324	JUP cDNA FLJ60424, highly similar to Junction plakoglobin	355	62577
8	IPI00300376	TGM3 Protein-glutamine gamma-glutamyltransferase E	303	76584
9	IPI00013885	CASP14 Caspase-14	303	27662
10	IPI00398625	HRNR Hornerin	276	282228
11	IPI00027547	DCD Dermcidin	273	11277
12	IPI00334627	ANXA2P2 Putative annexin A2-like protein	263	38635
13	IPI00025491	SNORA67;EIF4A1 Eukaryotic initiation factor 4A-I	262	46125
14	IPI00291560	ARG1 Isoform 1 of Arginase-1	254	34713
15	IPI00216099	DSC1 Isoform 1A of Desmocollin-1	240	99924
16	IPI00219575	BLMH Bleomycin hydrolase	240	52528
17	IPI00554711	JUP Junction plakoglobin	211	81693
18	IPI00003881	HNRNPF Heterogeneous nuclear ribonucleoprotein F	206	45643
19	IPI00021536	CALML5 Calmodulin-like protein 5	189	15883
20	IPI00790298	- 20 kDa protein	184	19534
21	IPI00465248	ENO1 Isoform alpha-enolase of Alpha-enolase	166	47139
22	IPI00465436	CAT Catalase	155	59719
23	IPI00247167	NCCRP1 Non-specific cytotoxic cell receptor protein 1 homolog	155	30828
24	IPI00021439	ACTB Actin, cytoplasmic 1	151	41710
25	IPI00216298	TXN Thioredoxin	146	11730
26	IPI00027462	S100A9 Protein S100-A9	135	13234
27	IPI00219018	GAPDH Glyceraldehyde-3-phosphate dehydrogenase	132	36030
28	IPI00022974	PIP Prolactin-inducible protein	128	16562

29	IPI00219525	PGD 6-phosphogluconate dehydrogenase, decarboxylating	127	53106
30	IPI00305622	TGM1 Protein-glutamine gamma-glutamyltransferase K	118	89730
31	IPI00022434	ALB Putative uncharacterized protein ALB	115	71658
32	IPI00033583	SERPINB12 Serpin B12	112	46247
33	IPI00166729	AZGP1 alpha-2-glycoprotein 1, zinc precursor	107	34237
34	IPI00179330	UBC;RPS27A;UBB ubiquitin and ribosomal protein S27a precursor	104	17953
35	IPI00013847	UQCRC1 Cytochrome b-c1 complex subunit 1, mitochondrial	104	52612
36	IPI00299000	PA2G4 Proliferation-associated protein 2G4	100	43759
37	IPI00386809	CDSN Corneodesmosin	91	51463
38	IPI00009328	EIF4A3 Eukaryotic initiation factor 4A-III	88	46841
39	IPI00103242	POF1B Isoform 1 of Protein POF1B	86	68653
40	IPI00419215	A2ML1 Alpha-2-macroglobulin-like protein 1	77	161001
41	IPI00021435	PSMC2 26S protease regulatory subunit 7	76	48603
42	IPI00156689	VAT1 Synaptic vesicle membrane protein VAT-1 homolog	74	41893
43	IPI00219806	S100A7 Protein S100-A7	74	11464
44	IPI00654755	HBB Hemoglobin subunit beta	68	15988
45	IPI00654788	FLG Profilaggrin (Fragment)	68	133528
46	IPI00032325	CSTA Cystatin-A	67	11000
47	IPI00219221	LGALS7;LGALS7B Galectin-7	66	15066
48	IPI00007047	S100A8 Protein S100-A8	59	10828
49	IPI00031461	GDI2 cDNA FLJ60299, highly similar to Rab GDP dissociation inhibitor beta	58	51121
50	IPI00023078	C1orf68 Skin-specific protein 32	53	26219
51	IPI00514908	KPRP Keratinocyte proline-rich protein	50	64093

Table 2.6: MS results from DMSO sample (70 kDa)

rank	prot_acc	prot_desc (Tax_Id=9606 Gene_Symbol)	prot_score	prot_mass
1	IPI00008557	IGF2BP1 Insulin-like growth factor 2 mRNA-binding protein 1	477	63417
2	IPI00304925	HSPA1A;HSPA1B Heat shock 70 kDa protein 1A/1B	436	70009
3	IPI00004860	RARS Isoform Complexed of Arginyl-tRNA synthetase, cytoplasmic	300	75331
4	IPI00017617	DDX5 Probable ATP-dependent RNA helicase DDX5	291	69105
5	IPI00027547	DCD Dermcidin	279	11277
6	IPI00025753	DSG1 Desmoglein-1	222	113644
7	IPI00643920	TKT cDNA FLJ54957, highly similar to Transketolase	153	68698
8	IPI00216694	PLS3 Plastin-3	141	70766
9	IPI00022434	ALB Putative uncharacterized protein ALB	135	71658
10	IPI00300074	FARSB Phenylalanyl-tRNA synthetase beta chain	126	66088
11	IPI00015614	PRSS3 Isoform A of Trypsin-3	125	32508
12	IPI00012442	G3BP1 Ras GTPase-activating protein-binding protein 1	120	52132
13	IPI00217182	DSP Isoform DPII of Desmoplakin	111	259957
14	IPI00020599	CALR Calreticulin	111	48112
15	IPI00008603	ACTA2 Actin, aortic smooth muscle	108	41982
16	IPI00789324	JUP cDNA FLJ60424, highly similar to Junction plakoglobin	106	62577
17	IPI00179953	NASP Isoform 1 of Nuclear autoantigenic sperm protein	105	85186
18	IPI00025874	RPN1 Dolichyl-diphosphooligosaccharide--protein glycosyltransferase subunit	86	72733
19	IPI00217975	LMNB1 Lamin-B1	75	66368
20	IPI00294879	RANGAP1 Ran GTPase-activating protein 1	70	63502
21	IPI00000690	AIFM1 Isoform 1 of Apoptosis-inducing factor 1, mitochondrial	66	66859
22	IPI00179330	UBC;RPS27A;UBB ubiquitin and ribosomal protein S27a precursor	58	17953
23	IPI00009771	LMNB2 Lamin-B2	58	69906
24	IPI00398625	HRNR Hornerin	54	282228
25	IPI00219077	LTA4H Isoform 1 of Leukotriene A-4 hydrolase	50	69241
26	IPI00216298	TXN Thioredoxin	50	11730
27	IPI00465233	EIF3L Eukaryotic translation initiation factor 3, subunit E interacting pro	49	70857
28	IPI00032325	CSTA Cystatin-A	48	11000

29	IPI00027462	S100A9 Protein S100-A9	44	13234

Table 2.7: MS results from Probe sample (70 kDa)

rank	prot_acc	prot_desc (Tax_Id=9606 Gene_Symbol)	prot_score	prot_mass
1	IPI00304925	HSPA1A;HSPA1B Heat shock 70 kDa protein 1A/1B	1604	70009
2	***IPI00012912***	***CPT2 Carnitine O-palmitoyltransferase 2, mitochondrial***	***1421***	***73730***
3	IPI00911039	HSPA1A;HSPA1B cDNA FLJ54408, highly similar to Heat shock 70 kDa protein 1	1340	63885
4	IPI00644712	XRCC6 ATP-dependent DNA helicase 2 subunit 1	1242	69799
5	IPI00004860	RARS Isoform Complexed of Arginyl-tRNA synthetase, cytoplasmic	1191	75331
6	IPI00217975	LMNB1 Lamin-B1	843	66368
7	IPI00221226	ANXA6 Annexin A6	613	75826
8	IPI00643920	TKT cDNA FLJ54957, highly similar to Transketolase	500	68698
9	IPI00411937	NOP56 Nucleolar protein 56	468	66009
10	IPI00300074	FARSB Phenylalanyl-tRNA synthetase beta chain	467	66088
11	IPI00216694	PLS3 Plastin-3	423	70766
12	IPI00025874	RPN1 Dolichyl-diphosphooligosaccharide--protein glycosyltransferase subunit	416	72733
13	IPI00012442	G3BP1 Ras GTPase-activating protein-binding protein 1	409	52132
14	IPI00017617	DDX5 Probable ATP-dependent RNA helicase DDX5	391	69105
15	IPI00020127	RPA1 Replication protein A 70 kDa DNA-binding subunit	376	68095
16	IPI00007084	SLC25A13 Calcium-binding mitochondrial carrier protein Aralar2	353	74129
17	IPI00305166	SDHA cDNA FLJ61478, highly similar to Succinate dehydrogenase (ubiquinone)	347	72641
18	IPI00217143	SDHA SDHA protein	347	56716
19	IPI00294879	RANGAP1 Ran GTPase-activating protein 1	296	63502
20	IPI00219077	LTA4H Isoform 1 of Leukotriene A-4 hydrolase	276	69241
21	IPI00027547	DCD Dermcidin	276	11277
22	IPI00658000	IGF2BP3 Isoform 1 of Insulin-like growth factor 2 mRNA-binding protein 3	224	63666
23	IPI00064328	PRMT5 protein arginine methyltransferase 5 isoform b	192	71275
24	IPI00022434	ALB Putative uncharacterized protein ALB	179	71658
25	IPI00552546	C10orf119 Isoform 2 of UPF0557 protein C10orf119	166	72703
26	IPI00179953	NASP Isoform 1 of Nuclear autoantigenic sperm protein	163	85186
27	IPI00021338	DLAT Dihydrolipoyllysine-residue acetyltransferase component of pyruvate de	154	68953
28	IPI00003886	GNL3 Isoform 2 of Guanine nucleotide-binding protein-like 3	144	60503

29	IPI00022395	C9 Complement component C9	131	63133
30	IPI00100460	DARS2 Aspartyl-tRNA synthetase, mitochondrial	123	73516
31	IPI00032304	PLS1 Plastin-1	113	70209
32	IPI00018140	SYNCRIP Isoform 1 of Heterogeneous nuclear ribonucleoprotein Q	104	69560
33	IPI00394679	WHSC2 Wolf-Hirschhorn syndrome candidate 2 protein	104	58462
34	IPI00008557	IGF2BP1 Insulin-like growth factor 2 mRNA-binding protein 1	99	63417
35	IPI00171903	HNRNPM Isoform 1 of Heterogeneous nuclear ribonucleoprotein M	93	77464
36	IPI00027462	S100A9 Protein S100-A9	92	13234
37	IPI00019463	EIF2AK2 Interferon-induced, double-stranded RNA-activated protein kinase	88	62056
38	IPI00306043	YTHDF2 Isoform 1 of YTH domain family protein 2	86	62296
39	IPI00013894	STIP1 Stress-induced-phosphoprotein 1	86	62599
40	IPI00012074	HNRNPR Isoform 1 of Heterogeneous nuclear ribonucleoprotein R	81	70899
41	IPI00179330	UBC;RPS27A;UBB ubiquitin and ribosomal protein S27a precursor	78	17953
42	IPI00008603	ACTA2 Actin, aortic smooth muscle	78	41982
43	IPI00219221	LGALS7;LGALS7B Galectin-7	78	15066
44	IPI00642862	PPIL4 Peptidyl-prolyl cis-trans isomerase-like 4	76	57189
45	IPI00382470	HSP90AA1 Isoform 2 of Heat shock protein HSP 90-alpha	66	98099
46	IPI00009057	G3BP2 Isoform A of Ras GTPase-activating protein-binding protein 2	57	54088
47	IPI00014424	EEF1A2 Elongation factor 1-alpha 2	54	50438
48	IPI00166768	TUBA1C TUBA1C protein	53	36719
49	IPI00296563	GUF1 GTP-binding protein GUF1 homolog	52	74281
50	IPI00163505	RBM39 Isoform 1 of RNA-binding protein 39	51	59343

The identities of the top three proteins found by MS were confirmed by repeating the biotin pull-down experiment and Western blotting with specific antibodies (**Figure 2.5**). The probe was also able to pull down 14DM, but this binding was barely detectable (**Figure 2.6**), consistent with previous reports that show itraconazole has minimal activity against human 14DM[15,16]. Interestingly, when the photolabeling experiment was repeated in HUVEC, it appeared that the vast majority of the probe bound to VDAC1 (**Figure 2.7**), suggesting that in endothelial cells the other two proteins are minor targets, and providing a possible explanation for the cell-type to cell-type differences in itraconazole's activity.

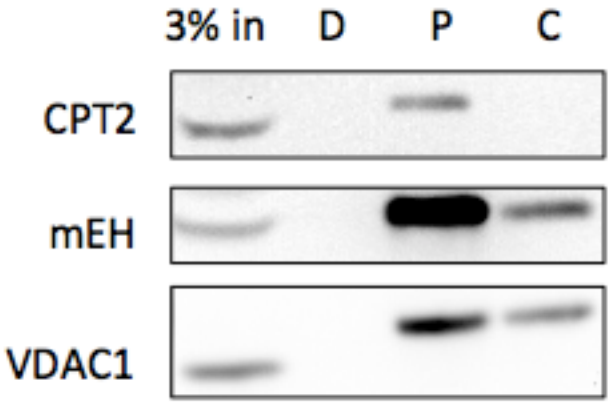

Figure 2.5: Western blot validation of the proteins identified by MS. After photolabeling and biotin pull-down in 293T cells, Western blots were performed using antibodies against each of the 3 highest scoring proteins by MS. The results demonstrate that the proteins identified by MS were specifically pulled down by the probe and competed away by excess itraconazole. (D = DMSO only; P = Probe; C = Competition)

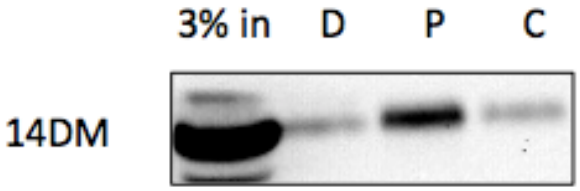

Figure 2.6: Western blot of 14-alpha demethylase after pull down by the itra probe. 14DM labeling by the itra probe was detectable by western blot after biotin pull-down, but the amount of protein detected compared with the input is much lower than for the other three target proteins, as shown in figure 2.5. (D = DMSO only; P = Probe; C = Competition)

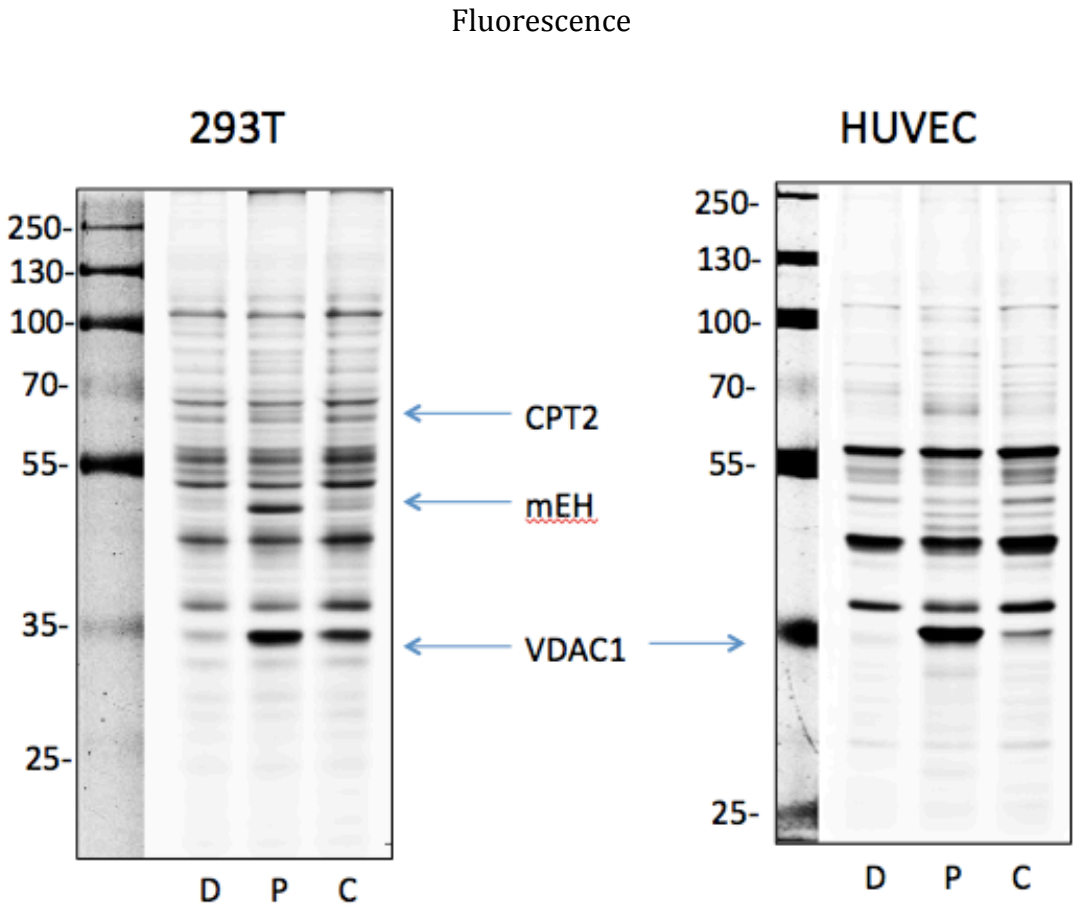

Figure 2.7: Live-cell photoaffinity labeling in 293T vs. HUVEC. The photoaffinity labeling experiment was repeated in HUVEC, where the vast majority of the probe bound to VDAC1, as visualized by fluorescence gel scan. (D = DMSO; P = Probe; C = Competition)

Validation experiments narrow down targets

To determine which of the three newly identified itraconazole-binding proteins might be relevant to its antiangiogenic mechanism of action, we first knocked down each protein individually in HUVEC. Two shRNA sequences were designed for each target and packaged in lentivirus for delivery to the cells. After 2-3 days transduction, the cells were assessed for any changes in the phenotypes associated with itraconazole, including cell proliferation (by thymidine incorporation), cholesterol distribution (by filipin staining), mTOR activity and VEGFR2 glycosylation (by Western blot). All of the knockdown cells showed decreased rates of cell proliferation to varying degrees, although none showed a significant difference in sensitivity to itraconazole (**Figures 2.8 and 2.9**). None of the knockdown cells showed induction of NPC phenotype or changes in VEGFR2 glycosylation (data not shown). However, knockdown of VDAC1 and CPT2 decreased basal mTOR activity as measured by phosphorylation of S6K (**Figure 2.10a,b**), whereas mEH knockdown did not affect mTOR activity (**Figure 2.10c**). This result suggested that VDAC1 and/or CPT2 might be relevant to the mechanism of mTOR inhibition in HUVEC.

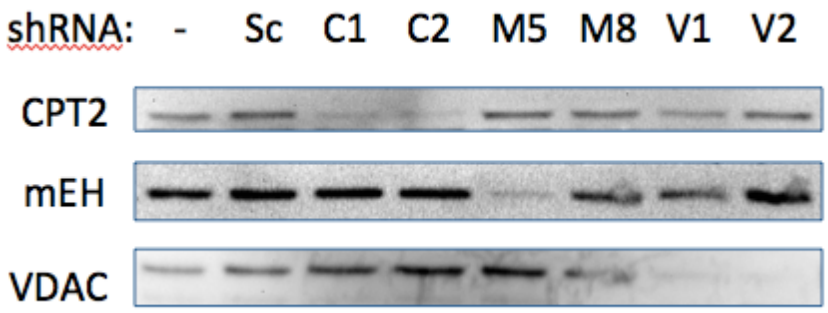

Figure 2.8: Knockdown of the three putative targets in HUVEC. Cells were treated with lentivirus for 3 days before expression of the targets was measured by Western blot. Two different shRNA sequences were used for each target protein. Sc = scrambled shRNA; C1 = CPT2 sh#1; C2 = CPT2 sh#2; M5 = mEH sh#5; M8 = mEH sh#8; V1 = VDAC1 sh#1; V2 = VDAC1 sh#2.

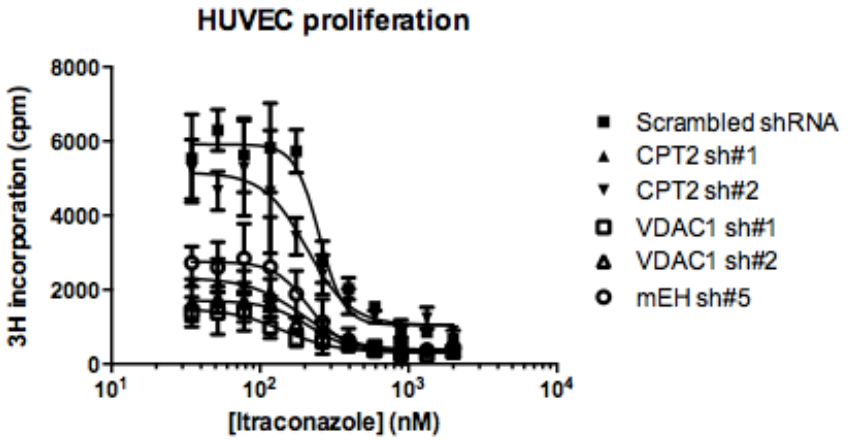

	Scrambled shRNA	CPT2 sh#1	CPT2 sh#2	mEH sh#5	VDAC1 sh#1	VDAC1 sh#2
IC50	250.4	190.1	207.3	210.4	143.5	217.0

Figure 2.9: Knockdown cells display decreased proliferation rate in HUVEC.

Proliferation of the lentivirus-transduced cells was assessed by thymidine incorporation assay. The cells displayed a decrease in the overall rate of proliferation (total cpm), with VDAC1 knockdown cells having the lowest proliferation rate. However, none of the cells showed a significant difference in their sensitivity to proliferation inhibition by itra.

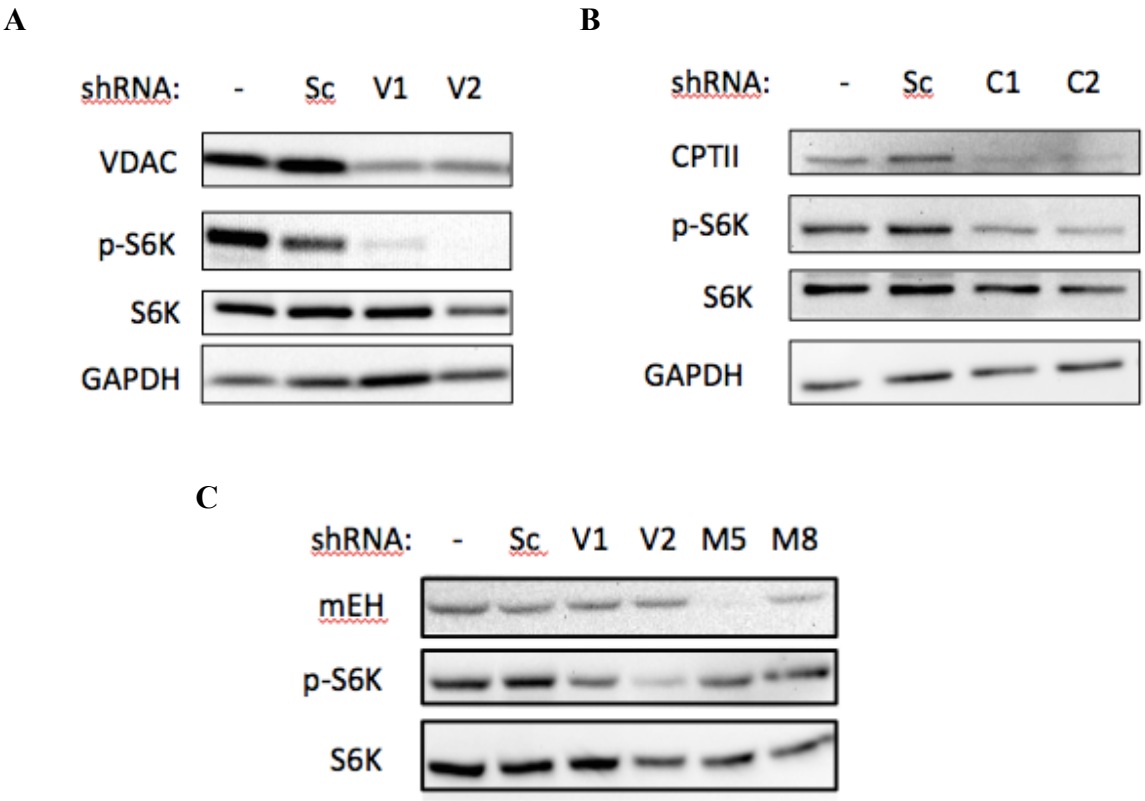

Figure 2.10: Effect of knockdowns on mTOR signaling in HUVEC. Knockdown of A) VDAC1 and B) CPT2 both caused a significant decrease in basal S6K phosphorylation, indicating mTOR was inhibited in these cells. C) Knockdown of mEH does not change S6K phosphorylation, as compared with knockdown of VDAC1.

The relevance of mEH was further ruled out by demonstrating that another azole antifungal drug, miconazole, could compete with binding of the itraconazole probe to mEH, but an analog of itraconazole lacking the azole ring (triazole-deleted [TD]-itra) could not (**Figure 2.11**). This result suggested that the binding to mEH was likely mediated by the azole ring and not specifically by itraconazole itself. Since the antiangiogenic activity of itraconazole is unique among the azole antifungals tested, it was concluded that mEH was unlikely to be a relevant target of itraconazole.

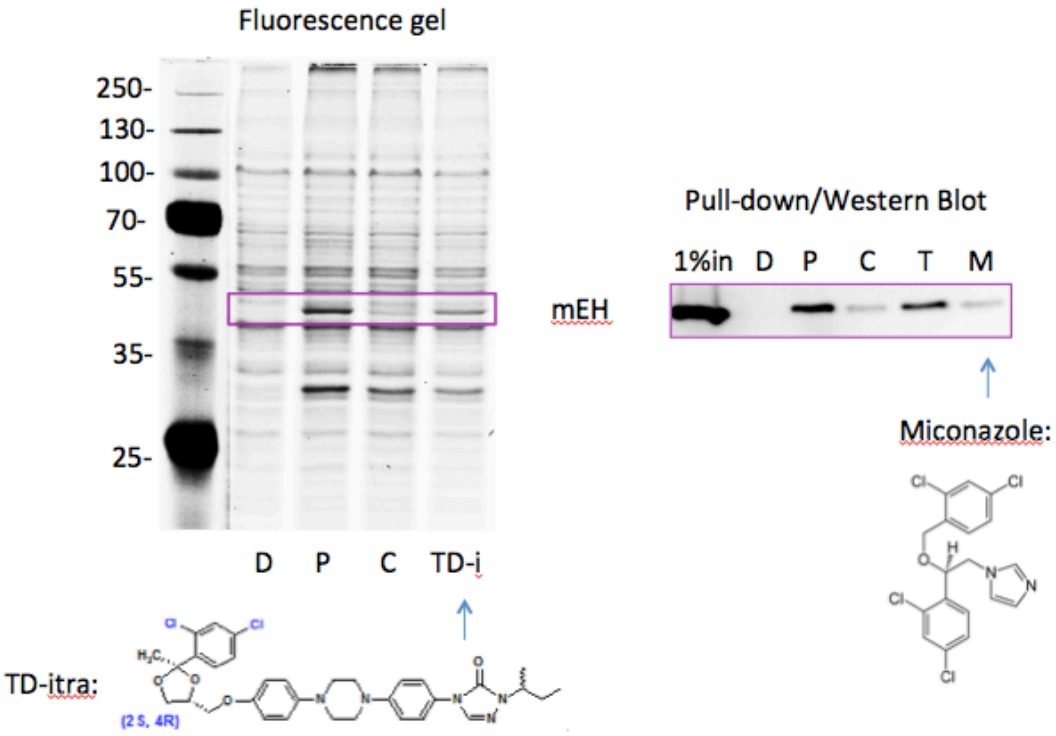

Figure 2.11: Competition of the probe binding to mEH is mediated by the azole ring of itraconazole. The photoaffinity labeling experiment was performed using TD-itra or miconazole as competitors, and the labeled proteins were either detected by fluorescence gel scan (left) or pull-down followed by Western blot (right). These results demonstrate that itraconazole is able to compete with the probe binding to mEH, but TD-itra is not.

CPT2 is a resident protein of the inner mitochondrial membrane (IMM), where it is involved in transporting fatty acids into the mitochondria to undergo beta-oxidation[33]. To assess whether itraconazole is able to inhibit CPT2 activity in cells, we measured beta-oxidation in the presence and absence of itraconazole by observing the conversion of ^{14}C-oleic acid to $^{14}CO_2$. Compared with the positive control inhibitor etomoxir, which significantly inhibited beta-oxidation in this assay, itraconazole did not have any obvious effect (**Figure 2.12**). In addition, there was no observable build-up of palmitoyl-carnitine in itraconazole-treated cells measured by LC-MS, which would be expected if the enzyme's activity were inhibited by itraconazole (data not shown). Thus, with no evidence of any effect of itraconazole on CPT2 function in cells, we concluded that CPT2 is also unlikely to be a physiologically relevant target of itraconazole and subsequently turned our attention toward VDAC1.

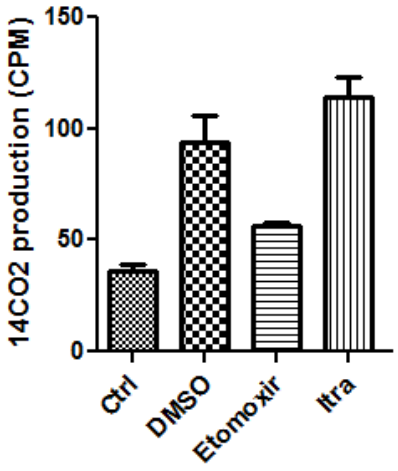

Figure 2.12: Itraconazole does not inhibit fatty acid oxidation in HUVEC. Compared with DMSO treatment alone, etomoxir inhibits β-oxidation almost to control levels, while 10 μM itraconazole has no effect.

VDAC, also known as mitochondrial porin, is a β barrel protein channel that sits in the outer mitochondrial membrane (OMM) and regulates the movement of ions and small metabolites into and out of the mitochondria. First, to confirm the specificity of itraconazole's binding to VDAC1, we repeated the photoaffinity labeling and pull-down experiment in HUVEC and assessed binding to another β barrel protein of the OMM, Tom 40[34], by Western blot (**Figure 2.13**). As expected, there was no labeling of Tom 40 by the itraconazole probe, showing that the binding between itraconazole and VDAC1 is indeed specific and not due to non-specific hydrophobic interactions or accumulation in the membrane.

There are three isoforms of VDAC found in mammals: VDAC1, VDAC2, and VDAC3[35]. Although VDAC1 was the primary isoform identified by MS and Western blot as binding to the itraconazole probe, we wanted to assess whether this binding was isoform specific. We therefore expressed each individual VDAC isoform with a C-terminal V5 tag in 293T cells and repeated the pull-down experiment. By Western blotting with a V5 antibody, we were able to observe clear labeling of the exogenously expressed VDAC1, whereas labeling of VDAC2 and VDAC3 was barely detectable (**Figure 2.14**), suggesting that binding of the itraconazole probe is selective for VDAC1 over the other two isoforms.

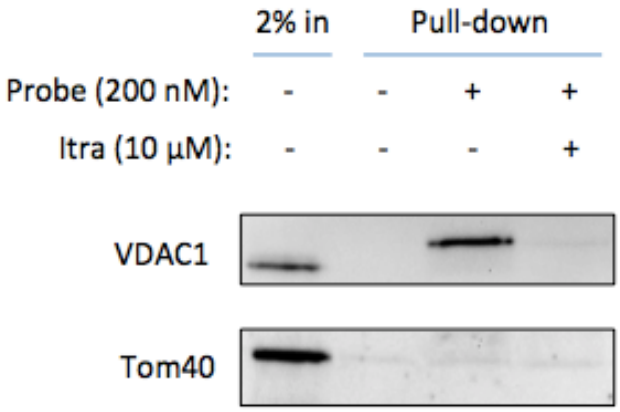

Figure 2.13: The itraconazole probe does not bind to Tom40. Biotin pull-down and Western blot with antibodies against VDAC1 and another β-barrel protein of the outer mitochondrial membrane, Tom40, shows that the binding of the itraconazole probe is specific to VDAC1.

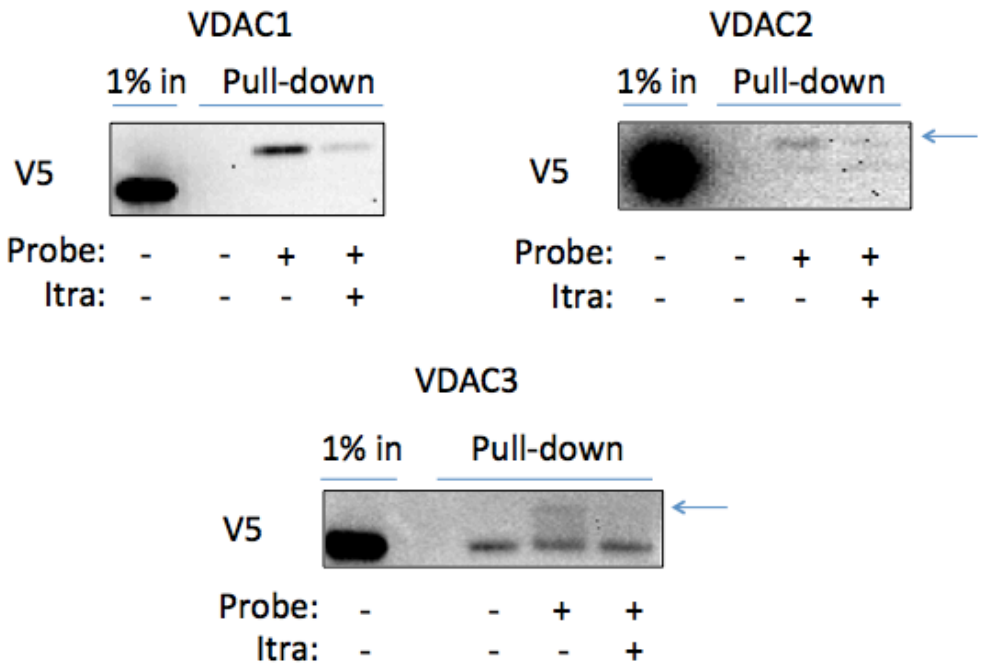

Figure 2.14: The itraconazole probe selectively binds to VDAC1 over VDAC 2 or 3. Each individual VDAC isoform with a C-terminal V5 tag was expressed in 293T cells before labeling with the itraconazole probe and biotin pull-down. Detection of the expressed protein by western blotting with a V5 antibody revealed clear labeling of VDAC1 and only very faint labeling of VDACs 2 and 3 (indicated by arrows).

Itraconazole activates AMPK in HUVEC

The primary cellular function of VDAC is to regulate mitochondrial function by controlling the movement of ions and small metabolites across the OMM[36,37]. Because of the central role of mitochondria in a myriad of cellular processes, we reasoned that there is likely to be a pathway by which mitochondrial function is connected to mTOR activity; however, this link has not been directly demonstrated[38]. mTOR is known to be regulated by multiple upstream signaling pathways, responding to changes in cellular nutrient availability and energy stress. One of these is the 5' AMP-activated protein kinase (AMPK) pathway, which is activated by an increase in the cellular AMP:ATP ratio, indicating that energy levels are low[39,40]. Because VDAC is known to regulate mitochondrial ATP production by transporting ADP and ATP across the OMM[37], we hypothesized that itraconazole binding to VDAC1 might perturb ATP production and cause activation of the AMPK pathway.

We therefore examined the effect of itraconazole on AMPK activity in HUVEC. Upon binding of AMP to the γ-subunit of the heterotrimeric AMPK complex, a conformational change takes place that allows phosphorylation of threonine 172 of the α-subunit to occur, leading to activation of its kinase activity. As shown in **Figure 2.15**, treatment of HUVEC with itraconazole increased the phosphorylation of AMPKα at Thr172 within 5 minutes of drug treatment, with maximal activation occurring after 15 minutes, after which time levels dropped slightly but remained elevated compared to control. The level of AMPK phosphorylation induced by itraconazole at 15 minutes was similar to that of a positive control compound, thapsigargin[41]. Importantly,

phosphorylation of the mTOR substrate S6K did not begin to decrease until 15 minutes after itraconazole treatment, and was maximally inhibited after 30 minutes. The slower onset of mTOR inhibition by itraconazole suggests that AMPK activation is likely upstream of mTOR inhibition by itraconazole, consistent with a possible causal relationship between AMPK activation and mTOR inhibition.

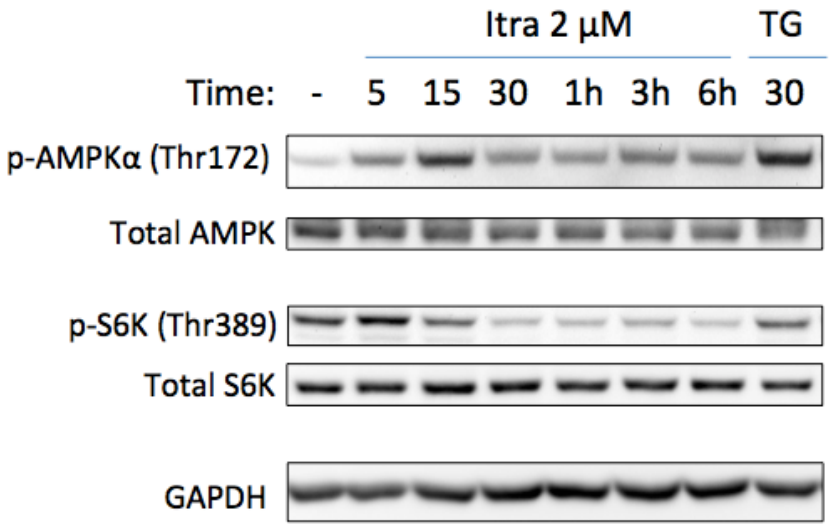

Figure 2.15: Itraconazole activates AMPK prior to the onset of mTOR inhibition in HUVEC. The activating phosphorylation of AMPKα increases within 5 min of itraconazole treatment, but mTOR inhibition is not observed until 15 min after itraconazole treatment, suggesting that mTOR is downstream of AMPK.

Activation of AMPK leads to restoration of cellular energy levels by upregulating ATP-producing pathways and downregulating ATP-consuming ones. One canonical substrate of AMPK is acetyl-CoA carboxylase 1 (ACC1), which is involved in the synthesis of fatty acids during times of excess energy availability and is inactivated upon phosphorylation at Serine 79 by AMPK[42]. As expected, itraconazole treatment also led to increased phosphorylation of ACC1 in HUVEC (**Figure 2.16**), demonstrating that stimulation of AMPKα by itraconazole indeed increases the kinase activity of AMPK and affects downstream signaling pathways.

AMPK activation is known to lead to mTOR inhibition through direct phosphorylation of two mTOR regulatory proteins: tuberous sclerosis 2 (TSC2) and the regulatory associated protein of mTOR (raptor)[38,40]. Phosphorylation of raptor on Serine 792 by AMPK increases the association of raptor with the scaffold protein 14-3-3, leading to dissociation and inactivation of the mTOR complex 1. We found that treatment of HUVEC with itraconazole led to an increase in the phosphorylation of raptor at Serine 792, similar to that induced by the known AMPK activating compound 2-deoxyglucose (2DG) (**Figure 2.16**). Interestingly, we did not observe increased phosphorylation of TSC2 by either itraconazole or 2DG in these cells, indicating that inhibition of mTOR by itraconazole is likely mediated by raptor rather than TSC2.

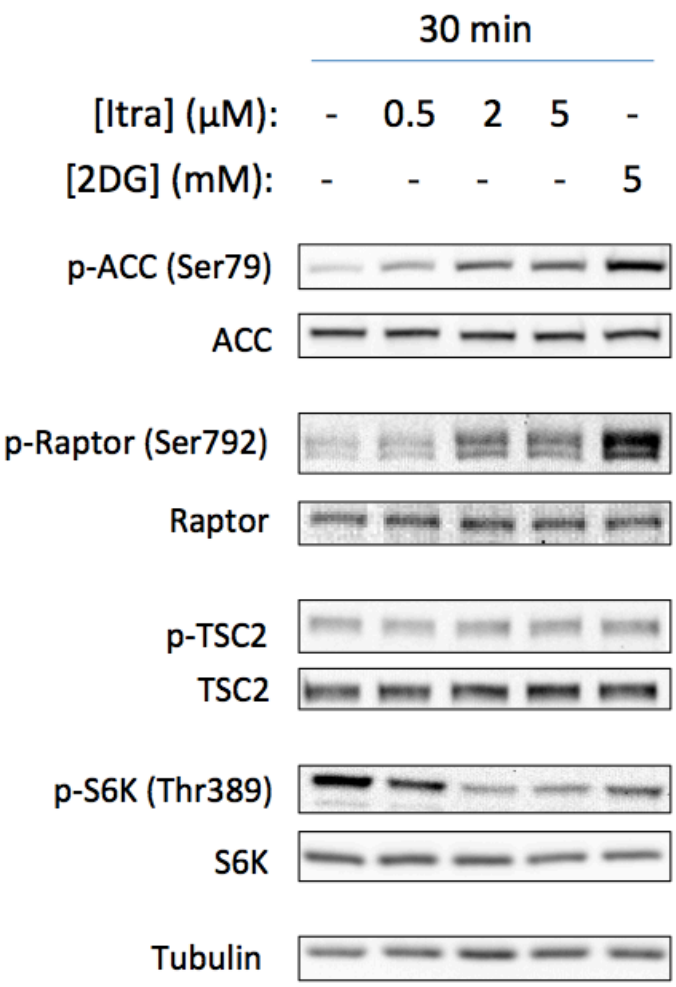

Figure 2.16: Itraconazole increases phosphorylation of AMPK substrates.

Phosphorylation of the AMPK substrates ACC and raptor increases dose-dependently with itraconazole treatment, concomitant with a decrease in S6K phosphorylation. However, phosphorylation of TSC2 at Ser1387 is not affected by either itraconazole or 2DG under the same conditions, suggesting that itraconazole's inhibition of mTOR is mediated by raptor rather than TSC2.

Given that AMPK activation leads to mTOR inhibition, and mTOR positively regulates proliferation, we wanted to specifically test the effect of AMPK activation on proliferation in HUVEC. A769662 is a direct and specific activator of AMPK, which binds in the interface between the AMPK α- and β-subunits and allosterically activates the complex[43]. We therefore tested A769662 in HUVEC and found that it inhibited proliferation with an IC_{50} of 73 μM (+/- 8.34, SEM) (**Figure 2.17a**). Conversely, inhibition of AMPK using the small molecule AMPK inhibitor Compound C significantly reversed the proliferation inhibition caused by itraconazole in HUVEC (**Figure 2.17b**). These results demonstrate a causal relationship between AMPK activation and proliferation inhibition in HUVEC and support the hypothesis that proliferation inhibition by itraconazole is downstream of its activation of AMPK.

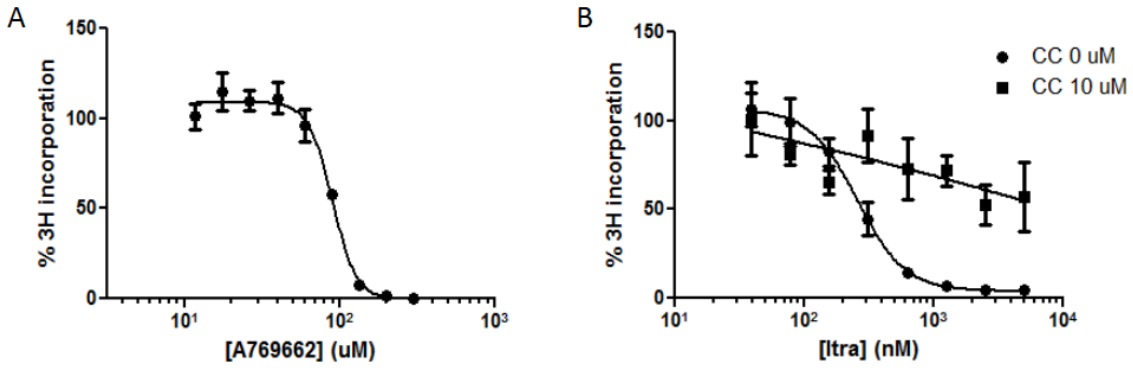

Figure 2.17: AMPK activation causes proliferation inhibition in HUVEC.

(A) HUVEC were treated with varying concentrations of A769662 for 24 hours before being pulsed for 6 hours with 3H-thymidine. The average IC50 from 3 independent experiments was 73 μM +/- 8.34 (SEM). (B) HUVEC were pretreated with 10 μM Compound C for 30 minutes before being treated with varying concentrations of itraconazole for 24 hours. Cells were then pulsed for 6 hours with 3H-thymidine. Results shown are averaged from 3 independent experiments, and error bars represent SEM.

To further verify the activation of AMPK by itraconazole in cells and to follow the time course of AMPK activation in higher resolution, we used a genetically encoded FRET-based biosensor which allows AMPK activity to be measured directly in real time[26]. The reporter contains a phosphorylation motif identified through a positional peptide library screen[27] and undergoes a conformational change upon phosphorylation by AMPK leading to an increase in the yellow/cyan FRET emission ratio of the reporter. Consistent with the results obtained by Western blot, 2 μM itraconazole caused a rapid increase in FRET ratio beginning about 5 minutes after drug addition and peaking between 10-15 minutes, before slowly tapering off again (**Figure 2.18a,b**). After 30 minutes, 20 mM 2DG was added to maximize the FRET response of the reporter. From this experiment, we determined that 2 μM itraconazole was able to activate AMPK to approximately 70% of the maximum achievable response induced by 20 mM 2DG. The specificity of the FRET reporter response was confirmed by using a version of the reporter containing a T/A mutation in the phosphorylation motif, which renders it insensitive to AMPK activation; as expected, neither itraconazole nor 2DG induced any changes in the emission ratio of the mutated reporter (**Figure 2.18c**). Taken together, these results confirmed that itraconazole causes activation of AMPK and its downstream signaling pathways in endothelial cells.

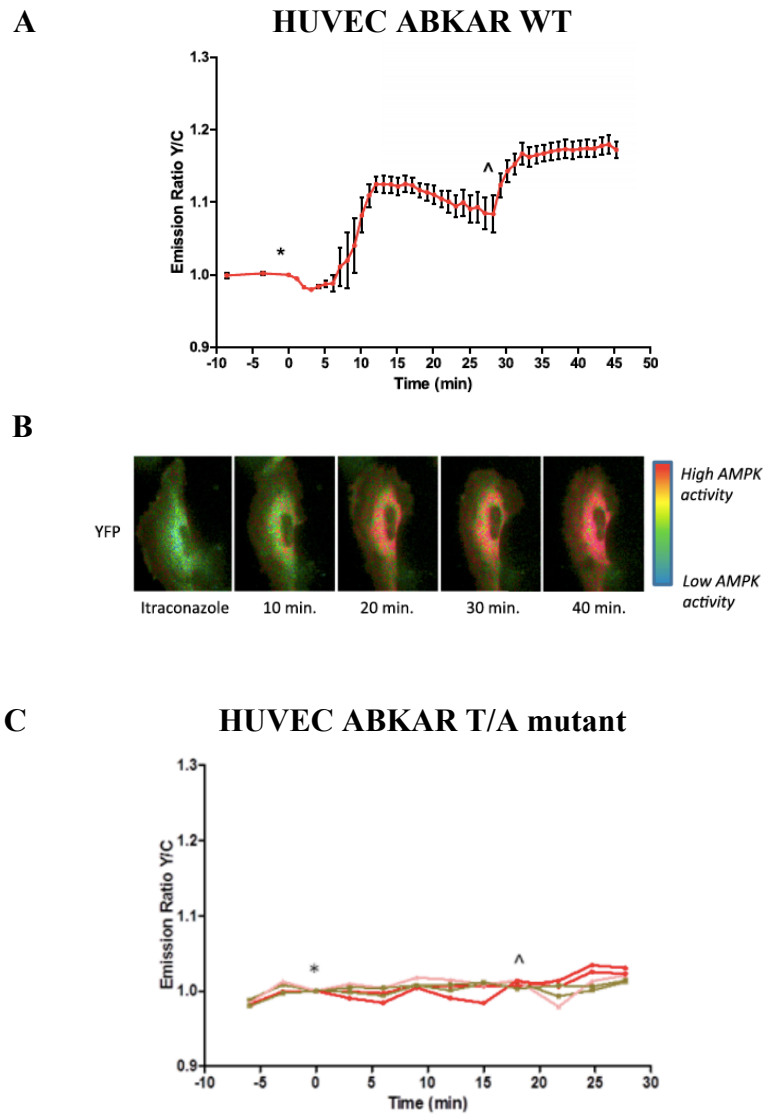

Figure 2.18: A FRET-based AMPK activity reporter demonstrates increased AMPK activation in live cells. A) HUVEC expressing the AMPK-activity reporter ABKAR show an increased yellow/cyan emission ratio after treatment with 2 μM itraconazole (*); this increase peaks 10–15 min after treatment. The effect of itraconazole was ~70% of the maximal response of the reporter induced by 20 mM 2DG (^). (B) Pseudocolor images of an itraconazole-treated HUVEC cell expressing ABKAR. (C) Cells expressing the reporter with a T/A mutation in the substrate motif, which cannot be phosphorylated by AMPK, show no response to itraconazole (*) or 2DG (^) treatment.

AMPK activation by itraconazole is caused by an increase in AMP:ATP ratio

The activating phosphorylation of AMPKα at Thr172 is known to be carried out by two upstream kinases, LKB1 and CaMKKβ[44]. LKB1 is thought to be constitutively active, but it can only efficiently phosphorylate AMPKα after the conformational change induced by AMP binding to the γ subunit when AMP:ATP ratios are high. On the other hand, CaMKKβ is a calmodulin-dependent kinase that is activated by increased intracellular calcium levels. To determine which of these two mechanisms is involved in AMPK activation by itraconazole, we measured AMP, ADP, and ATP levels in extracts of DMSO- or itraconazole-treated cells by LC-MS/MS. We found that itraconazole treatment caused a rapid increase in both AMP:ATP and ADP:ATP ratios (**Figure 2.19a,b**) compared with DMSO treatment, indicating a drop in cellular energy levels after itraconazole treatment. Further, the activation of AMPK by itraconazole was not blocked in cells pretreated with the CaMKKβ inhibitor STO-609, whereas activation by the calcium ionophore ionomycin was reversed (**Figure 2.19c**), suggesting that unlike ionomycin, itraconazole does not activate AMPK through a calcium-dependent mechanism.

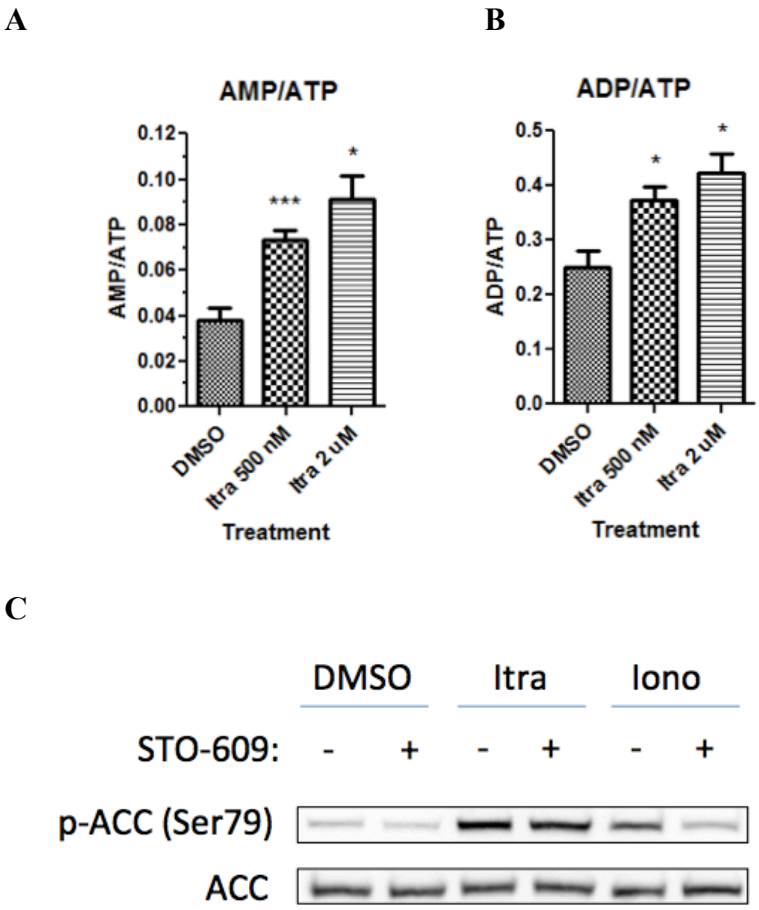

Figure 2.19: Itraconazole-induced AMPK activation is the result of the increased AMP:ATP ratio. Itraconazole treatment increases the AMP:ATP (A) and ADP:ATP (B) ratio in HUVEC, as measured by LC-MS/MS. Cells were treated with 0.5 or 2 μM itraconazole for 2 min followed by metabolite extraction. Error bars represent SEMs of three independent experiments. A statistically significant increase in AMP:ATP or ADP:ATP was calculated by paired, one-tailed t test. *P < 0.05, ***P < 0.001. (C) Pretreatment of HUVEC with the CaMKKβ inhibitor STO-609 (30 min, 10 μM) does not prevent activation of AMPK by itraconazole (15 min, 2 μM), as opposed to the calcium ionophore ionomycin (15 min, 3 μM), indicating that itraconazole does not activate AMPK through a calcium/calmodulin/CaMKKβ-dependent pathway.

In addition, two commonly used cell lines which lack LKB1, A549 and HeLa (**Figure 2.20a)**, did not display any AMPK activation by itraconazole, and the effect on mTOR in these cell lines was also greatly diminished (**Figure 2.20b-d**), further demonstrating that AMPK activation is upstream of mTOR inhibition by itraconazole. In contrast to itraconazole, ionomycin was able to activate AMPK in A549 and HeLa cells, demonstrating that an increase in cytosolic calcium was able to induce AMPK activation in these cells and again suggesting that itraconazole does not act through a calcium-dependent mechanism (**Figure 2.20e**). Taken together, these results strongly suggest that activation of AMPK by itraconazole in HUVEC is caused by an increase in cellular AMP:ATP ratio, rather than through the calcium/calmodulin/CaMKKβ pathway.

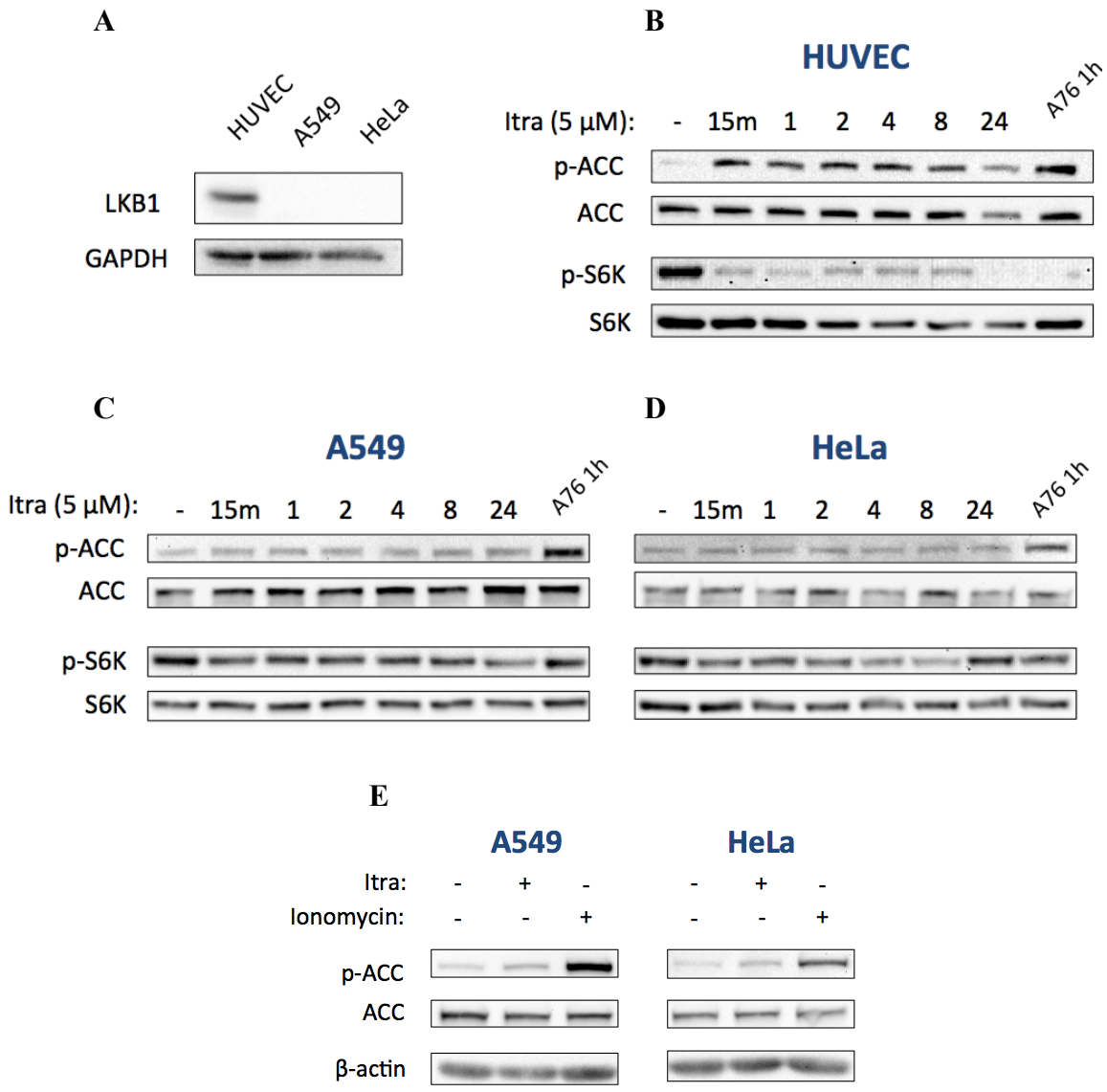

Figure 2.20: LKB1-deficient cells are insensitive to itraconazole. (A) A549 and HeLa, two commonly used cell lines which are reported to be LKB1-deficient, do not express LKB1 as measured by western blot. (B) HUVEC, (C) A549, and (D) HeLa cells were treated with 5 μM itraconazole for the indicated times (in hours except where indicated) or 100 μM A769662 for 1 hour. (E) A549 and HeLa cells were treated with either 5 μM itraconazole or 3 μM ionomycin for 15 minutes. Ionomycin activates AMPK in these cell lines while itraconazole does not.

VDAC1-/- cells are resistant to AMPK activation and mTOR inhibition by itraconazole

We next sought to determine whether the activation of AMPK by itraconazole can be explained by the observed binding to VDAC1. Because the efficiency of VDAC1 knockdown achieved in HUVEC by lentivirus was not high, we sought to generate VDAC1 null cells for further studies with itraconazole. However HUVEC are primary cells that only survive several passages in culture, rendering it unsuitable for such genetic manipulation as gene knockout. We thus turned to VDAC1 knockout MEFs which were generated previously[19]. VDAC1 knockout was complete as confirmed by Western blot (**Figure 2.21a**). Wild type and VDAC1-/- MEFs were treated in parallel with itraconazole and assessed for AMPK activation and mTOR inhibition by Western blot analysis. Consistent with what was seen in VDAC1 knockdown HUVEC, basal mTOR signaling appeared to be lower in VDAC1-/- cells than the wild type. In wild type MEFs, 5 μM itraconazole robustly activated AMPK, as measured by ACC phosphorylation, and also inhibited mTOR, as measured by S6K phosphorylation. Strikingly, VDAC1-/- cells were completely resistant to AMPK activation by 5 μM itraconazole, and they also showed significantly less mTOR inhibition (**Figure 2.21a**). The insensitivity to itraconazole was also sustained for up to 24 h, demonstrating that there is no change in the time course of AMPK activation in these cells. In contrast, 2DG, which inhibits glycolysis and thus should activate AMPK independently of VDAC1 status, was still able to activate AMPK in VDAC1-/- cells, demonstrating that the lack of AMPK response in VDAC1-/- cells is specific to itraconazole's mechanism (**Figure 2.21b**). These results clearly draw a direct link between VDAC1 function and AMPK activation/mTOR inhibition and strongly

suggest that direct binding to VDAC1 mediates the activation of AMPK and inhibition of mTOR by itraconazole.

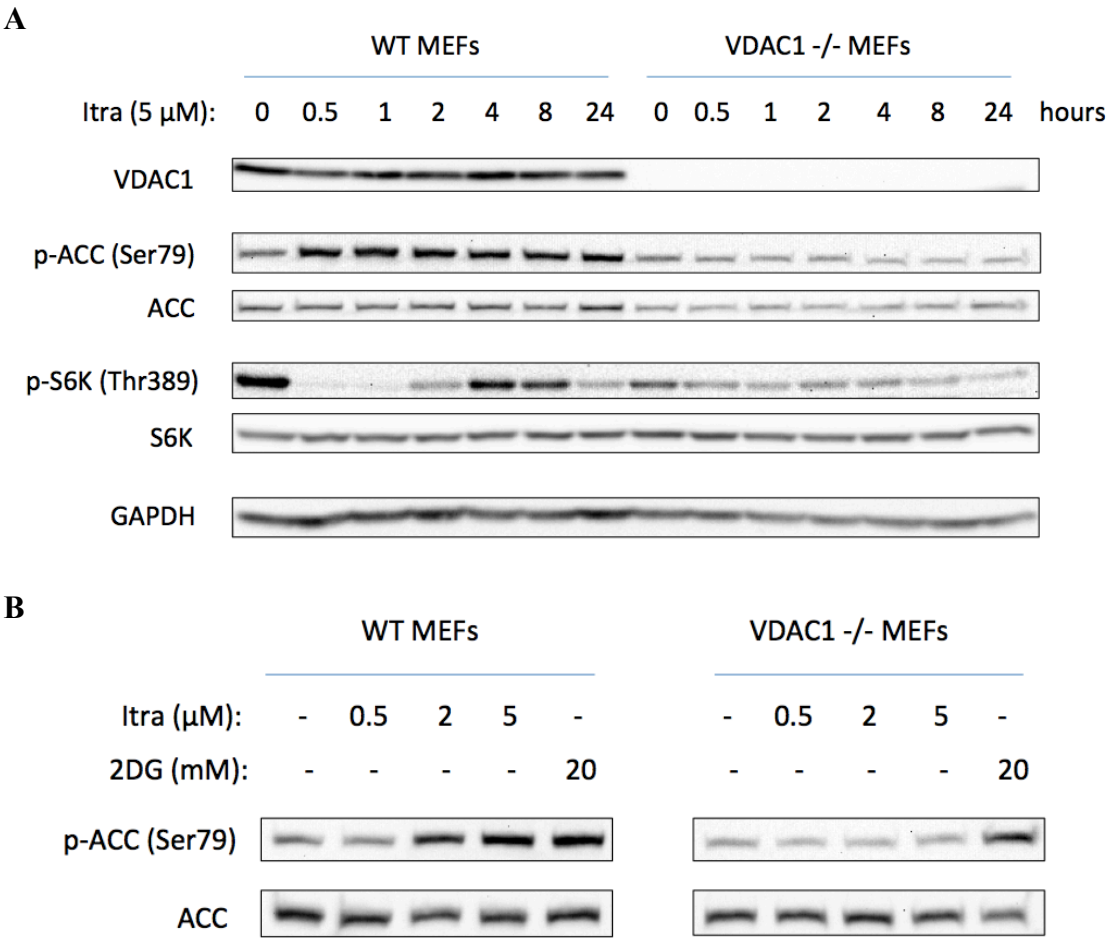

Figure 2.21: VDAC1-knockout cells are resistant to AMPK activation by itraconazole. (A) Itraconazole (5 μM) causes robust activation of AMPK and inhibition of mTOR in wild-type MEFs, whereas VDAC1-knockout (VDAC1−/−) MEFs treated with itraconazole display no activation of AMPK and markedly reduced inhibition of mTOR. (B) Itraconazole has no effect in VDAC1−/− cells, whereas 2DG activates AMPK in both WT and VDAC1−/− cells, demonstrating that the lack of AMPK activation in VDAC1−/− is specific to the mechanism of itraconazole.

A known VDAC inhibitor, erastin, also activates AMPK and inhibits mTOR and proliferation of HUVEC

It has been reported previously that the small molecule erastin also binds to VDAC[45]. We therefore tested whether erastin was also able to activate AMPK and inhibit mTOR in HUVEC. Cells were treated with a range of concentrations of erastin and itraconazole for 30 minutes before harvesting. Indeed, erastin dose-dependently increased AMPK activation as measured by ACC phosphorylation, similar to itraconazole, albeit with a significantly lower potency (**Figure 2.22a**). Erastin also inhibited mTOR signaling as measured by S6K phosphorylation. We then tested erastin for inhibition of HUVEC proliferation, and again found it to be active but less potent than itraconazole, with an IC_{50} of ~1.5 μM (**Figure 2.22b**). These results further suggest that binding to VDAC likely mediates the AMPK activation of both compounds. In support of this hypothesis, erastin also partially competed binding of the itraconazole probe to VDAC in HUVEC (**Figure 2.22c**), suggesting the two drugs likely bind to the same site on the channel.

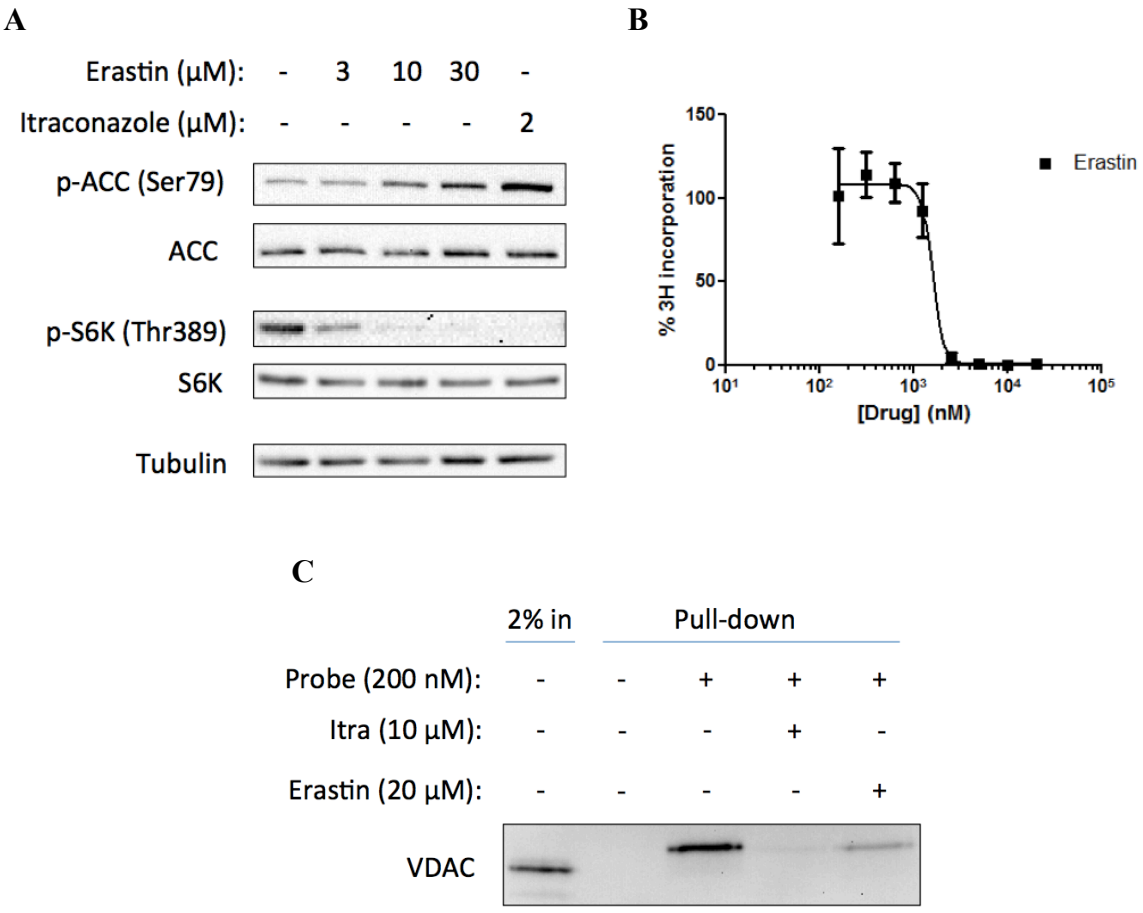

Figure 2.22: The known VDAC antagonist erastin induces effects similar to those of itraconazole in HUVEC. (A) HUVEC were treated with erastin for 30 min at the indicated concentrations. Erastin, similar to itraconazole, dose-dependently activates AMPK and inhibits mTOR in HUVEC. (B) Erastin also inhibits HUVEC proliferation, with an IC50 of about 1.5 μM. (C) Erastin competes with binding of the itraconazole probe to VDAC in HUVEC.

Correlation between VDAC1 binding and HUVEC inhibition by itraconazole analogs

One way of determining the physiological relevance of a drug target is to see whether there is a pharmacological correlation between binding of different analogs of the drug to the target and their cellular activity[46]. As previously reported, miconazole, terconazole, and fluconazole have IC_{50} values for HUVEC proliferation of about 2.5, 7, and >100 μM, respectively[8]. We thus performed the pull-down assay using pretreatment with high concentrations of these three drugs (20 μM miconazole/terconazole, 50 μM fluconazole) as competitors. Accordingly, 20 μM miconazole was able to partially compete with binding of the itraconazole probe to VDAC1, consistent with its moderate potency against HUVEC proliferation. However, terconazole and fluconazole were unable to compete with binding at the concentrations tested, suggesting that these less active analogs of itraconazole do not bind to VDAC1 appreciably (**Figure 2.23a**). In contrast, an analog of itraconazole that lacks the triazole moiety (triazole-deleted itraconazole or TD-itra) retains activity in HUVEC (**Figure 2.23b-d**) and was also able to compete with binding of the itraconazole probe to VDAC1. Further, the binding of these compounds to VDAC1 also correlated with their ability to activate AMPK (**Figure 2.23e**). Collectively, these results further support the notion that VDAC1 is a physiologically relevant target of itraconazole.

A

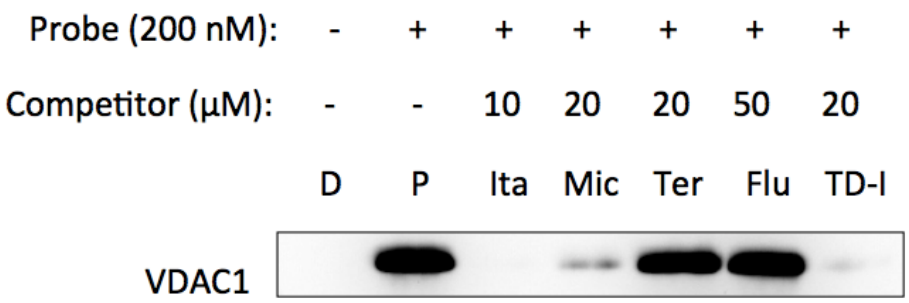

B

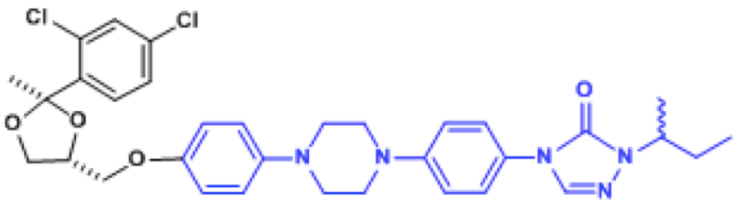

C

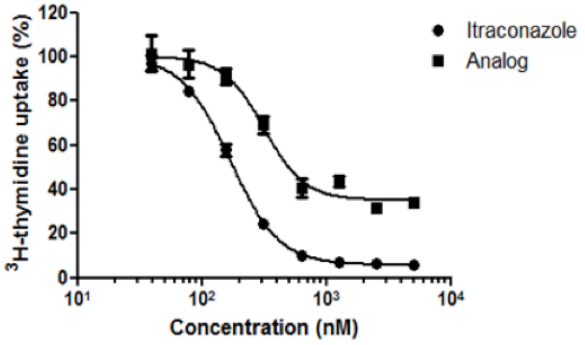

	Itraconazole	Analog
EC50	168.7	314.3

D

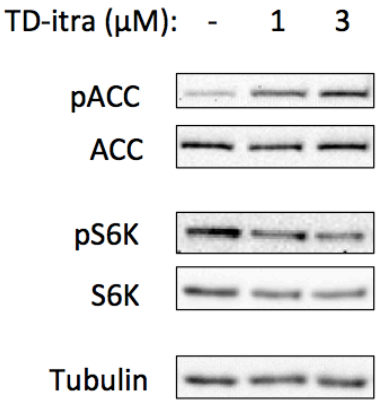

E

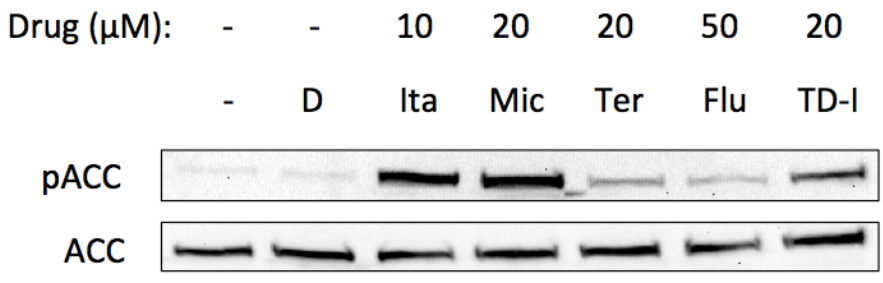

Figure 2.23: Inactive azoles do not bind VDAC1, but non-azole analog does. A) The ability of itraconazole-like molecules to bind to VDAC1 was assessed by their ability to compete with binding of the itraconazole probe to VDAC1. Cells were treated with DMSO alone (D), probe alone (P), or probe plus itraconazole (Ita), miconazole (Mic), terconazole (Ter), Fluconazole (Flu), or analog TD-itra (shown in panel b) at the indicated concentrations. B) Chemical structure of TD-itra. C) Dose-response curves of itraconazole and TD-itra against HUVEC proliferation. D) TD-itra is able to activate AMPK and inhibit mTOR in HUVEC after a 15-minute treatment. E) Compounds that bind to VDAC1 also activate AMPK.

Itraconazole increases the rate of calcium-induced mitochondrial swelling

It has previously been observed that erastin increases the permeability of isolated mitochondria to calcium ions (Wenzhi Tan and Marco Colombini, unpublished). Because VDAC is known to be the main point of passage in the OMM for calcium ions, the rate of calcium entry into mitochondria may also be considered a measure of VDAC function. Calcium entry through VDAC causes mitochondrial swelling, and the rate of this swelling, which is easily monitored by a change in absorbance at 400 nm, is thus proportional to the rate of calcium transport. We therefore tested whether itraconazole could also induce the same effects as erastin in this calcium-induced mitochondrial swelling assay. Freshly isolated rat liver mitochondria were preincubated with drugs for 10 minutes before addition of calcium and monitored at 400 nm. The absorbance was plotted over time, and the initial slope after calcium addition was considered the maximum rate of swelling. We found that itraconazole caused a dose-dependent increase in the rate of calcium-induced mitochondrial swelling, similar to erastin (**Figure 2.24**). The fact that another VDAC inhibitor exhibited similar effects on AMPK and mTOR in endothelial cells as well as calcium permeability in isolated mitochondria provides strong evidence that inhibition of VDAC mediates these activities of itraconazole as well as erastin.

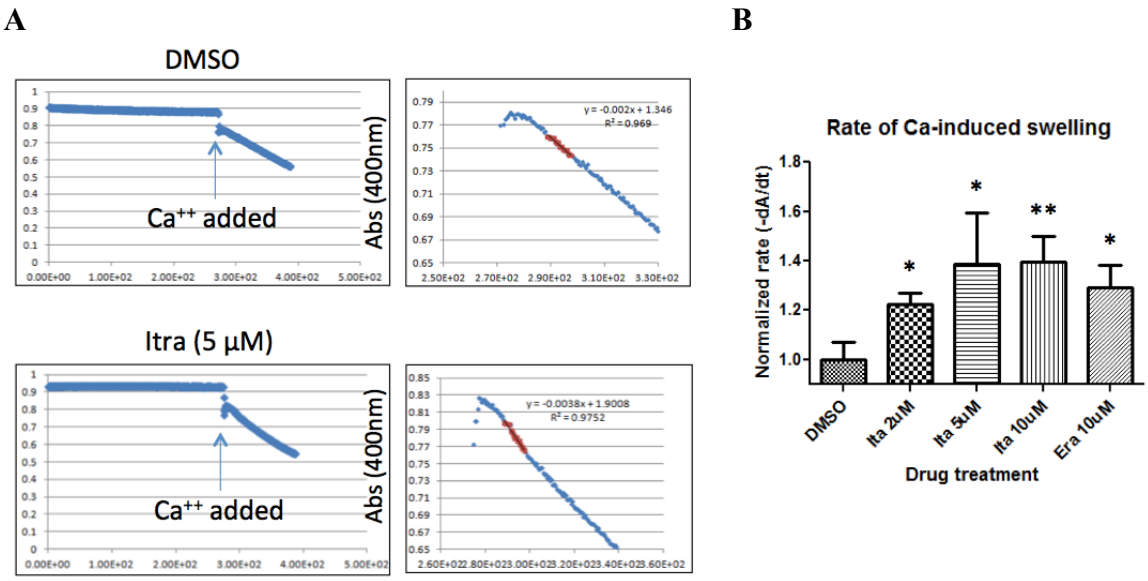

Figure 2.24: Itraconazole and erastin increase the rate of calcium–induced mitochondrial swelling. A) Purified rat liver mitochondria were preincubated with itraconazole or erastin at the concentrations shown for 10 minutes before the addition of calcium, and mitochondrial swelling was monitored at 400 nm. The initial rate of swelling was calculated by linear fitting. A representative plot of absorbance vs. time is shown for DMSO treated and 5 µM itraconazole-treated mitochondria. B) Itraconazole and erastin significantly increase the rate of calcium-induced mitochondrial swelling as compared to DMSO treatment. Error bars represent SEM of 4-5 experimental replicates. Statistically significant increase in swelling rate was calculated by an unpaired, one-tailed t-test. * $p < 0.05$, ** $p < 0.01$.

In vitro experiments with VDAC reconstituted in planar lipid bilayers

To determine whether the effects of itraconazole observed in cellular assays were due to a direct effect on intrinsic VDAC channel activity, we initiated a collaboration with Drs. Tatiana Rostovtseva and Sergei Bezrukov at the National Institutes of Health who specialize in electrophysiological measurements of VDAC channels. Experiments were performed with single channels to measure the conductance of the open and closed states of the channel, as well as the frequency of channel closure, in the presence of applied voltage with and without itraconazole. Single channel experiments were also performed in the presence of dimeric tubulin, a soluble factor that has been shown to directly block VDAC channels *in vitro*[47], to determine whether itraconazole affected the interaction between VDAC and tubulin. In addition to the single channel experiments, multichannel experiments were also performed to measure the averaged gating properties of many channels.

In the multichannel experiments, initial experiments performed at pH 7.4 showed a small but reproducible effect of itraconazole addition, which was to increase G_{min}, or the minimum conductance achieved at high applied voltages (i.e. voltage gating) (**Figure 2.25a**). Because G_{min} was already high under these conditions (channels were not gating significantly), making it difficult to detect a further increase in G_{min}, we changed the conditions to increase gating by either decreasing the pH of the buffer (**Figure 2.25b**) or adding tubulin before drug (**Figure 2.25c**). In both cases, we were on multiple occasions able to observe a significant reversal of gating activity after itraconazole addition. Unfortunately, these effects were not reproducible in later experiments, and many attempts to determine the cause of the lost effect were unsuccessful.

A

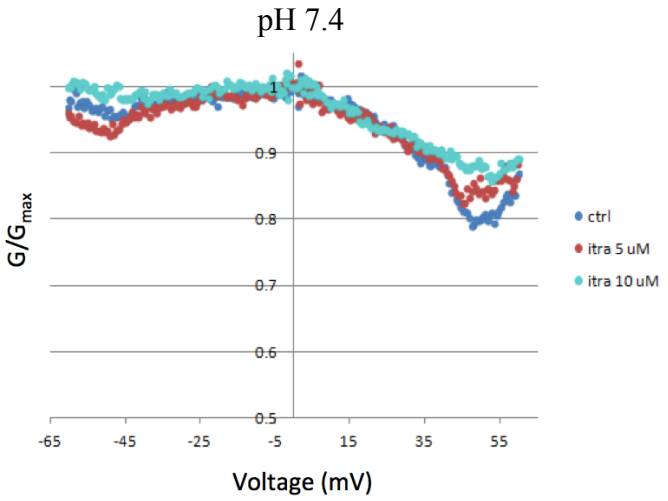
pH 7.4
G/Gmax
1
0.9
0.8
0.7
0.6
0.5
-65
-45
-25
-5
15
35
55
Voltage (mV)
ctrl
itra 5 uM
itra 10 uM

B

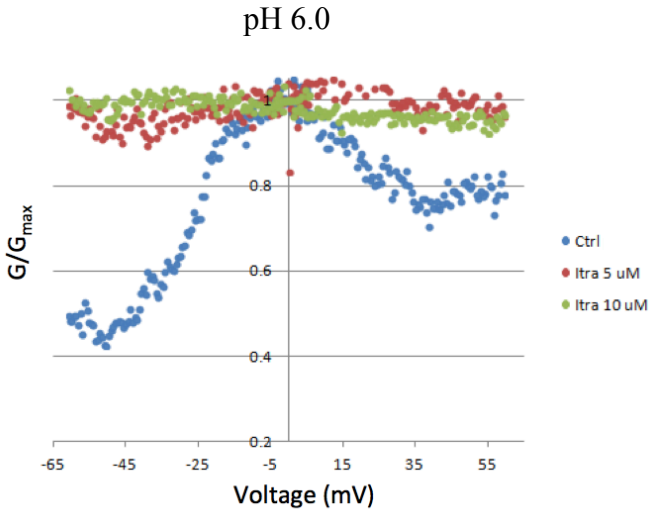
pH 6.0
G/Gmax
1
0.8
0.6
0.4
0.2
-65
-45
-25
-5
15
35
55
Voltage (mV)
Ctrl
Itra 5 uM
Itra 10 uM

C

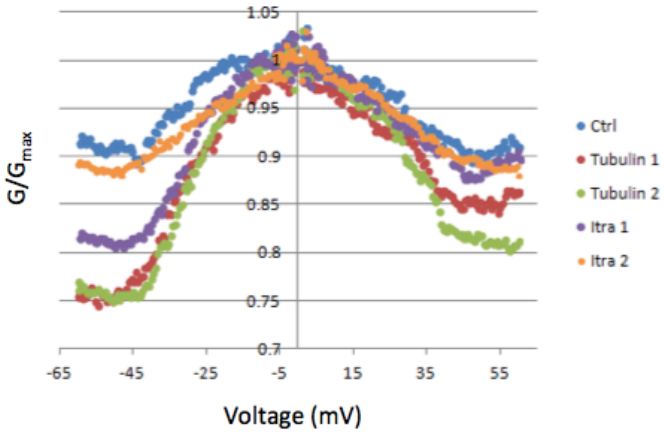
pH 7.4
G/Gmax
1.05
1
0.95
0.9
0.85
0.8
0.75
0.7
-65
-45
-25
-5
15
35
55
Voltage (mV)
Ctrl
Tubulin 1
Tubulin 2
Itra 1
Itra 2

Figure 2.25: Effect of itraconazole on purified VDAC channels in multichannel experiments. Conductance vs. Voltage (G/V) plots are used to visualize channel gating activity, i.e. the voltage-dependent closure of the channels. On the x-axis is the voltage applied to the channels (in mV), and on the y-axis, G/G_0 is the observed conductance normalized to the conductance of the open state of the channel ($G_0 = 1$). A) Itraconazole treatment lead to a small increase in conductance at high applied voltages (increased G_{min}); however the change was difficult to detect because the channels did not show significant gating activity before drug addition ($G_{min} \sim 0.8$). B) Reducing the pH of the buffer to 6.0 significantly increases channel gating activity ($G_{min} \sim 0.4$) and therefore the increase in G_{min} after itraconazole treatment is more pronounced. C) Addition of tubulin (3.4 nM x 2 additions) similarly increases channel gating activity ($G_{min} \sim 0.75$), and subsequent addition of itraconazole (5 μM x 2 additions) reverses the tubulin-induced gating back to control levels.

In the single channel experiments, we decreased the pH to ~6 to induce measurable gating activity at +/-50-60mV. Each voltage condition was recorded for approximately 10 minutes, and the T_{open} (channel open time), frequency of closure, and closed state conductances were measured. After recording each voltage for the control, DMSO or itraconazole (500 nM-10 μM) was added to both sides of the membrane. Several experiments (n = 9) were performed with a single VDAC channel at pH 6. There was a large degree of variability in gating activity from one channel to another, where some channels had measurable gating activity at 50 mV while others did not close until 60 mV was applied. The direction and degree of gating asymmetry was also inconsistent, but this may be due in part to the sign of the voltage being applied at the time of channel insertion. In order to compare results from one experiment to another, the voltage that induced the most closures was used for measurements (generally negative voltage at cis side), and the frequency of closure (closures per minute, or CPM) was normalized to the control recorded at the beginning of each experiment.

We found that in the majority of experiments, there was an increase in the frequency of closures and a corresponding decrease in T_{open} after itraconazole addition (**Figure 2.26a**). The effect was fairly consistent, but the degree of the effect was highly variable, ranging from 50-500% increase in CPM. In two out of nine experiments there was no effect of itraconazole addition, which could potentially be explained by isoform selectivity as the rat liver VDAC used contains a mixture of isoforms. Two experiments were also performed with DMSO alone, and a small increase in CPM (between 25-75%) was observed. However, in one experiment where the channel was recorded over an extended period of time with no drug addition, there was also a large increase in the

frequency of channel closures (**Figure 2.26b**). The fact that such an increase was not observed in all of the experiments indicates that this increase in gating over time does not occur with all channels; however, the possibility of such a large change in channel activity throughout the experiment makes it practically impossible to differentiate drug effects from fluctuating channel activity. Therefore, we could not conclude whether there was an effect of itraconazole on the intrinsic VDAC channel activity in these experiments.

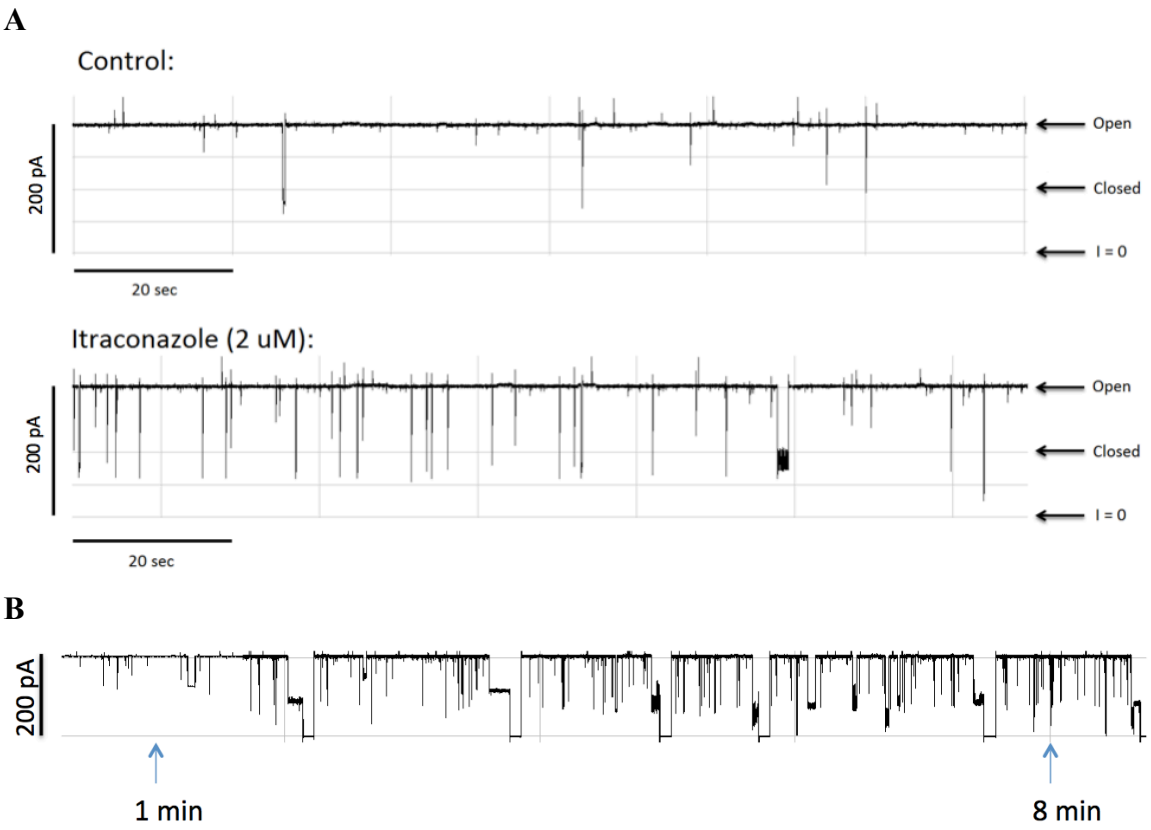

Figure 2.26: Effects of itraconazole on individual VDAC channels. Channel recordings showing the conductance (y-axis) over time (x-axis), where channel closure is detected as a downward spike in conductance. A) Compared with the control trace, the itraconazole-treated channel displays an increased frequency of channel closures. B) The frequency of closures of this particular channel increased dramatically over time on its own, without any drug addition.

To determine whether itraconazole may be affecting VDAC activity indirectly by altering lipid properties of the membrane, its effects on Gramicidin A channels, which are highly sensitive to any membrane perturbations, were measured. The voltage applied was 150mV, and because of the low conductance and relatively long lifetime of these channels, the recordings were filtered at 200 Hz instead of 500 Hz. Channel lifetime and conductance were measured for control, DMSO (0.1%), and 10 μM itraconazole (0.2% DMSO) treatments. There was no obvious change in any of the treatment groups by eye. After data analysis, there appeared to be a very slight increase in channel lifetime and low conductance channel formation, but these effects were very small (**Figure 2.27**). These results suggest that itraconazole is either not altering membrane properties, or is not being effectively delivered to membranes.

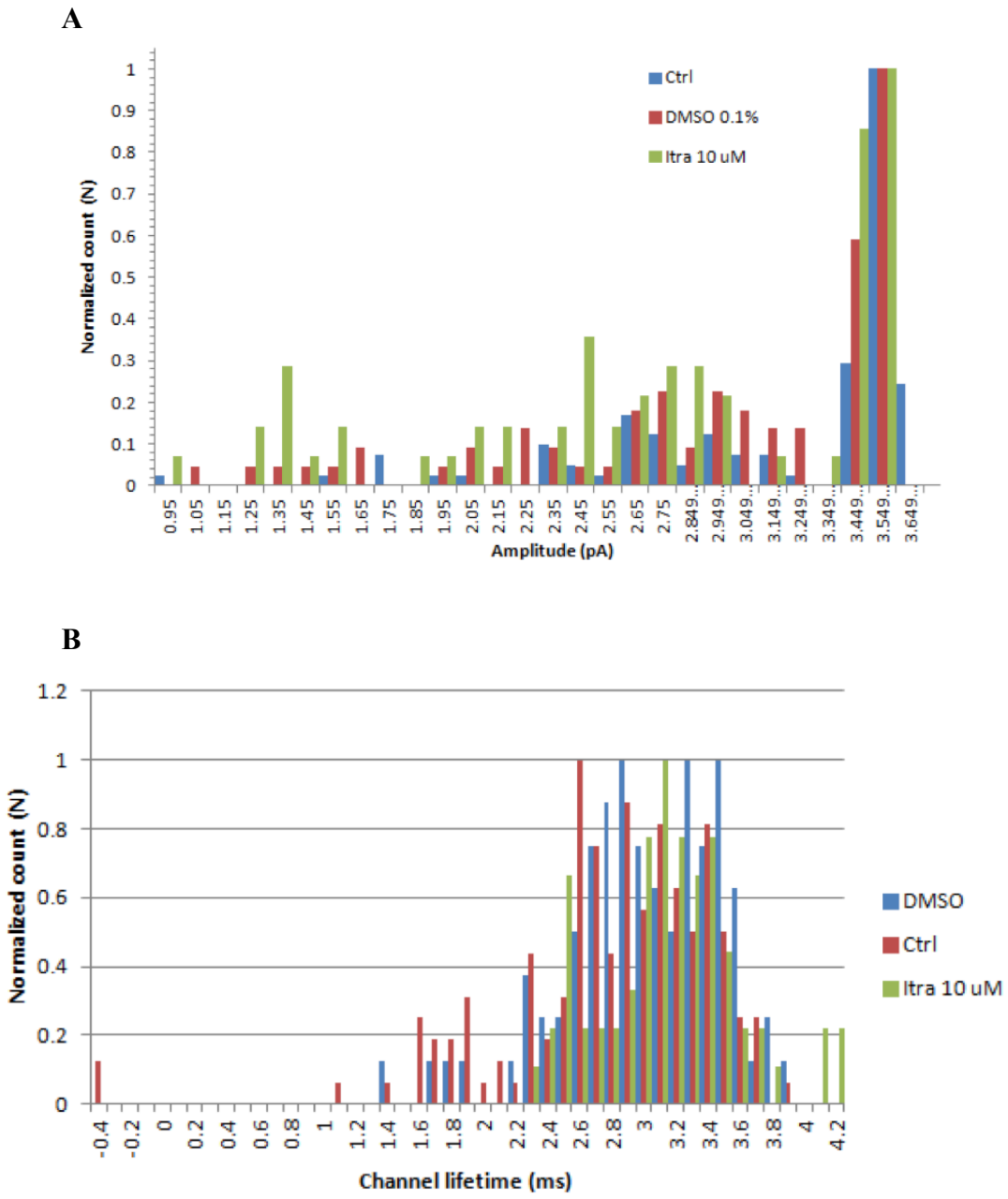

Figure 2.27: Effects of itraconazole on Gramicidin A channel conductance and lifetime. Histograms depicting the frequency of gramicidin channel conductance (A) and lifetime (B). No significant change was observed upon DMSO or itraconazole addition.

2.5: Discussion

Since itraconazole was identified as a novel inhibitor of angiogenesis, multiple newly initiated Phase 2 clinical studies and retrospective analyses have shown efficacy of itraconazole in the treatment of different types of cancer, suggesting that it is a promising antiangiogenic and anticancer drug candidate. Our previous mechanistic investigation ruled out lanosterol 14α-demethylase, the molecular target mediating the antifungal activity of itraconazole, as its antiangiogenic target. Using a phenotypic approach starting with the effect of itraconazole on the G1-S cell cycle transition of endothelial cells, we found that itraconazole specifically inhibited the mTOR signaling pathway by downregulating the kinase activity of mTORC1. The underlying molecular mechanism of inhibition of endothelial cell proliferation by itraconazole, however, has remained largely unknown. In the present study, we employed a photoaffinity labeling approach using a biologically active itraconazole photoaffinity probe in live cells to identify the mitochondrial outer membrane channel VDAC1 as a molecular target of itraconazole. Importantly, we were able to establish a previously unknown link between VDAC1 and mTOR via modulation of cellular AMP/ATP ratio and the activation of AMPK, elucidating the molecular basis of inhibition of mTOR activity by itraconazole.

Classical approaches for direct identification of small molecule targets have largely relied on affinity-based methods[46]; however, for such an approach to be successful, the target protein must retain its ability to bind the small molecule outside of the native cellular environment. This is particularly problematic for integral membrane proteins, which often do not retain their native conformation upon cell lysis. The development of cell-permeable photoaffinity labels has helped to circumvent this issue by

allowing a probe to bind covalently to its target protein within the native environment of the cell, so that upon cell lysis the interaction is preserved and the target protein can be easily detected and isolated[20]. In this study, we utilized information from our previous structure-activity studies of itraconazole[31,32] to design a cell-active photoaffinity probe, which enabled the identification of VDAC1 as a direct protein target of itraconazole. Had we used the conventional affinity pull-down approach, we may not have succeeded in this endeavor.

It was once thought that the outer mitochondrial membrane (OMM) was essentially freely permeable, or "leaky", to most small molecules. But more recently it has become clear that the permeability of the OMM is actually regulated by the channels that transport these molecules, the so-called Voltage Dependent Anion Channels[48]. It was predicted in 1979 that these channels would be involved in regulating mitochondrial metabolism[49], and in the ensuing decades numerous studies have proven this to be true[50–54]. The name of the channel is somewhat misleading, as although it was originally thought to be anion-selective, VDAC has also been shown to transport cations such as calcium, as well as numerous small metabolites including ATP, ADP, NADH, pyruvate, and others[55,56]. The voltage-dependent property of the channel when reconstituted into planar lipid bilayers leads to channel closure in the presence of ~40-50 mV applied voltage. However, the physiologic potential across the OMM is a matter of debate, and it remains unclear how this voltage-dependence translates to the signals which induce channel closure in the cell. The selectivity of VDAC channels is known to switch from anions to cations upon channel closure due to electrostatic changes within the pore; therefore, permeability to anions (such as ATP) and cations (such as calcium) are

inversely correlated[55,57]. Thus, the observation that itraconazole caused a decrease in cellular ATP levels and also increased mitochondrial permeability to calcium ions is consistent with this inverse relationship of VDAC charge selectivity.

The discovery that itraconazole binds to a mitochondrial protein involved in regulating metabolism made sense in the context of the drug's ability to activate AMPK. Mitochondria are critical for ATP production, and many small molecules which activate AMPK have been shown to inhibit mitochondrial function, including metformin, resveratrol, berberine, and rotenone [58–62]. In order to produce ATP, ADP must enter the mitochondria through VDAC in the outer membrane and ANT (adenine nucleotide translocase) in the inner membrane, be converted to ATP through oxidative phosphorylation, and then exit the mitochondria again through ANT and VDAC. Indeed, it has been reported recently that VDAC closure reduces mitochondrial energy conversion and decreases cytosolic ATP:ADP ratios[37]. It is therefore logical that disruption of VDAC function by small molecules such as itraconazole would lead to a drop in cellular ATP levels, causing an increase in AMP:ATP ratio and the ensuing activation of AMPK.

The connection between AMPK, mTOR, and angiogenesis has been firmly established in a number of previous studies. AMPK can regulate mTOR via two alternative pathways, mediated by the tumor suppressor protein TSC2 and the mTOR binding partner raptor[38,40]. Thus, upon phosphorylation by AMPK, TSC2 has an enhanced GTPase activity for its substrate Rheb, leading to mTOR inhibition. Unlike TSC2, phosphorylation of raptor leads to its association with 14-3-3, decreasing mTOR activity. Interestingly, we found activation of AMPK by itraconazole increased

phosphorylation of raptor but did not affect phosphorylation of TSC2. However, phosphorylation of raptor alone has been shown to be sufficient for inhibition of mTOR by AMPK in the absence of TSC2[40], so it is unnecessary for AMPK to affect mTOR activity via both TSC2 and raptor simultaneously. Thus, these results support the hypothesis that AMPK activation by itraconazole is upstream of mTOR inhibition.

Several drugs modulating the AMPK pathway have also been evaluated as potential antiangiogenic and anticancer agents. The widely prescribed, AMPK-activating antidiabetic drug, metformin, has been shown to inhibit angiogenesis *in vitro* and *in vivo*[63] and is currently being evaluated in several clinical trials for various types of cancer[64]. However, the concentrations of metformin required to activate AMPK in HUVEC are at least 1,000 times higher than those required of itraconazole (in the range of low mM[63]), suggesting that itraconazole might be significantly more effective than metformin at inhibiting angiogenesis in patients. Another drug in trials for cancer, the natural product curcumin, has also been shown to activate AMPK and inhibit mTOR[65–67]. Interestingly, a recent study demonstrated that it also interferes with VDAC1 function[68], similar to itraconazole.

In this study, we have demonstrated that the binding of itraconazole to VDAC1 mediates its AMPK activation in endothelial cells. However, exactly how itraconazole binding affects VDAC1 function is a question that remains to be answered. *In vitro* VDAC activity assays, electrophysiological and crystallographic studies have been initiated, but are complicated by the fact that itraconazole is virtually insoluble in aqueous solution, and thus measurements of binding outside of the environment of the cell are difficult. This speaks to a major advantage of the live-cell photoaffinity labeling

approach, which is particularly well suited for hydrophobic molecules that would likely not interact with their target in solution. Another possibility is that itraconazole binding to VDAC1 does not affect its channel activity directly, but either requires or disrupts the interaction of another protein, with functional consequences. VDAC has been reported to interact with other proteins of diverse functions, including tubulin, hexokinase, ANT, Bcl-2, Bcl-XL, cyclophilin D, and TSPO, providing a multitude of other potential regulatory mechanisms[47,69–73]. Interestingly, itraconazole was shown to be synergistic with the cyclophilin-targeting drug cyclosporine A for angiogenesis inhibition[74], so it is possible that simultaneous inhibition of VDAC1 and cyclophilin D could be the cause of this observed synergy.

In summary, we have identified VDAC1 as a direct target of itraconazole and the AMPK signaling pathway as a key mediator of its inhibition of mTOR and endothelial cell proliferation. Thus, binding of itraconazole to VDAC1 leads to a decrease in mitochondrial ATP production and a corresponding increase in AMP:ATP ratio, which in turn leads to activation of AMPK. Phosphorylation of raptor by AMPK then causes inhibition of mTOR. These results elucidated a previously unknown connection between the mitochondrial VDAC1 channel and mTOR. The identification of VDAC1 as the molecular target of itraconazole will also facilitate the future discovery and development of novel angiogenesis inhibitors.

2.6: References

1. Carmeliet, P. Angiogenesis in health and disease. *Nat. Med.* **9,** 653–660 (2003).
2. Distler, J. H. W. *et al.* Angiogenic and angiostatic factors in the molecular control of angiogenesis. *Q. J. Nucl. Med. Off. Publ. Ital. Assoc. Nucl. Med. AIMN Int. Assoc. Radiopharmacol. IAR* **47,** 149–161 (2003).
3. Folkman, J. Tumor angiogenesis: therapeutic implications. *N. Engl. J. Med.* **285,** 1182–1186 (1971).
4. Franson, P. J. & Lapka, D. V. Antivascular endothelial growth factor monoclonal antibody therapy: a promising paradigm in colorectal cancer. *Clin. J. Oncol. Nurs.* **9,** 55–60 (2005).
5. Jain, R. K. Tumor angiogenesis and accessibility: role of vascular endothelial growth factor. *Semin. Oncol.* **29,** 3–9 (2002).
6. Fine, S. L., Martin, D. F. & Kirkpatrick, P. Pegaptanib sodium. *Nat. Rev. Drug Discov.* **4,** 187–188 (2005).
7. Cohen, R. B. & Oudard, S. Antiangiogenic therapy for advanced renal cell carcinoma: management of treatment-related toxicities. *Invest. New Drugs* **30,** 2066–2079 (2012).
8. Chong, C. R. *et al.* Inhibition of angiogenesis by the antifungal drug itraconazole. *ACS Chem. Biol.* **2,** 263–270 (2007).
9. Sporanox [package insert]. Titusville, NJ: Janssen Pharmaceuticals, Inc.; 2014.
10. Aftab, B. T., Dobromilskaya, I., Liu, J. O. & Rudin, C. M. Itraconazole inhibits angiogenesis and tumor growth in non-small cell lung cancer. *Cancer Res.* **71,** 6764–6772 (2011).
11. Kim, J. *et al.* Itraconazole, a commonly used antifungal that inhibits Hedgehog pathway activity and cancer growth. *Cancer Cell* **17,** 388–399 (2010).
12. Rudin, C. M. *et al.* Phase 2 study of pemetrexed and itraconazole as second-line therapy for metastatic nonsquamous non-small-cell lung cancer. *J. Thorac. Oncol. Off. Publ. Int. Assoc. Study Lung Cancer* **8,** 619–623 (2013).

13. Antonarakis, E. S. *et al.* Repurposing itraconazole as a treatment for advanced prostate cancer: a noncomparative randomized phase II trial in men with metastatic castration-resistant prostate cancer. *The oncologist* **18,** 163–173 (2013).
14. Kim, D. J. *et al.* Open-label, exploratory phase II trial of oral itraconazole for the treatment of basal cell carcinoma. *J. Clin. Oncol. Off. J. Am. Soc. Clin. Oncol.* **32,** 745–751 (2014).
15. Lamb, D. C. *et al.* Characteristics of the heterologously expressed human lanosterol 14alpha-demethylase (other names: P45014DM, CYP51, P45051) and inhibition of the purified human and Candida albicans CYP51 with azole antifungal agents. *Yeast Chichester Engl.* **15,** 755–763 (1999).
16. Trösken, E. R. *et al.* Comparison of lanosterol-14 alpha-demethylase (CYP51) of human and Candida albicans for inhibition by different antifungal azoles. *Toxicology* **228,** 24–32 (2006).
17. Xu, J., Dang, Y., Ren, Y. R. & Liu, J. O. Cholesterol trafficking is required for mTOR activation in endothelial cells. *Proc. Natl. Acad. Sci. U. S. A.* **107,** 4764–4769 (2010).
18. Head, S. A. *et al.* Antifungal drug itraconazole targets VDAC1 to modulate the AMPK/mTOR signaling axis in endothelial cells. *Proc. Natl. Acad. Sci. U. S. A.* **112,** E7276–7285 (2015).
19. Wu, S., Sampson, M. J., Decker, W. K. & Craigen, W. J. Each mammalian mitochondrial outer membrane porin protein is dispensable: effects on cellular respiration. *Biochim. Biophys. Acta* **1452,** 68–78 (1999).
20. Mackinnon, A. L. & Taunton, J. Target Identification by Diazirine Photo-Cross-linking and Click Chemistry. *Curr. Protoc. Chem. Biol.* **1,** 55–73 (2009).
21. Yang, X. *et al.* A public genome-scale lentiviral expression library of human ORFs. *Nat. Methods* **8,** 659–661 (2011).
22. Keinan, N., Tyomkin, D. & Shoshan-Barmatz, V. Oligomerization of the mitochondrial protein voltage-dependent anion channel is coupled to the induction of apoptosis. *Mol. Cell. Biol.* **30,** 5698–5709 (2010).

23. Abu-Hamad, S., Sivan, S. & Shoshan-Barmatz, V. The expression level of the voltage-dependent anion channel controls life and death of the cell. *Proc. Natl. Acad. Sci. U. S. A.* **103,** 5787–5792 (2006).

24. Shryock, J. C., Rubio, R. & Berne, R. M. Extraction of adenine nucleotides from cultured endothelial cells. *Anal. Biochem.* **159,** 73–81 (1986).

25. Naldini, L. *et al.* In vivo gene delivery and stable transduction of nondividing cells by a lentiviral vector. *Science* **272,** 263–267 (1996).

26. Sample, V., Ramamurthy, S., Gorshkov, K., Ronnett, G. V. & Zhang, J. Polarized Activities of AMPK and BRSK in Primary Hippocampal Neurons. *Mol. Biol. Cell* (2015). doi:10.1091/mbc.E14-02-0764

27. Tsou, P., Zheng, B., Hsu, C.-H., Sasaki, A. T. & Cantley, L. C. A fluorescent reporter of AMPK activity and cellular energy stress. *Cell Metab.* **13,** 476–486 (2011).

28. Siskind, L. J., Kolesnick, R. N. & Colombini, M. Ceramide channels increase the permeability of the mitochondrial outer membrane to small proteins. *J. Biol. Chem.* **277,** 26796–26803 (2002).

29. Palmieri, F. & De Pinto, V. Purification and properties of the voltage-dependent anion channel of the outer mitochondrial membrane. *J. Bioenerg. Biomembr.* **21,** 417–425 (1989).

30. Rostovtseva, T. K. *et al.* α-Synuclein Shows High Affinity Interaction with Voltage-dependent Anion Channel, Suggesting Mechanisms of Mitochondrial Regulation and Toxicity in Parkinson Disease. *J. Biol. Chem.* **290,** 18467–18477 (2015).

31. Shi, W., Nacev, B. A., Bhat, S. & Liu, J. O. Impact of Absolute Stereochemistry on the Antiangiogenic and Antifungal Activities of Itraconazole. *ACS Med. Chem. Lett.* **1,** 155–159 (2010).

32. Shi, W. *et al.* Itraconazole side chain analogues: structure-activity relationship studies for inhibition of endothelial cell proliferation, vascular endothelial growth factor receptor 2 (VEGFR2) glycosylation, and hedgehog signaling. *J. Med. Chem.* **54,** 7363–7374 (2011).

33. Rufer, A. C. *et al.* The crystal structure of carnitine palmitoyltransferase 2 and implications for diabetes treatment. *Struct. Lond. Engl. 1993* **14,** 713–723 (2006).

34. Bay, D. C., Hafez, M., Young, M. J. & Court, D. A. Phylogenetic and coevolutionary analysis of the β-barrel protein family comprised of mitochondrial porin (VDAC) and Tom40. *Biochim. Biophys. Acta* **1818,** 1502–1519 (2012).

35. Messina, A., Reina, S., Guarino, F. & De Pinto, V. VDAC isoforms in mammals. *Biochim. Biophys. Acta* **1818,** 1466–1476 (2012).

36. Lemasters, J. J., Holmuhamedov, E. L., Czerny, C., Zhong, Z. & Maldonado, E. N. Regulation of mitochondrial function by voltage dependent anion channels in ethanol metabolism and the Warburg effect. *Biochim. Biophys. Acta* **1818,** 1536–1544 (2012).

37. Maldonado, E. N. & Lemasters, J. J. ATP/ADP ratio, the missed connection between mitochondria and the Warburg effect. *Mitochondrion* **19 Pt A,** 78–84 (2014).

38. Laplante, M. & Sabatini, D. M. mTOR signaling at a glance. *J. Cell Sci.* **122,** 3589–3594 (2009).

39. Hardie, D. G. AMP-activated protein kinase: an energy sensor that regulates all aspects of cell function. *Genes Dev.* **25,** 1895–1908 (2011).

40. Gwinn, D. M. *et al.* AMPK phosphorylation of raptor mediates a metabolic checkpoint. *Mol. Cell* **30,** 214–226 (2008).

41. Tamás, P. *et al.* Regulation of the energy sensor AMP-activated protein kinase by antigen receptor and Ca2+ in T lymphocytes. *J. Exp. Med.* **203,** 1665–1670 (2006).

42. Davies, S. P., Sim, A. T. & Hardie, D. G. Location and function of three sites phosphorylated on rat acetyl-CoA carboxylase by the AMP-activated protein kinase. *Eur. J. Biochem. FEBS* **187,** 183–190 (1990).

43. Xiao, B. *et al.* Structural basis of AMPK regulation by small molecule activators. *Nat. Commun.* **4,** 3017 (2013).

44. Carling, D., Sanders, M. J. & Woods, A. The regulation of AMP-activated protein kinase by

upstream kinases. *Int. J. Obes. 2005* **32 Suppl 4,** S55–59 (2008).

45. Yagoda, N. *et al.* RAS-RAF-MEK-dependent oxidative cell death involving voltage-dependent anion channels. *Nature* **447,** 864–868 (2007).
46. Titov, D. V. & Liu, J. O. Identification and validation of protein targets of bioactive small molecules. *Bioorg. Med. Chem.* **20,** 1902–1909 (2012).
47. Rostovtseva, T. K. *et al.* Tubulin binding blocks mitochondrial voltage-dependent anion channel and regulates respiration. *Proc. Natl. Acad. Sci. U. S. A.* **105,** 18746–18751 (2008).
48. Colombini, M. VDAC: the channel at the interface between mitochondria and the cytosol. *Mol. Cell. Biochem.* **256-257,** 107–115 (2004).
49. Colombini, M. A candidate for the permeability pathway of the outer mitochondrial membrane. *Nature* **279,** 643–645 (1979).
50. Maldonado, E. N. *et al.* Voltage-dependent anion channels modulate mitochondrial metabolism in cancer cells: regulation by free tubulin and erastin. *J. Biol. Chem.* **288,** 11920–11929 (2013).
51. Shoshan-Barmatz, V., Israelson, A., Brdiczka, D. & Sheu, S. S. The voltage-dependent anion channel (VDAC): function in intracellular signalling, cell life and cell death. *Curr. Pharm. Des.* **12,** 2249–2270 (2006).
52. Lemasters, J. J. & Holmuhamedov, E. Voltage-dependent anion channel (VDAC) as mitochondrial governator--thinking outside the box. *Biochim. Biophys. Acta* **1762,** 181–190 (2006).
53. Lemasters, J. J. Modulation of mitochondrial membrane permeability in pathogenesis, autophagy and control of metabolism. *J. Gastroenterol. Hepatol.* **22 Suppl 1,** S31–37 (2007).
54. Kholmukhamedov, E. L. *et al.* [The role of the voltage-dependent anion channels in the outer membrane of mitochondria in the regulation of cellular metabolism]. *Biofizika* **55,** 822–833 (2010).
55. Hodge, T. & Colombini, M. Regulation of metabolite flux through voltage-gating of VDAC

channels. *J. Membr. Biol.* **157,** 271–279 (1997).

56. Rostovtseva, T. & Colombini, M. ATP flux is controlled by a voltage-gated channel from the mitochondrial outer membrane. *J. Biol. Chem.* **271,** 28006–28008 (1996).
57. Tan, W. & Colombini, M. VDAC closure increases calcium ion flux. *Biochim. Biophys. Acta* **1768,** 2510–2515 (2007).
58. Viollet, B. *et al.* Cellular and molecular mechanisms of metformin: an overview. *Clin. Sci. Lond. Engl. 1979* **122,** 253–270 (2012).
59. Ferretta, A. *et al.* Effect of resveratrol on mitochondrial function: implications in parkin-associated familiar Parkinson's disease. *Biochim. Biophys. Acta* **1842,** 902–915 (2014).
60. Pereira, G. C. *et al.* Mitochondrially targeted effects of berberine [Natural Yellow 18, 5,6-dihydro-9,10-dimethoxybenzo(g)-1,3-benzodioxolo(5,6-a) quinolizinium] on K1735-M2 mouse melanoma cells: comparison with direct effects on isolated mitochondrial fractions. *J. Pharmacol. Exp. Ther.* **323,** 636–649 (2007).
61. Pung, Y. F. *et al.* Mitochondrial oxidative stress corrupts coronary collateral growth by activating adenosine monophosphate activated kinase-α signaling. *Arterioscler. Thromb. Vasc. Biol.* **33,** 1911–1919 (2013).
62. Hawley, S. A. *et al.* Use of cells expressing gamma subunit variants to identify diverse mechanisms of AMPK activation. *Cell Metab.* **11,** 554–565 (2010).
63. Soraya, H. *et al.* Anti-angiogenic Effects of Metformin, an AMPK Activator, on Human Umbilical Vein Endothelial Cells and on Granulation Tissue in Rat. *Iran. J. Basic Med. Sci.* **15,** 1202–1209 (2012).
64. He, H. *et al.* Metformin, an old drug, brings a new era to cancer therapy. *Cancer J. Sudbury Mass* **21,** 70–74 (2015).
65. Beevers, C. S., Li, F., Liu, L. & Huang, S. Curcumin inhibits the mammalian target of rapamycin-mediated signaling pathways in cancer cells. *Int. J. Cancer J. Int. Cancer* **119,** 757–764 (2006).

66. Kang, O. H. *et al.* Curcumin decreases oleic acid-induced lipid accumulation via AMPK phosphorylation in hepatocarcinoma cells. *Eur. Rev. Med. Pharmacol. Sci.* **17,** 2578–2586 (2013).

67. Xiao, K. *et al.* Curcumin induces autophagy via activating the AMPK signaling pathway in lung adenocarcinoma cells. *J. Pharmacol. Sci.* **123,** 102–109 (2013).

68. Tewari, D. *et al.* Modulation of the mitochondrial voltage dependent anion channel (VDAC) by curcumin. *Biochim. Biophys. Acta* **1848,** 151–158 (2015).

69. Veenman, L., Shandalov, Y. & Gavish, M. VDAC activation by the 18 kDa translocator protein (TSPO), implications for apoptosis. *J. Bioenerg. Biomembr.* **40,** 199–205 (2008).

70. Crompton, M., Virji, S. & Ward, J. M. Cyclophilin-D binds strongly to complexes of the voltage-dependent anion channel and the adenine nucleotide translocase to form the permeability transition pore. *Eur. J. Biochem. FEBS* **258,** 729–735 (1998).

71. Pastorino, J. G. & Hoek, J. B. Regulation of hexokinase binding to VDAC. *J. Bioenerg. Biomembr.* **40,** 171–182 (2008).

72. Huang, H. *et al.* An Interaction between Bcl-xL and the Voltage-dependent Anion Channel (VDAC) Promotes Mitochondrial Ca2+ Uptake. *J. Biol. Chem.* **288,** 19870–19881 (2013).

73. Shimizu, S., Narita, M. & Tsujimoto, Y. Bcl-2 family proteins regulate the release of apoptogenic cytochrome c by the mitochondrial channel VDAC. *Nature* **399,** 483–487 (1999).

74. Nacev, B. A. & Liu, J. O. Synergistic inhibition of endothelial cell proliferation, tube formation, and sprouting by cyclosporin A and itraconazole. *PloS One* **6,** e24793 (2011).

Chapter 3: NPC1 as a Secondary Target of Itraconazole and a Dual-Targeted Mechanism of mTOR Inhibition

3.1: Abstract

In Chapter 2, I described the use of a photoaffinity probe of itraconazole to identify VDAC1 as its major binding partner in endothelial cells, as well as the validation studies connecting VDAC1 to the observed mTOR inhibition through activation of the AMPK pathway. However, the connection between VDAC1/AMPK and the previously described inhibition of cholesterol trafficking (i.e. Niemann-Pick type C, or NPC, phenotype induction) by itraconazole was not clear. Here, I demonstrate that NPC phenotype and AMPK activation are parallel effects of itraconazole, as other known NPC phenotype inducers do not activate AMPK, and other AMPK activators do not induce NPC phenotype. In addition, VDAC1 knockdown does not induce NPC phenotype in HUVEC, although it does inhibit mTOR, suggesting that another as yet unidentified target likely mediates the NPC phenotype induction by itraconazole. Using the photoaffinity probe to directly test whether itraconazole binds to either of the two critical NPC proteins (NPC1 and NPC2), I found that the probe does crosslink to NPC1 and the crosslinking is competed away by excess itraconazole, suggesting that it is a direct binding protein of itraconazole. We therefore hypothesized that by simultaneously inhibiting two targets that lead to mTOR inhibition via distinct mechanisms (AMPK activation and NPC phenotype induction), itraconazole inhibits mTOR much more potently than AMPK activators or NPC inducers alone. In support of this hypothesis, preliminary results show that the combination of a known AMPK activator (A769662)

and NPC inducer (U18666A) is synergistic for mTOR inhibition in HUVEC. Thus, itraconazole appears to act through a novel, dual-targeted mechanism to inhibit mTOR.

ABBREVIATIONS

14DM, lanosterol 14-α-demethylase; 2DG, 2-deoxyglucose; ACC, acetyl coA carboxylase; AMPK, AMP-activated protein kinase; CPT2, carnitine palmitoyltransferase 2; DMSO, dimethyl sulfoxide; FRET, fluorescence resonance energy transfer; GAPDH, glyceraldehyde 3-phosphate dehydrogenase; HUVEC, human umbilical vein endothelial cells; IC50, 50% inhibitory concentration; Itra, itraconazole; MEF, mouse embryonic fibroblast; mEH, microsomal epoxide hydrolase; mTOR, mechanistic target of rapamycin; NPC, Niemann-Pick type C; NTD, N-terminal domain; Raptor, regulatory associated protein of TOR; S6K, ribosomal protein S6 kinase; TD-itra, triazole deleted itraconazole; VDAC, voltage-dependent anion channel.

3.2: Introduction

The mechanistic Target of Rapamycin (mTOR) pathway is a critical regulator of cell growth and proliferation. As such, it has been implicated in diseases such as cancer where growth and proliferation are dysregulated, and mTOR inhibitors have been pursued as cancer therapeutics[1]. The canonical inhibitor for which the pathway was named, rapamycin, inhibits the mTOR kinase directly by inducing dimerization of mTOR and FKBP12, physically preventing the assembly of mTOR complex 1 (mTORC1) that is required for phosphorylation of the downstream effectors such as S6 kinase (S6K) and eukaryotic translation initiation factor 4E-binding protein 1 (4EBP1). Rapamycin and its analogs have been demonstrated to have antitumor and antiangiogenic activity; however, in practice their efficacy in clinical trials has been limited, likely due to insensitivity resulting from a signaling feedback loop that leads to activation of AKT upon prolonged treatment[2,3]. Other direct mTOR inhibitors have been designed which are mostly active site ATP-competitive kinase inhibitors, but like other drugs of this class these inhibitors often have off-target effects on other kinases and can lead to the development of resistance conferring mutations[4]. Thus, mTOR inhibitors with novel mechanisms may be useful in overcoming these limitations.

The antifungal drug itraconazole was found to inhibit mTOR signaling and angiogenesis through a mechanism distinct from its antifungal target, 14-alpha demethylase (14DM), and unique to itraconazole over other azole antifungals[5]. Similarly to rapamycin, itraconazole induced an upregulation of p27 expression and downregulation of p21 in endothelial cells, and led to cell cycle arrest in the G1 phase[6]. It also inhibited the phosphorylation of mTORC1 substrates S6K and 4EBP1 with an IC_{50}

between 100-300 nM, the same concentration range required for inhibition of HUVEC proliferation. Unlike rapamycin, however, itraconazole was also shown to have a striking effect on the intracellular distribution of cholesterol, as visualized by the fluorescent cholesterol-binding dye filipin. After itraconazole treatment, the cellular cholesterol rapidly became sequestered in perinuclear punctae that were shown to colocalize with the late endosomal-lysosomal marker LAMP-1, and was no longer distributed throughout the plasma membrane. This cholesterol distribution pattern is also observed in the cells of patients with a rare genetic disease called Niemann-Pick Type C (NPC) disease, where mutations in one of two lysosomal cholesterol-binding proteins (NPC1 and NPC2) prevents the release of cholesterol from the lysosome to the rest of the cell. The fact that rapamycin did not induce a similar NPC-like phenotype suggested that the cholesterol redistribution was not a downstream effect of mTOR inhibition. It was shown that knocking down either NPC1 or NPC2 led to inhibition of mTOR in HUVEC, and that two other NPC-inducing small molecules, U18666A and imipramine, also inhibited mTOR and proliferation in HUVEC, although at much higher concentrations than itraconazole (IC_{50} values of ~3 and 10 μM, respectively). Taken together, these results suggested that NPC phenotype was likely to be upstream of mTOR inhibition by itraconazole.

The identification of VDAC1 as a direct target of itraconazole, as described in Chapter 2, appeared to partially explain the inhibition of mTOR by itraconazole as a consequence of AMPK activation. However, it remained to be shown whether AMPK activation and NPC phenotype induction were interrelated or separate effects of itraconazole, and whether one or both of these effects was responsible for the

downstream mTOR inhibition and antiproliferative effects. In this chapter, I demonstrate that NPC phenotype and AMPK activation are in fact parallel effects of itraconazole, and that the photoaffinity probe of itraconazole directly binds to NPC1. I also demonstrate that combining the NPC inducer U18666A and the AMPK activator A769662 leads to a greater inhibition of mTOR than would be expected by adding the effects of the two drugs individually, suggesting that the simultaneous targeting of these two pathways synergistically inhibits mTOR. This unique dual-targeted mechanism of mTOR inhibition may underlie the higher potency of itraconazole for mTOR compared with other AMPK activators and NPC inducers, and its polypharmacology may help itraconazole to overcome the weaknesses of other clinically used mTOR inhibitors.

3.3: Materials and Methods

Reagents and antibodies

Itraconazole was purchased from TCI Chemicals (I0732; Philadelphia, PA). 2DG was from LKT laboratories (D1859; St. Paul, MN). Filipin (F4767) was from Sigma-Aldrich (St Louis, MO). Alexa Fluor 647-azide (A10277), TCEP (20490) and High Capacity Streptavidin Agarose beads (20359) were from Life Technologies (Grand Island, NY). Biotin-azide was from Click Chemistry Tools (AZ104-100; Scottsdale, AZ). TBTA was from Anaspec (63360-50; Fremont, CA). Copper Sulfate was from LabChem Inc (LC13440-1; Pittsburgh, PA). A769662 was from Abcam (ab120335; Cambridge, MA). Antibodies against ACC (3676), phospho-ACC Ser79 (3661), and phospho-p70 S6K Thr389 (9205), were from Cell Signaling Technologies (Danvers, MA). Antibodies against p70 S6K (sc-8418), GAPDH (sc-20357), Tubulin (sc-5286), VDAC1 (sc-58649), and NPC2 (sc-33776) were from Santa Cruz Biotechnologies (Santa Cruz, CA). The antibody against NPC1 was from Proteintech (13926-1-AP; Chicago, IL).

Cell culture

Primary HUVEC pooled from 4 donors (Lonza) were cultured in complete EGM-2 (Lonza) and subcultured every 2 days at a density of 1:4, or 3 days at 1:8, and discarded after passage 8. HEK 293T, HeLa, and A549 were cultured in low glucose DMEM (Gibco; Gaithersburg, MD) supplemented with 10% filtered FBS (Gibco) and 1% penicillin/streptomycin (Gibco). All cells were cultured at 37°C with 5% CO_2.

Plasmids

The plasmids used in this study were created by a previous member of the Liu lab (Dr. Jing Xu). NPC1 and NPC2 cDNAs were cloned into the pcDNA3.1 myc his-A vector digested with BamHI and XhoI, resulting in expression of the proteins with a C-terminal myc-his tag. NPC1 NTD (aa 1-264) was cloned into the p3xflag CMV vector digested with NotI and XbaI, resulting in expression of the truncated protein with an N-terminal 3x-FLAG tag.

Filipin Staining

HUVEC 2-3 days post-transduction (as described in the Materials and Methods section of Chapter 2) were plated in an 8-well slide chamber at a density of 1000/well in 1 mL of media and allowed to settle overnight. The media was removed and cells were fixed with 4% paraformaldehyde for 15 min at room temperature. Cells were then washed twice with PBS before being incubated with 500 μL of filipin solution (diluted from 5 mg/ml DMSO stock solution to 50 μg/mL in PBS) for 1 h in the dark. The cells were then carefully washed twice more with PBS, mounted and covered with coverslip and observed using a 710NLO-Meta multiphoton microscope (Carl Zeiss, Thornwood, NY) using DAPI wavelengths (360/460 nm) at the Johns Hopkins Microscope Facility.

Photoaffinity labeling

Photoaffinity labeling and pull-down experiments were performed as described in the Materials and Methods section of Chapter 2.

Western blot

Western blotting was performed as described in the Materials and Methods section of Chapter 2.

3.4: Results

AMPK activation and NPC phenotype induction are parallel effects of itraconazole

AMPK is a well-established upstream regulator of mTOR signaling and, as described in Chapter 2, several pieces of evidence suggested that AMPK activation by itraconazole likely contributed to the observed mTOR inhibition in HUVEC. AMPK activation occurred rapidly after itraconazole treatment, as demonstrated by time-course Western blot and live cell imaging with a FRET reporter of AMPK activity, and shortly before the onset of mTOR inhibition. Increased phosphorylation of raptor on the AMPK phosphorylation site demonstrated that the known AMPK-activated feedback mechanism to inhibit mTOR was also triggered. In addition, cell lines in which AMPK activation did not occur (A549, HeLa, and VDAC1-/- MEFs) also displayed little to no mTOR inhibition by itraconazole. However, these results did not take into account the previously uncovered evidence that appeared to connect the cholesterol trafficking inhibition by itraconazole to mTOR. It remained a possibility that NPC phenotype induction by itraconazole somehow led to AMPK activation, or conversely that AMPK activation induced NPC phenotype by an unknown mechanism, which then led to mTOR inhibition.

To address these possibilities, we therefore tested whether two other commonly used NPC phenotype-inducing compounds that had previously been shown to inhibit mTOR, U18666A and imipramine, could also activate AMPK in HUVEC. At concentrations where mTOR inhibition was clearly observed, there was no detectable activation of AMPK (**Figure 3.1**), demonstrating that inhibition of cholesterol trafficking alone is not sufficient to activate AMPK, and therefore that NPC phenotype is not upstream of AMPK activation by itraconazole.

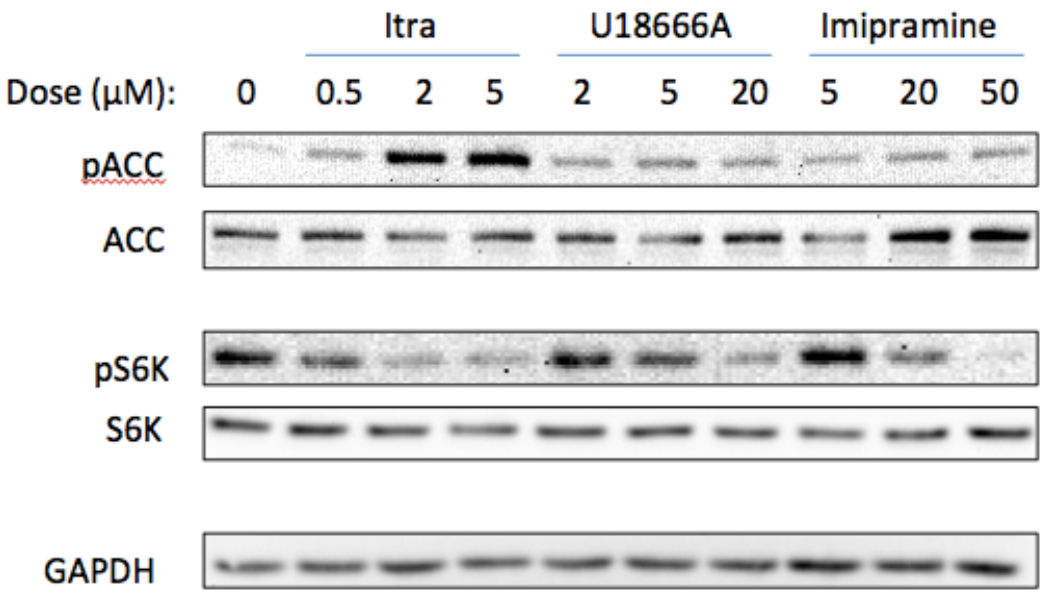

Figure 3.1: Other NPC inducers do not activate AMPK. HUVEC were treated with the indicated concentrations of NPC inducing compounds U18666A and imipramine for 1 hour. Neither compound had any observable effect on AMPK, as measured by ACC phosphorylation, at concentrations that inhibit mTOR.

We next tested whether other AMPK activators could induce NPC phenotype. Two AMPK activating compounds very commonly used in the literature are 2-deoxyglucose (2DG) and metformin. 2DG is an analog of glucose that cannot undergo glycolysis and thus causes a drop in cellular energy levels by acting as a competitive inhibitor of glycolysis. Metformin inhibits mitochondrial ATP production through a mechanism that has been debated in the field but is now generally thought to involve inhibition of complex I of the respiratory chain[7]. Another compound that has been shown to activate AMPK and inhibit mTOR is the common drug aspirin[8]. Notably, aspirin displayed a similar biphasic time-course of mTOR inhibition as itraconazole, where there was a slight recovery of mTOR activity around 4-8 hours that dropped off again to complete inhibition after 24 hours (**Figure 3.2**). In addition, one study that used a clickable probe designed to detect proteins alkylated by aspirin included VDAC1 among the list of modified proteins[9]. These interesting results prompted the question of whether itraconazole and aspirin might share a common mechanism of mTOR inhibition. However, none of the three AMPK activating drugs induced NPC phenotype (data not shown), and neither aspirin nor metformin competed with binding of the itraconazole probe to VDAC1 (**Figure 3.3**), demonstrating that they activated AMPK through a different mechanism than itraconazole. Taken together, these results suggested that AMPK activation and NPC phenotype induction are separate, parallel effects of itraconazole.

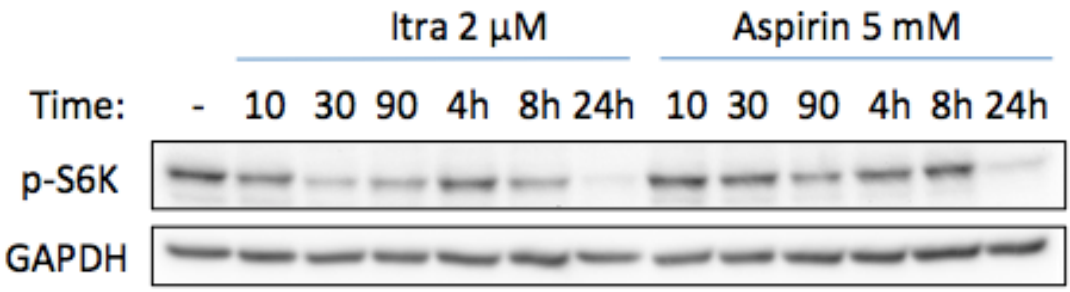

Figure 3.2: Itraconazole and aspirin both inhibit mTOR in HUVEC. HUVEC were treated with itra or aspirin for the indicated times. Both displayed a biphasic time-course of mTOR inhibition, where phosphorylation of S6K initially decreased rapidly, recovered between 4-8 hours, and then became inhibited completely by 24 hours.

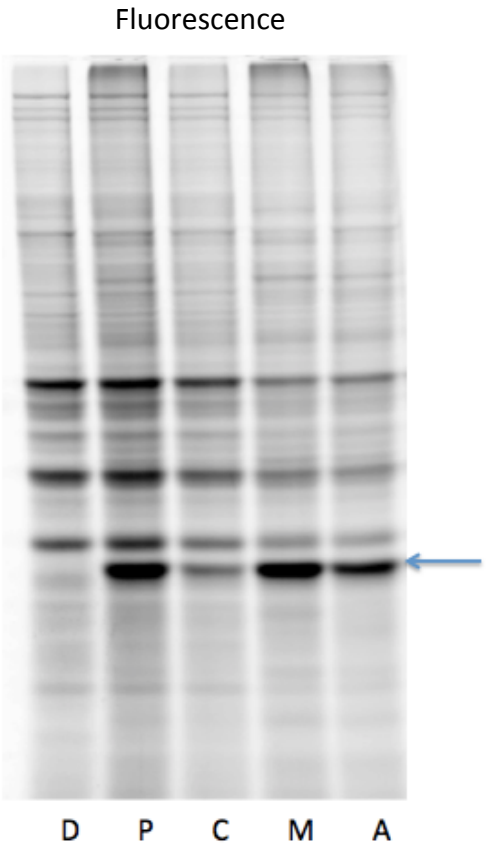

Figure 3.3: Neither aspirin nor metformin competes with binding of the itraconazole probe to VDAC1. The binding of the photoaffinity probe to VDAC1 (blue arrow) is competed away by itraconazole, but not by metformin or aspirin. (D = DMSO; P = Probe; C = Competition with Itraconazole; M = Competition with Metformin; A = Competition with aspirin)

NPC phenotype is not explained by the known targets of itraconazole

We previously demonstrated that knockdown of VDAC1 in HUVEC inhibited mTOR and proliferation as compared to wild-type cells. To determine if these effects were related to the NPC phenotype, we visualized cholesterol in VDAC1 knockdown cells and found that there was no difference in the distribution of cholesterol in wild-type vs. knockdown cells. This result suggested that NPC phenotype induction by itraconazole was likely mediated by a target other than VDAC1. Similarly, mEH and CPT2 knockdown did not affect cholesterol distribution in HUVEC. We also considered the possibility that inhibition of 14DM is responsible for NPC phenotype induction, as other azole antifungals were able to induce NPC phenotype at high concentrations[6]. However, the triazole-deleted itraconazole analog (TD-itra) was clearly able to induce NPC phenotype at 100 nM, suggesting that the azole ring was not required for this activity and thus not mediated by 14DM inhibition (**Figure 3.4**). These results led us to wonder if an additional target that had not yet been identified might be involved, and because the photoaffinity probe was also able to induce NPC phenotype (**Figure 2.2c**) we reasoned that it should also bind to the responsible target.

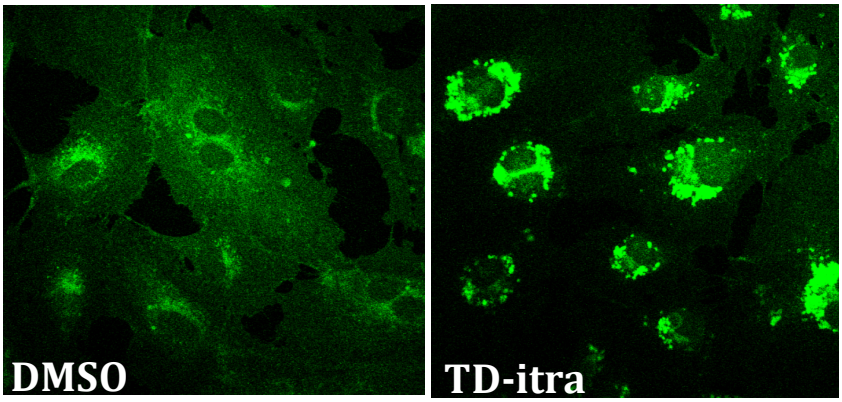

Figure 3.4: TD-itra induces NPC phenotype in HUVEC. HUVEC were treated with DMSO or TD-itra (2 μM) for 24 hours before staining with filipin to visualize cellular cholesterol. Data provided by Ruojing Li.

Itraconazole binds directly to NPC1

Niemann-Pick type C disease results from mutations in one of two lysosomal proteins, NPC1 and NPC2, with predicted molecular weights of 142 and 16.5 kDa, respectively. Although we did not observe any proteins of these molecular weights in the whole cell photolabeling experiment, we decided to specifically test whether the itraconazole photoaffinity probe could bind to either or both of these proteins by expressing tagged versions of the proteins in 293T cells and performing Western blots to detect the tag after the photocrosslinking and biotin pull-down. Surprisingly, myc-tagged NPC1 was pulled down by the probe, and was also competed away by excess itraconazole (**Figure 3.5**), suggesting that itraconazole is able to bind NPC1 directly. Myc-tagged NPC2, on the other hand, did not show any labeling by the probe. Endogenous NPC1, but not NPC2, could also be pulled down from 293T cells (**Figure 3.6a,b**), although the expression of NPC1 protein appeared to be fairly low in these cells. After testing NPC1 expression in several cell lines we found that A549 expressed higher levels of NPC1 (**Figure 3.6c**), and upon repeating the photolabeling experiment in A549 the pull-down of endogenous NPC1 could clearly be observed by Western blot (**Figure 3.6d**).

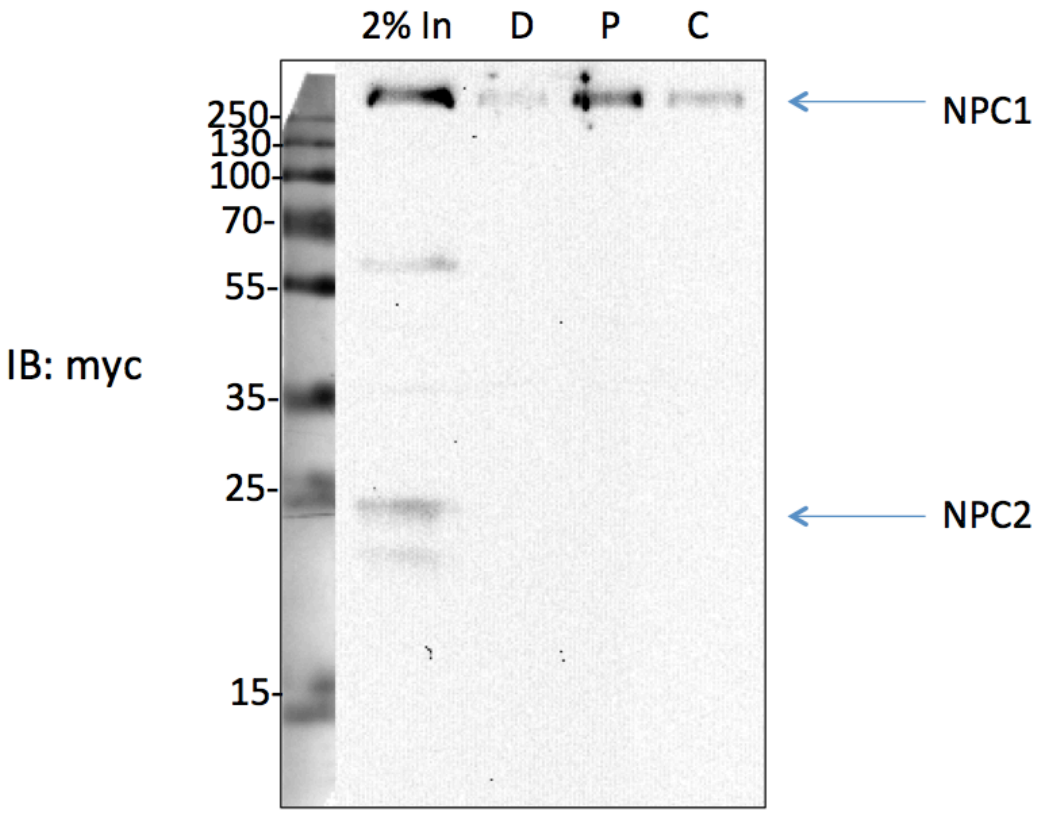

Figure 3.5: Photolabeling of exogenously expressed, myc-tagged NPC1 and NPC2. The photoaffinity labeling and biotin pull-down was performed in 293T cells co-transfected with plasmids expressing myc-tagged NPC1 and NPC2. Tagged NPC1 is clearly pulled down by the probe and competed away by itraconazole, whereas no NPC2 is detected after biotin pull-down.

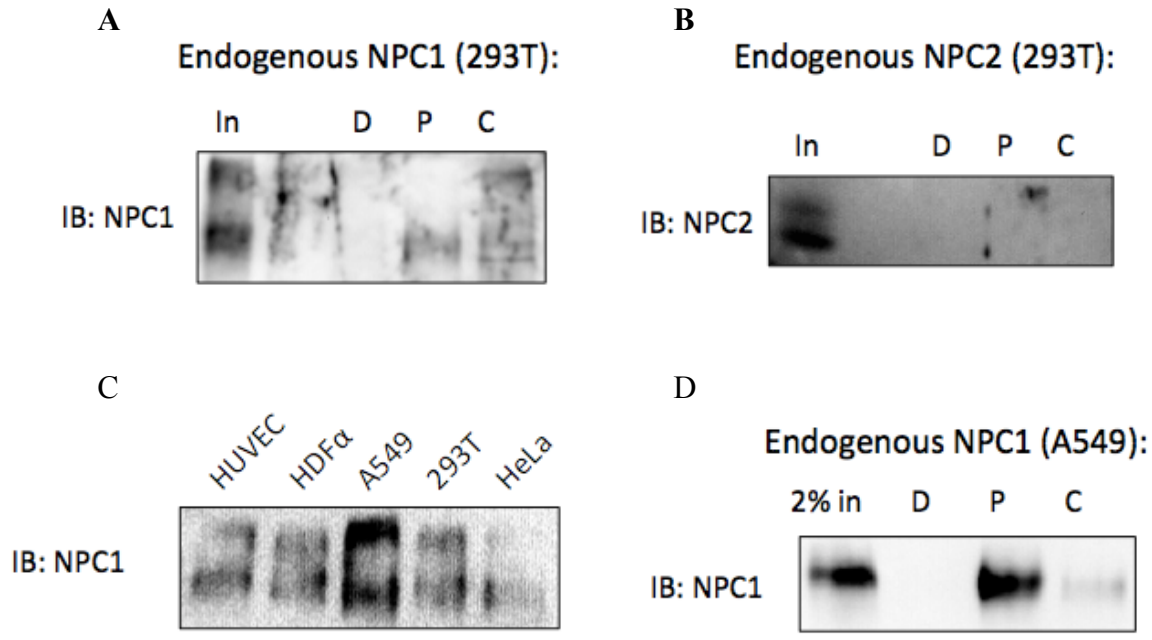

Figure 3.6: Photolabeling of endogenous NPC1 and NPC2. A) Labeling of endogenous NPC1 was detectable in 293T cells. B) No labeling of endogenous NPC2 was detectable in 293T cells. C) A549 cells were found to express the highest levels of NPC1 out of several cell lines tested. D) Labeling of endogenous NPC1 was clearly detectable in A549 cells.

NPC1 is an integral membrane protein with a 13-pass transmembrane C-terminal domain and a soluble N-terminal domain (NTD) that faces into the lumen of the lysosome and interacts directly with NPC2 to transfer cholesterol between the two proteins. To determine whether itraconazole binds to the integral membrane or soluble portion of the protein, we expressed the NTD alone (aa 1-264) with a FLAG tag and repeated the photocrosslinking and pull-down experiment. There was no observable photocrosslinking to the NTD as compared with the full-length protein (**Figure 3.7**), suggesting that the integral membrane portion of the protein is required for probe crosslinking.

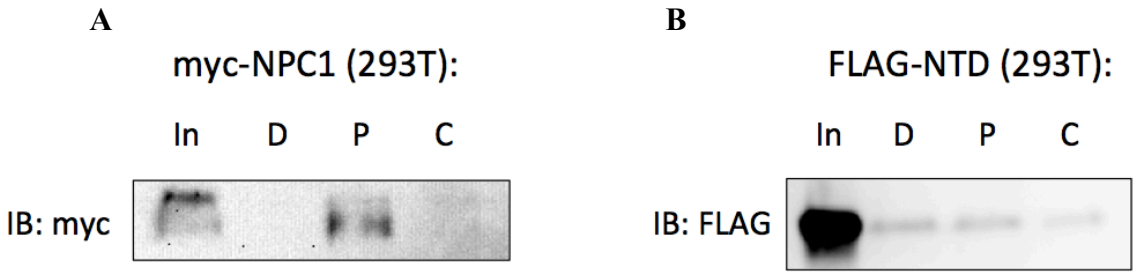

Figure 3.7: Photolabeling of expressed tagged NPC1 and NPC1(NTD). 293T cells were transfected with either A) myc-tagged NPC1 or B) FLAG-tagged NPC1(NTD) before photolabeling and biotin pull-down. Only the full-length protein could be pulled down by the probe.

Several small molecules that induce NPC phenotype have been identified and used as tool compounds to study the cholesterol trafficking defect found in patients with NPC disease. One of these is the sterol analog U18666A, which was recently shown to bind directly to the sterol-sensing domain of NPC1[15]. Another drug, indatraline, was also found to induce NPC phenotype through an unknown mechanism (**Figure 3.8**). To determine if these drugs were able to bind to NPC1 at the same site as itraconazole, we tested whether they could compete the binding of the itraconazole probe to NPC1. We also tested triazole-deleted itraconazole (TD-itra) and terconazole, another azole antifungal drug, as both had been shown to induce NPC phenotype. Thus, cells were pre-incubated with 10 μM of itraconazole or 20 μM of the other competitors for 30 min, before adding the itraconazole probe and performing the photoaffinity labeling experiment followed by biotin pull-down and Western blot for NPC1 (**Figure 3.9a**). As before, itraconazole clearly competed away binding of the itraconazole probe, while the other 4 competitors all appeared to partially compete with the binding (**Figure 3.9b**). This experiment suggested that these other NPC-inducing compounds might also bind directly to the same site on NPC1 but with lower affinity than itraconazole.

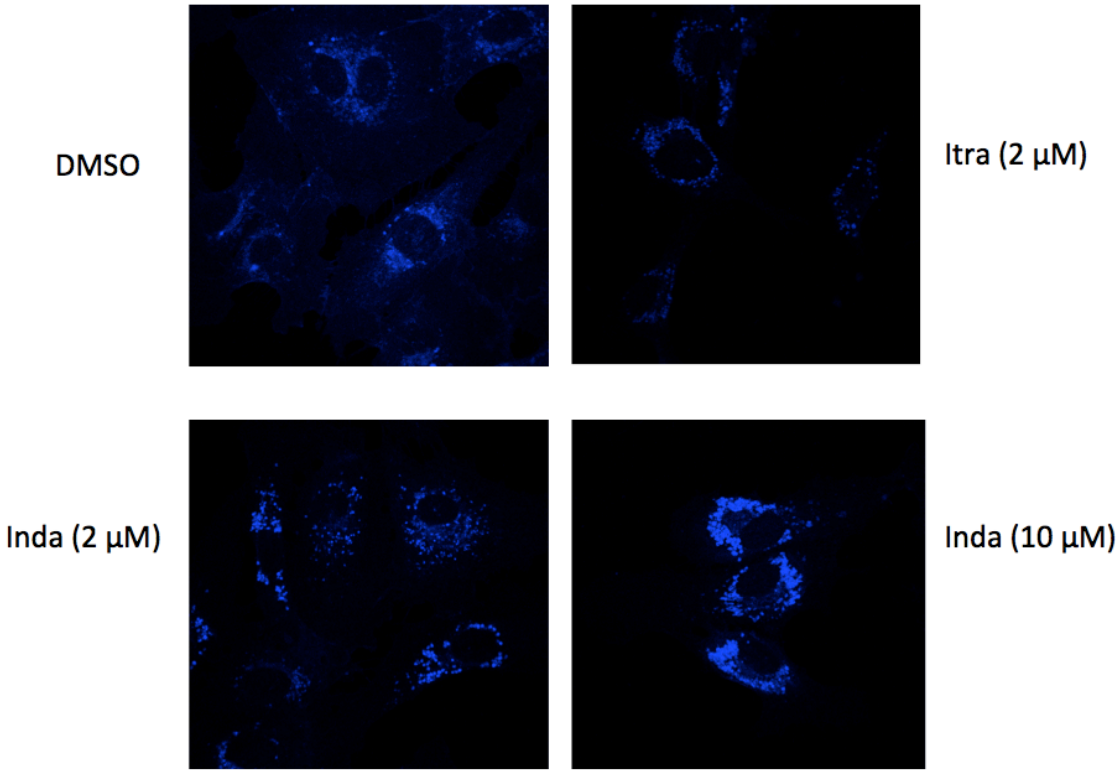

Figure 3.8: Indatraline induces NPC phenotype in HUVEC. HUVEC were treated with the indicated concentrations of itraconazole or indatraline (inda) for 24 hours and cholesterol distribution was observed by filipin staining.

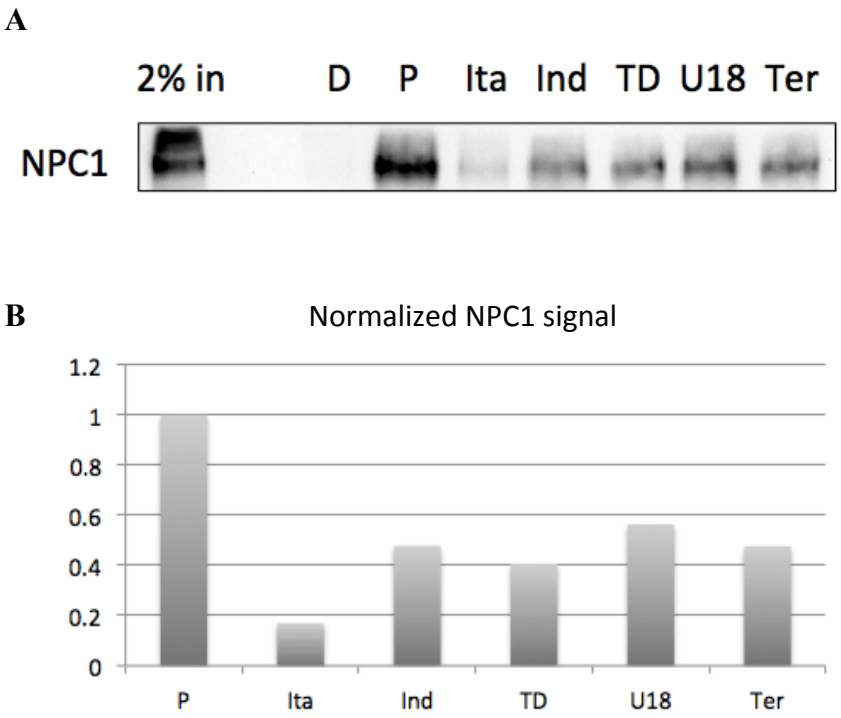

Figure 3.9: Photolabeling of NPC1 is partially competed by other NPC-inducing compounds. A) Photolabeling in A549 cells using itraconazole (ita), indatraline (ind), triazole-deleted itra (TD), U18666A (U18), or terconazole (ter) as competitors (itraconazole was used at 10 μM, all other compounds at 20 μM). B) Quantification of the western blot shown in figure A by densitometry shows that the NPC1 signal in the itraconazole competition sample is about 15% of the probe sample, while the other 4 competitor molecules have about 40-50% signal remaining.

AMPK activation and NPC induction lead to synergistic inhibition of mTOR

The fact that itraconazole binds directly to both VDAC1 and NPC1 suggested that AMPK activation and NPC phenotype induction might be two unrelated effects of itraconazole that both result in mTOR inhibition by different mechanisms. Inhibitors of cholesterol trafficking (U18666A, imipramine) and activators of AMPK (2DG, aspirin) were both previously shown to inhibit mTOR individually. We therefore wondered if simultaneously targeting these two upstream pathways would lead to a synergistic effect on mTOR. Synergy, or superadditivity, is observed when the effect of the combination of two or more compounds is greater than the sum of the effects of those compounds individually. Thus, if the sum of the individual effects of AMPK activation and NPC induction on mTOR were less than the effect of simultaneous AMPK activation and NPC induction on mTOR, then the effect would be considered synergistic. Accordingly, HUVEC were treated with the NPC inducer U18666A, as well as a direct AMPK activator called A769662 (the direct AMPK activator was used instead of 2DG or aspirin to avoid confounding effects on other cellular processes). A range of concentrations of each drug was chosen that had little or no effect on mTOR when given to cells individually (3-30 μM U18, 10-100 μM A76). However, when an intermediate concentration of each drug was combined with the other, there was a clear intensification of the effect on mTOR (**Figure 3.10**). For example, 10 μM U18 did not show obvious inhibition of mTOR on its own, but when combined with A76 the effect of A76 was significantly increased at all concentrations tested. Likewise, 30 μM A76 alone did not have an obvious effect on mTOR, but when combined with U18 it significantly enhanced the inhibition of mTOR by U18. These preliminary results support the hypothesis that the

combination of cholesterol trafficking inhibitors and AMPK activators can synergistically inhibit mTOR. Thus, by binding directly to both VDAC1 and NPC1, itraconazole simultaneously targets both pathways to produce a stronger effect on mTOR than an individual inhibitor of either protein would be able to. To our knowledge, this makes itraconazole the first known dual inhibitor of ATP production and cholesterol trafficking.

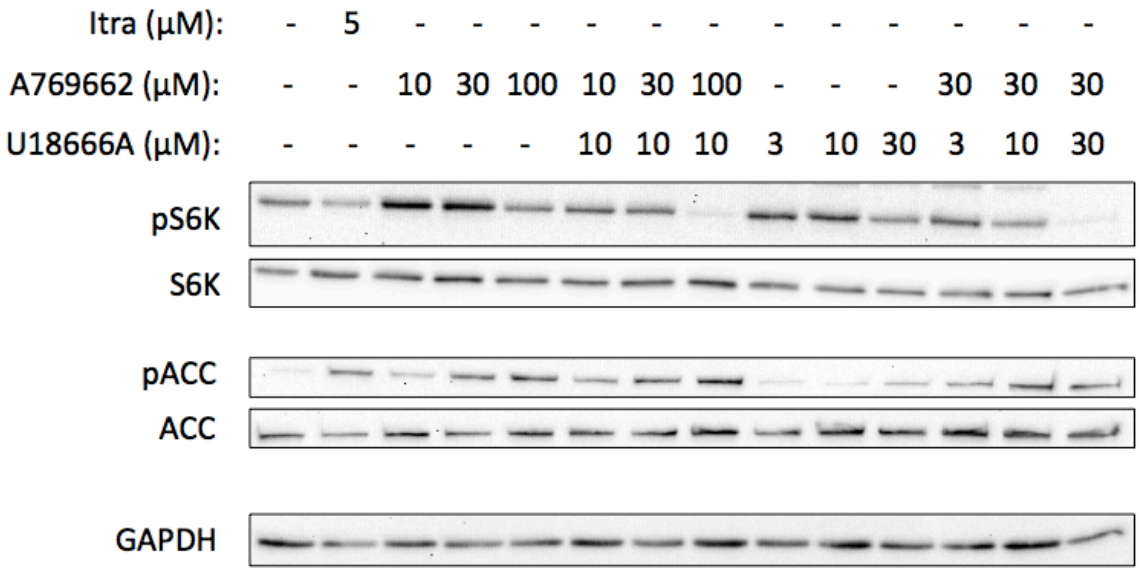

Figure 3.10: Combination treatment of HUVEC with the NPC inducer U18666a and the AMPK activator A769662. At 30 μM, A769662 does not significantly inhibit mTOR on its own (lane 4), but it does enhance the inhibition of mTOR by U18666A (lanes 9-14). Likewise, 10 μM U18666A does not inhibit mTOR in its own (lane 7), but enhances the inhibition by A769662 (lanes 3-8).

3.5: Discussion

NPC1 inhibition prevents the trafficking of cholesterol from the late endosomal-lysosomal compartment, leading to its accumulation in this compartment and its depletion from other cellular membranes. The observation that itraconazole induced this so-called NPC phenotype in HUVEC led to the connection being made between cholesterol trafficking and mTOR inhibition in endothelial cells[6]. However, the direct target of itraconazole that mediated this NPC phenotype induction was not known. In this chapter, we demonstrate that the antifungal drug itraconazole binds directly to NPC1 using a photoaffinity labeling approach in live cells.

Previous work had shown that the inhibition of mTOR and HUVEC proliferation by itraconazole could be partially rescued by adding back cholesterol in complex with the carrier molecule β-cyclodextrin. This result suggested that these effects of itraconazole might be mediated by a target whose activity is sensitive to cellular cholesterol levels. NPC1 contains a sterol-sensing domain (SSD) that has been shown to be critical for its ability to sense cholesterol in the membrane and promote its egress from the lysosome[10]. Recently, the NPC inducing compound U18666A was shown to bind directly to NPC1, and this binding was mapped to residues in the SSD by a point mutation within this domain (P691S) that prevented U18 binding. The fact that the itraconazole probe was unable to crosslink to the NTD alone and that photoaffinity labeling of NPC1 by the itraconazole probe is partially competed by U18 (**Figure 3.9a**) suggests that itraconazole's binding site on NPC1 may be located in the transmembrane portion of the protein, possibly that same SSD site to which U18 binds.

The minimal structural determinants for binding of itraconazole to NPC1 are not

clear. From the competition experiment in **figure 3.9**, it appears that neither the azole ring nor a large portion of the distal structure (phenyl-triazolone-isobutyl chain) are required for binding NPC1, as both TD-itra and terconazole are able to partially compete the binding of the itraconazole probe. The fact that U18666A and indatraline are also able to partially compete this binding suggests that the itraconazole binding pocket on NPC1 may be relatively non-specific. Indeed, in the recent report of U18666A binding to NPC1, it was suggested that the binding site "may lack the exquisite sensitivity of the [cholesterol binding site in the] NTD, and it may bind U18666A and other cationic amphiphiles that thereby block cholesterol egress from lysosomes"[15]. This hypothesis is also supported by the fact that every itraconazole analog synthesized and tested by our lab to date is able to induce NPC phenotype (data not shown). However, further work will determine whether any analogs diverge in their ability to activate AMPK and inhibit cholesterol trafficking, which would give interesting insights into the differences of the binding sites on NPC1 and VDAC1. In addition, if itraconazole does bind to the SSD of NPC1, it would be important to determine whether it also binds to other members of the SSD-containing family of proteins, which include the cholesterol biosynthetic enzymes HMG-CoA-reductase (HMGCR) and 7-dehydrocholesterol reductase (7DHCR), the SREBP-cleavage activating protein (SCAP), and the Hedgehog receptor patched.

The concept of polypharmacology, or a drug acting on more than one target, is not a new idea but has been recently gaining a renewed appreciation[18]. Until recently, most people considered so-called "dirty drugs" to be undesirable, as a high specificity and potency for a single target would presumably have powerful activity against the target with minimal side effects. However, this idea of a "magic bullet" to cure disease has not

been borne out clinically; in many situations, cells can compensate for inhibition of a single target either by developing resistance mutations or otherwise decreasing their dependence on that target. In cancer treatment in particular, due to an increased rate of genetic mutation, treatment with single targeted drugs often leads to selection of drug-resistant mutants. The same can be said for antimicrobial and antiviral drugs, due to the rapid proliferation rate and difficulty in achieving 100% eradication of the microorganism. Therefore, there is an increasing appreciation that simultaneous inhibition of multiple targets may lead to a decreased incidence of drug resistance, as the probability of a cell mutating or compensating for the loss of two targets at the same time is greatly reduced. One strategy to accomplish this is to use one or more single-targeted drugs in combination, such as with the cocktail of drugs used to treat HIV known as highly active antiretroviral therapy (HAART). However, this approach has the disadvantage of compounding side effects and the possibility of drug-drug interactions due to drug metabolism or other factors. In addition, individual pharmacokinetic differences between patients can make the dosing of multiple drugs at once even more challenging for physicians. Alternatively, using one drug with multiple targets can accomplish the same goal of combating resistance mechanisms while avoiding problems of drug-drug interactions, complicated dosing schedules, and increased side effects. To design a drug for the specific purpose of targeting multiple proteins simultaneously is more challenging, but can be accomplished through counterscreening. For example, receptor tyrosine kinases (such as EGFR or HER2) are a common target in cancer treatment, but their inhibition by small molecules can induce resistance mechanisms involving upregulation of PI3K activity. By screening a library of tyrosine kinase

inhibitors for PI3K activity, the kinase inhibitor PP121 was found that inhibits both targets, thus preventing this mechanism of resistance from occurring[18].

A related concept in drug combinations and polypharmacology is the concept of synergy. By definition, synergy is when the combination of two or more compounds produces an effect that is greater than the sum of its individual parts. In pharmacology, drugs that target multiple upstream inputs to a single cellular process are often found to be synergistic in combination. Similarly, it is possible for a single drug to induce an apparent synergistic effect by simultaneous targeting of multiple pathways. Although quantifying the synergy of a single drug is challenging without finding a way to measure its effects on one individual target at a time, we can use other specific inhibitors of each pathway to provide proof-of-concept for the synergistic inhibition of a downstream effect. Thus, in a preliminary experiment, we approximated the inhibition of the two targets of itraconazole (NPC1 and VDAC1) by combining the NPC1 inhibitor U18666A and the direct AMPK activator A769662 and measuring the effects on mTOR. By Western blotting for phosphorylation of the mTOR substrate S6K, we clearly observed a greater effect on mTOR activity by the combination of the two compounds than by each compound individually. In follow-up studies, we plan to further confirm the synergistic effect of other AMPK activators (including the VDAC inhibitor erastin) and NPC inducers on mTOR and HUVEC proliferation by using a larger number of drug doses and quantifying the synergy by calculating the combination index.

3.6: References

1. Pópulo, H., Lopes, J. M. & Soares, P. The mTOR Signalling Pathway in Human Cancer. *Int. J. Mol. Sci.* **13,** 1886–1918 (2012).
2. Huang, J. & Manning, B. D. A complex interplay between Akt, TSC2 and the two mTOR complexes. *Biochem. Soc. Trans.* **37,** 217–222 (2009).
3. O'Reilly, K. E. *et al.* mTOR inhibition induces upstream receptor tyrosine kinase signaling and activates Akt. *Cancer Res.* **66,** 1500–1508 (2006).
4. Zaytseva, Y. Y., Valentino, J. D., Gulhati, P. & Evers, B. M. mTOR inhibitors in cancer therapy. *Cancer Lett.* **319,** 1–7 (2012).
5. Chong, C. R. *et al.* Inhibition of angiogenesis by the antifungal drug itraconazole. *ACS Chem. Biol.* **2,** 263–270 (2007).
6. Xu, J., Dang, Y., Ren, Y. R. & Liu, J. O. Cholesterol trafficking is required for mTOR activation in endothelial cells. *Proc. Natl. Acad. Sci. U. S. A.* **107,** 4764–4769 (2010).
7. Wheaton, W. W. *et al.* Metformin inhibits mitochondrial complex I of cancer cells to reduce tumorigenesis. *eLife* **3,** (2014).
8. Din, F. V. N. *et al.* Aspirin inhibits mTOR signaling, activates AMP-activated protein kinase, and induces autophagy in colorectal cancer cells. *Gastroenterology* **142,** 1504–1515.e3 (2012).
9. Bateman, L. A., Zaro, B. W., Miller, S. M. & Pratt, M. R. An alkyne-aspirin chemical reporter for the detection of aspirin-dependent protein modification in living cells. *J. Am. Chem. Soc.* **135,** 14568–14573 (2013).
10. Millard, E. E. *et al.* The sterol-sensing domain of the Niemann-Pick C1 (NPC1) protein regulates trafficking of low density lipoprotein cholesterol. *J. Biol. Chem.* **280,** 28581–28590 (2005).

11. Côté, M. *et al.* Small molecule inhibitors reveal Niemann-Pick C1 is essential for Ebola virus infection. *Nature* **477,** 344–348 (2011).
12. Carette, J. E. *et al.* Ebola virus entry requires the cholesterol transporter Niemann-Pick C1. *Nature* **477,** 340–343 (2011).
13. Miller, E. H. *et al.* Ebola virus entry requires the host-programmed recognition of an intracellular receptor. *EMBO J.* **31,** 1947–1960 (2012).
14. Tang, Y., Leao, I. C., Coleman, E. M., Broughton, R. S. & Hildreth, J. E. K. Deficiency of niemann-pick type C-1 protein impairs release of human immunodeficiency virus type 1 and results in Gag accumulation in late endosomal/lysosomal compartments. *J. Virol.* **83,** 7982–7995 (2009).
15. Lu, F. *et al.* Identification of NPC1 as the target of U18666A, an inhibitor of lysosomal cholesterol export and Ebola infection. *eLife* **4,** (2015).
16. Strating, J. R. P. M. *et al.* Itraconazole inhibits enterovirus replication by targeting the oxysterol-binding protein. *Cell Rep.* **10,** 600–615 (2015).
17. Poh, M. K. *et al.* U18666A, an intra-cellular cholesterol transport inhibitor, inhibits dengue virus entry and replication. *Antiviral Res.* **93,** 191–198 (2012).
18. Apsel, B. *et al.* Targeted polypharmacology: discovery of dual inhibitors of tyrosine and phosphoinositide kinases. *Nat. Chem. Biol.* **4,** 691–699 (2008).
19. Hawley, S. A. *et al.* The ancient drug salicylate directly activates AMP-activated protein kinase. *Science* **336,** 918–922 (2012).

Chapter 4: Perspectives and Future Directions

Target identification is a challenging but critical step in the phenotypic drug discovery process. Many different methods have been developed for this purpose and each has advantages and disadvantages (as summarized in Chapter 1). Generally, however, it is not possible to know beforehand which approach will be successful for a given molecule, particularly without prior information about the type of target. Certain characteristics of the small molecule may be helpful in determining which methods are more likely to succeed; for example, water soluble drugs are generally more likely to bind to soluble proteins, for which affinity purification from cellular lysates may be appropriate, while lipid soluble drugs may be more likely to bind to membrane proteins, in which case a native approach that does not require cell lysis may be more effective. Molecules containing a reactive group such as epoxide, fluorophosphonate, or β-lactam are more likely to bind their target covalently[1], while those with bulky hydrophobic structures may interact non-covalently with their target, for which a crosslinking strategy may be preferable[2]. Many molecules interact with a specific binding pocket of a protein receptor, but others exert their effects through binding to DNA, RNA, lipids or carbohydrates, or otherwise non-specifically affect cellular function by mechanisms such as aggregation or alteration of organellar pH, in which case a target ID method with a protein-only readout will never be successful. Certain structural features have been observed in the types of molecules that act in these ways[3–7]; however, there are exceptions to every rule and it cannot be predicted with absolute certainty that a given strategy will be effective in identifying the target of a particular molecule. It is therefore

critical to be aware of the inherent biases and pitfalls of each method, and whenever possible combine the use of multiple techniques with minimal overlap in their particular weaknesses.

The antifungal drug itraconazole was identified in a high-throughput screen of clinically used drugs for its ability to selectively inhibit endothelial cell proliferation. Through a top-down, or phenotype-based approach, it was subsequently found to inhibit the mTOR signaling pathway, cholesterol trafficking, and VEGFR2 glycosylation in HUVEC. Each of these processes have been studied extensively by other researchers and many key molecular players identified, and as such a significant amount of luck would have been required to find the relevant target of itraconazole by testing each one individually. Thus, we sought to identify the molecular target(s) directly using a "bottom-up", or unbiased chemical approach. Initially, a biotinylated version of itraconazole was synthesized and used in affinity pull-down experiments with cellular lysates, but no obvious binding proteins were observed by silver staining. In retrospect, given the poor aqueous solubility of itraconazole and the lack of any reactive groups that might indicate covalent binding, we might have predicted that the biotin pull-down strategy was unlikely to succeed for this molecule. Therefore, a photoaffinity labeling approach was employed to allow binding and covalent modification of the target to occur in a native cellular environment. The proteins pulled down and identified by MS were all membrane proteins (mEH, CPT2, VDAC1, NPC1), suggesting that itraconazole probably does partition into cellular membranes. However, the fact that the photoaffinity probe did not pull down Tom40, another integral membrane protein, demonstrated that the probe did not non-specifically label all membrane proteins.

A major challenge with target identification, once one or more binding proteins are identified, is validation of the relevance of these proteins to the observed bioactivity of the small molecule. If only one binding protein is identified and its known function completely explains the observed phenotype, then validation will be straightforward. In the case of itraconazole, 3 major binding proteins were identified by the whole cell labeling experiment, none of which had been previously implicated in any of the observed effects of itraconazole in HUVEC. Additionally, a 4th binding protein, NPC1, was not detected using this "unbiased" method, possibly due to its low cellular abundance in comparison with the other binding proteins. Determining the relevance of any of these proteins to a drug phenotype then becomes challenging, particularly if the true effect of the drug involves activity against more than one protein at once. The discovery that itraconazole activated AMPK and this activity was mediated by VDAC1 was serendipitous, and still did not explain the full phenotype of the drug, which also involves inhibition of cholesterol trafficking by NPC1. We also cannot rule out the possibility that CPT2, mEH, or other unidentified targets may contribute to its effects.

To summarize, photoaffinity labeling can be a powerful tool for small molecule target identification in many situations. Its main advantages are that 1) ligand-target interaction occurs in the native environment of a living cell, making it highly useful for insoluble membrane proteins; 2) the binding partners are covalently attached by photocrosslinking, ensuring the interaction will be preserved after cell lysis and subsequent manipulation steps; 3) the specificity of the probe binding is measured directly by competition with the parent compound (or any other molecule that you want to know if it binds to the same site); and 4) the identification of targets is "unbiased" in

that all cellular proteins are present and available for labeling and identification, or alternatively, binding to specific targets can be tested by pull-down/Western blot without necessitating protein purification and binding assays for each one. Its disadvantages are that 1) it is more likely to detect more abundant cellular targets; 2) it requires that the target of the small molecule be a protein; and 3) it requires subsequent validation of the target's biological relevance through further functional experiments. Thus, as with all scientific techniques, it is best to use this photoaffinity labeling approach in combination with other techniques such as a top-down approach or genetic methods.

In this work, we used photoaffinity labeling to identify VDAC1 as a novel target of itraconazole, and employed genetic (knockdown/knockout) and various cell-based assays to validate that VDAC1 is relevant to the observed phenotype of itraconazole in endothelial cells. In the process, we also uncovered a new activity of itraconazole, the activation of the AMPK signaling pathway. A large number of AMPK activating small molecules have been discovered and used clinically or scientifically, including the clinical drugs metformin, phenformin, aspirin, and the thiazolinediones; the metabolite analogs 2DG and AICAR; synthetic direct AMPK activators A769662 and PT1; and natural products such as resveratrol and other polyphenols, berberine, and curcumin[8,9]. However, the concentrations of these drugs required to activate AMPK are generally very high (>1 mM for aspirin, 2DG, and AICAR; high μM range for metformin), and even for the synthetic direct AMPK activator A769662, concentrations in excess of 50 μM are required to activate AMPK in our experiments. Itraconazole, on the other hand, can induce detectable AMPK activation in HUVEC at concentrations as low as 300 nM, which to our knowledge makes it the most potent AMPK activator reported to date.

The discovery that itraconazole potently activates AMPK suggests new potential therapeutic applications of the drug in addition to its antifungal and antiangiogenic use. AMPK activators are most commonly used clinically as antidiabetic drugs, due to their ability to suppress hepatic glucose production. Although itraconazole has been shown to have hepatotoxicity in some patients at high doses during treatment for fungal infections, lower doses are generally very well tolerated in patients and might be sufficient to activate AMPK in the liver without inducing toxicity. In addition, the pure stereoisomer IT-C (2S,4R,2'S) was shown to have significantly lower hepatotoxicity with increased antiangiogenic activity[10]. If this isomer also induces AMPK with the same or greater potency than the mixture of cis-isomers, it would be worth investigating for this purpose, either alone or in combination with currently used diabetic drugs.

In addition to diabetes, AMPK has also been shown to be a potential target in acute lymphoblastic leukemia (ALL) and B-cell chronic lymphocytic leukemia (B-CLL)[11,12]. Interestingly, one study that investigated itraconazole in ALL and AML patients showed an increase in disease-free survival of ALL patients who were given itraconazole, which the authors suggested might be attributable to reversal of multidrug resistance through inhibition of p-glycoprotein[13]. We are currently testing itraconazole in several ALL cell lines to determine its effect on AMPK and proliferation, which may lead to a rationale for clinical trials to be expanded from the cancer types already being investigated. However, at a minimum, it could be argued that ALL patients who are already being given azole drugs for antifungal prophylaxis could potentially benefit more from itraconazole than the other azoles, which do not activate AMPK.

The identification of NPC1 as a target of itraconazole also opens up the

possibility for new potential therapeutic uses. In particular, NPC inducers have been shown to have activity against certain viruses, including Ebola, Marburg, Filovirus and HIV[14–18]. Itraconazole and U18666A were recently shown to have activity against enterovirus and hepatitis C replication, thought to be mediated by inhibition of oxysterol-binding protein (OSBP)[19]. U18666A was also shown in another study to inhibit dengue virus entry and replication[20]. It would be highly worthwhile to test itraconazole against a panel of different viruses to see if it has activity, as it is not only significantly more potent than U18 at inducing NPC phenotype but is also an FDA-approved drug that could be rapidly repurposed for short-term antiviral use.

Another intensive effort by our lab over the past several years has been the synthesis of structural analogs of itraconazole, and to date we have made over 75 such analogs[21–23]. Ongoing efforts to characterize the activity of these analogs against each of itraconazole's effects – mTOR inhibition, NPC phenotype, Hedgehog, proliferation – has revealed analogs with improved activity, better water solubility, and less cross-inhibition of drug metabolizing enzymes. Further studies will investigate whether any of these analogs might be more selective inhibitors of either VDAC1 or NPC1, which could potentially be useful therapeutics.

4.2: References

1. Johnson, D. S., Weerapana, E. & Cravatt, B. F. Strategies for discovering and derisking covalent, irreversible enzyme inhibitors. *Future Med. Chem.* **2,** 949–964 (2010).
2. Sumranjit, J. & Chung, S. J. Recent Advances in Target Characterization and Identification by Photoaffinity Probes. *Molecules* **18,** 10425–10451 (2013).
3. Paul, A. & Bhattacharya, S. Chemistry and biology of DNA-binding small molecules. *Curr. Sci.* **102,** 212–231 (2012).
4. DeJong, E. S., Luy, B. & Marino, J. P. RNA and RNA-protein complexes as targets for therapeutic intervention. *Curr. Top. Med. Chem.* **2,** 289–302 (2002).
5. Sudhahar, C. G., Haney, R. M., Xue, Y. & Stahelin, R. V. Cellular membranes and lipid-binding domains as attractive targets for drug development. *Curr. Drug Targets* **9,** 603–613 (2008).
6. Funk, R. S. & Krise, J. P. Cationic amphiphilic drugs cause a marked expansion of apparent lysosomal volume: Implications for an intracellular distribution-based drug interaction. *Mol. Pharm.* **9,** 1384–1395 (2012).
7. Seidler, J., McGovern, S. L., Doman, T. N. & Shoichet, B. K. Identification and prediction of promiscuous aggregating inhibitors among known drugs. *J. Med. Chem.* **46,** 4477–4486 (2003).
8. Fogarty, S. & Hardie, D. G. Development of protein kinase activators: AMPK as a target in metabolic disorders and cancer. *Biochim. Biophys. Acta BBA - Proteins Proteomics* **1804,** 581–591 (2010).
9. Steinberg, G. R. & Kemp, B. E. AMPK in Health and Disease. *Physiol. Rev.* **89,** 1025–1078 (2009).

10. Shim, J. S. *et al.* Divergence of Anti-angiogenic Activity and Hepatotoxicity of Different Stereoisomers of Itraconazole. *Clin. Cancer Res. Off. J. Am. Assoc. Cancer Res.* (2016). doi:10.1158/1078-0432.CCR-15-1888
11. Sengupta, T. K. *et al.* Cytotoxic effect of 5-aminoimidazole-4-carboxamide-1-beta-4-ribofuranoside (AICAR) on childhood acute lymphoblastic leukemia (ALL) cells: implication for targeted therapy. *Mol. Cancer* **6,** 46 (2007).
12. Campàs, C. *et al.* Acadesine activates AMPK and induces apoptosis in B-cell chronic lymphocytic leukemia cells but not in T lymphocytes. *Blood* **101,** 3674–3680 (2003).
13. Vreugdenhil, G., Raemaekers, J. M., van Dijke, B. J. & de Pauw, B. E. Itraconazole and multidrug resistance: possible effects on remission rate and disease-free survival in acute leukemia. *Ann. Hematol.* **67,** 107–109 (1993).
14. Côté, M. *et al.* Small molecule inhibitors reveal Niemann-Pick C1 is essential for Ebola virus infection. *Nature* **477,** 344–348 (2011).
15. Carette, J. E. *et al.* Ebola virus entry requires the cholesterol transporter Niemann-Pick C1. *Nature* **477,** 340–343 (2011).
16. Miller, E. H. *et al.* Ebola virus entry requires the host-programmed recognition of an intracellular receptor. *EMBO J.* **31,** 1947–1960 (2012).
17. Tang, Y., Leao, I. C., Coleman, E. M., Broughton, R. S. & Hildreth, J. E. K. Deficiency of niemann-pick type C-1 protein impairs release of human immunodeficiency virus type 1 and results in Gag accumulation in late endosomal/lysosomal compartments. *J. Virol.* **83,** 7982–7995 (2009).
18. Lu, F. *et al.* Identification of NPC1 as the target of U18666A, an inhibitor of lysosomal cholesterol export and Ebola infection. *eLife* **4,** (2015).
19. Strating, J. R. P. M. *et al.* Itraconazole inhibits enterovirus replication by targeting the oxysterol-binding protein. *Cell Rep.* **10,** 600–615 (2015).

20. Poh, M. K. *et al.* U18666A, an intra-cellular cholesterol transport inhibitor, inhibits dengue virus entry and replication. *Antiviral Res.* **93,** 191–198 (2012).
21. Shi, W. *et al.* Itraconazole Side Chain Analogues: Structure–Activity Relationship Studies for Inhibition of Endothelial Cell Proliferation, Vascular Endothelial Growth Factor Receptor 2 (VEGFR2) Glycosylation, and Hedgehog Signaling. *J. Med. Chem.* **54,** 7363–7374 (2011).
22. Head, S. A. *et al.* Antifungal drug itraconazole targets VDAC1 to modulate the AMPK/mTOR signaling axis in endothelial cells. *Proc. Natl. Acad. Sci. U. S. A.* **112,** E7276–7285 (2015).
23. Shi, W., Nacev, B. A., Bhat, S. & Liu, J. O. Impact of Absolute Stereochemistry on the Antiangiogenic and Antifungal Activities of Itraconazole. *ACS Med. Chem. Lett.* **1,** 155–159 (2010).

CURRICULUM VITAE

Sarah Alexandra Head
June 2016

Education

2010 – 2016 Johns Hopkins School of Medicine (Ph.D.) Baltimore, MD

Department of Pharmacology and Molecular Sciences; Affiliate of Chemistry-Biology Interface program

- Mentor: Dr. Jun Liu, Ph.D.

2005 – 2009 Boston University (B.A.) Boston, MA

College of Arts and Sciences

- B.A. in Biochemistry and Molecular Biology; B.A. in Psychology; Premedicine
- Studied abroad at the University of Auckland, NZ, Jan – June 2007.

Research Experience

Sep 2010 – Present Dr. Jun Liu (JHMI) Baltimore, MD

PhD student

- Identified VDAC1 as the antiangiogenic target of the clinical drug itraconazole, and elucidated a novel regulatory mechanism of the AMPK/mTOR signaling pathway.

Sep 2014 – Feb 2015 Drs. Sergei Bezukrov and Tatiana Rostovtseva Bethesda, MD

Special Volunteer, National Institutes of Health (NIH)

- Performed electrophysiology experiments on purified VDAC and gramicidin channels, as part of a collaboration related to thesis project.

Sep 2012 – July 2013 Dr. Marco Colombini (UMD) College Park, MD

PhD student collaborator

- Performed functional assays using isolated mitochondria to measure outer membrane permeability, as part of a collaboration related to thesis project.

Mar – Jun 2011 Drs. Jin Zhang & Heng Zhu (JHMI) Baltimore, MD

Rotation student

- Developing a FRET-based biosensor for the measurement of CaMKII activity in live cells.
- Using human protein microarrays to identify substrates of different CaMK isoforms.

Dec 2010 – Mar 2011 Dr. Philip Cole (JHMI) Baltimore, MD

Rotation student

- Measuring differential sensitivities of wild-type and mutated EGFR to inhibitors *in vitro*.

Jun 2009 – July 2010 Dr. Gene Blatt (Boston University) Boston, MA

Research Technician

- Investigating neuroanatomical differences between autistic and normal post-mortem human brains.

Publications

Shah AK, Qian S, Zhang D, **Head SA**, Liu JO, Jin Z (2016). Insights into the structure activity relationship of the anticancer compound ZJ-101: a critical role played by cyclohexene ring. Bioorgan Med Chem, in press.

Head SA, Liu JO. (2016) Identification of small molecule-binding proteins in a native cellular environment by live-cell photoaffinity labeling. J Vis Exp, in press.

Shim JS, Li R, Bumpus N, **Head S**, Pasunooti K, Shi W, Liu JO. (2016). Divergence of Anti-angiogenic Activity and Hepatotoxicity of Different Stereoisomers of Itraconazole. Clin Cancer Res, in press.

Head SA, Shi W, Zhao L, Gorshkov K, Pasunooti K, Chen Y, Deng Z, Li R, Shim JS, Tan W, Hartung T, Zhang J, Zhao Y, Colombini M, Liu JO (2015). Antifungal drug itraconazole targets VDAC1 to modulate the AMPK/mTOR signaling axis in endothelial cells. Proc Nat Acad Sci USA, 112(52):E7276-85.

Shim JS, Li R, Lv J, **Head S**, Yang EJ, Liu JO (2015). Inhibition of angiogenesis by selective estrogen receptor modulators through blockade of cholesterol trafficking rather than estrogen receptor antagonism. Cancer Lett, 362(1):106-15.

Strating JR, van der Linden L, Albulescu L, Bigay J, Arita M, Delang L, Leyssen P, van der Schaar HM, Lanke KH, Thibaut HJ, Ulferts R, Drin G, Schlinck N, Wubbolts RW, Sever N, **Head SA**, Liu JO, Beachy PA, De Matteis MA, Shair MD, Olkkonen VM, Neyts J, van Kuppeveld FJ (2015). Itraconazole Inhibits Enterovirus Replication by Targeting the Oxysterol-Binding Protein. Cell Rep, 10(4):600-15.

Shi W, Nacev BA, Aftab BT, **Head S**, Rudin CM, Liu JO (2011). Itraconazole Side Chain Analogues: Structure-Activity Relationship Studies for Inhibition of Endothelial Cell Proliferation, Vascular Endothelial Growth Factor Receptor 2 (VEGFR2) Glycosylation, and Hedgehog Signaling. J Med Chem, 54(20):7363-74.

Wang Z, Longo PA, Tarrant MK, Kim K, **Head S**, Leahy DJ, Cole PA (2011). Mechanistic Insights into the Activation of Oncogenic Forms of EGF Receptor. Nat Struct Mol Biol, 18(12):1388-93.

Awards and academic activities

- Awarded Predoctoral Fellowship in Pharmacology/Toxicology from the PhRMA Foundation in 2014
- Profiled two Pharmacology faculty members for JHM Science News newsletter, 2015.
- Student Research Mentor (2012, 2013, 2014, 2015).
- Graduated *cum laude;* Dean's list Fall 2006, Fall 2007, Fall 2008, Spring 2009.

Invited seminars and poster presentations

- Invited Seminar: Faculty of Health Sciences, University of Macau, Macau, China SAR. May 25, 2016.
- Invited Seminar: Department of Metabolism and Molecular Biology, Fudan University, Shanghai, China. June 1, 2016.
- Poster presentation: Gordon Research Seminar/Gordon Research Conference on High Throughput Chemistry & Chemical Biology, June 2015.
- Poster presentation (Best poster award): Johns Hopkins Chemistry-Biology Interface retreat, 2014.